



저작자표시-비영리-변경금지 2.0 대한민국

이용자는 아래의 조건을 따르는 경우에 한하여 자유롭게

- 이 저작물을 복제, 배포, 전송, 전시, 공연 및 방송할 수 있습니다.

다음과 같은 조건을 따라야 합니다:



저작자표시. 귀하는 원저작자를 표시하여야 합니다.



비영리. 귀하는 이 저작물을 영리 목적으로 이용할 수 없습니다.



변경금지. 귀하는 이 저작물을 개작, 변형 또는 가공할 수 없습니다.

- 귀하는, 이 저작물의 재이용이나 배포의 경우, 이 저작물에 적용된 이용허락조건을 명확하게 나타내어야 합니다.
- 저작권자로부터 별도의 허가를 받으면 이러한 조건들은 적용되지 않습니다.

저작권법에 따른 이용자의 권리는 위의 내용에 의하여 영향을 받지 않습니다.

이것은 [이용허락규약\(Legal Code\)](#)을 이해하기 쉽게 요약한 것입니다.

[Disclaimer](#)

**Doctor of Philosophy**

**Roles of translation inhibitors and  
eIF2alpha phosphorylation  
in TFEB and TFE3 nuclear translocation**

The Graduate school of the University of Ulsan

Department of Biological science

**Dang Thi Thao**

**Roles of translation inhibitors and  
eIF2alpha phosphorylation  
in TFEB and TFE3 nuclear translocation**

Supervisor: Professor **Sung Hoon Back**, Ph.D

A Dissertation

Submitted to

The Graduate School of the University of Ulsan

In partial Fulfillment of the Requirements

for the degree of

**Doctor of Philosophy**

By


**Dang Thi Thao**


Department of Biological Science


Ulsan, Korea


**Roles of translation inhibitors and  
eIF2alpha phosphorylation  
in TFEB and TFE3 nuclear translocation**


This certifies that the dissertation  
of Dang Thi Thao is approved by

Committee Chair Dr. IN SEOB HAN 

Committee Member Dr. HUN TAEG CHUNG 

Committee Member Dr. BYUNG JU LEE 

Committee Member Dr. CHAN YOUNG PARK 

Committee Member Dr. SUNG HOON BACK 

**Department of Biological Science  
Ulsan, Korea.  
August 2022**

# CONTENTS

## Roles of translation inhibitors and eIF2alpha phosphorylation in TFEB and TFE3 nuclear translocation

**Abstract** ----- 1

### **Chapter 1. Translation Inhibitors Activate Autophagy Master Regulators TFEB and TFE3**

Abstract ----- 4

Introduction -----5

Materials and Methods -----9

Results -----16

Discussion -----24

Figures -----26

Reference -----43

### **Chapter 2. Phosphorylation of eukaryotic translation initiation factor 2 $\alpha$ is indispensable for nuclear translocation of TFEB and TFE3 during ER stress**

Abstract -----51

Introduction -----52

Materials and Methods -----55

Results -----68

Discussion -----83

Figures -----88

Reference -----120

**Appendix 1. Translation Inhibitors Activate Autophagy Master Regulators TFEB and TFE3**

**Appendix 2. PERK but not eIF2 $\alpha$  phosphorylation is required for intracellular calcium dynamics during ER stress**

## Abstract

Macroautophagy/autophagy is important catabolic process responsible for the degradation of unnecessary or dysfunction cellular components via lysosomal pathway. Autophagy is triggered in diverse stress conditions such as food deprivation, hypoxia, misfolded proteins, damaged organelles, or intracellular pathogens. Therefore, autophagy is essential for balancing energy sources for protein synthesis. Moreover, protein biosynthesis is one of the major metabolic processes, which are crucial for maintaining cellular functions including autophagy.

In part 1, using three translation inhibitors with distinct inhibitory mechanisms, I analyzed their effects on the regulation of TFEB/TFE3 activity and autophagy. Cycloheximide (CHX) is a translation elongation inhibitor, which prevents tRNA translocation by skewing the binding of deacylated tRNA to the E-site. Lactimidomycin (LTM) is another translation elongation inhibitor, which binds to the ribosomal E-site and prevents translocation of the P-site tRNA into the E-site. However, CHX stalls ribosome during ongoing translation, whereas LTM preferentially arrests ribosomes during the very first round of elongation. Lastly, rocaglamide A (RocA) is an eIF4A RNA helicase inhibitor, which inhibits the translation of not only purine-rich 5' leader containing mRNAs but also normally unresponsive mRNAs via blockade of 43S PI scanning, 43S PIC recruitment block and bystander effect by eIF4F sequestration. In this study, I found that these translation inhibitors enhance TFEB/TFE3 autophagy master regulators nuclear translocation via dephosphorylation and 14-3-3 dissociation and significantly increases autophagy-related genes. Furthermore, I demonstrated that translation inhibition increased autophagosome biogenesis but impaired the degradative autolysosome formation because of lysosomal dysfunction. In addition, these findings suggest a new biological function of translation inhibition in autophagy regulation.

In part 2, I reveal the essential role of eIF2 $\alpha$  phosphorylation in the nuclear translocation of TFEB and TFE3. Eukaryotic translation of the mRNA molecule consists of 4 stages: initiation, elongation, termination, and recycle. Inhibition at any stages during translation process can lead to either change in the protein structure or their gene expression. However, protein synthesis is mostly and sensitively controlled at the initiation stage rather than elongation or termination stage. Phosphorylation of the  $\alpha$  subunit of the translation initiation factor eIF2 $\alpha$  at serine 51 mediates translational control and necessary for cell adaptation to cellular stress. Several reports suggest that the eIF2 $\alpha$  phosphorylation could play a key role in autophagy regulation. I found that eIF2 $\alpha$  phosphorylation-deficient (A/A) cells which have Serine to Alanine mutation at 51st amino acid have defective in autophagy process including autophagosome formation, autophagosome-lysosome fusion and autolysosome formation. These effects mainly caused by defective in TFEB and TFE3

nuclear translocation and reduced their activation in *A/A* cells during ER stress conditions. Therefore, eIF2 $\alpha$  phosphorylation was important for TFEB and TFE3 nuclear translocation under diverse autophagy inducing conditions including ER stress. I also found that TFEB dephosphorylation at both S211 and S142 residues and dissociation from 14-3-3 were not sufficient for its nuclear translocation in *A/A* cells during ER stress. However, overexpression of the activated ATF6 $\alpha$  form was necessary and sufficient to induce both TFEB dephosphorylation and its nuclear translocation in *A/A* cells during ER stress. Consequently, the activated ATF6 $\alpha$  or TFEB forms overexpression could restore impaired autophagic defects in eIF2 $\alpha$  phosphorylation-deficient (*A/A*) cells during ER stress. The data highlight a new mechanism controlling TFEB subcellular localization and activity via an eIF2 $\alpha$  phosphorylation-dependent component of UPR signaling pathways under ER stress conditions. Furthermore, the finding revealed that how eIF2 $\alpha$  phosphorylation connects the UPR pathways to autophagy.

Altogether, this study reveals that translation inhibition by translation inhibitors and eIF2 $\alpha$  phosphorylation have an important role in nuclear translocation of TFEB and TFE3. Both translation inhibitors-mediated translation inhibition and eIF2 $\alpha$  phosphorylation-mediated translation inhibition may share the TFEB/TFE3 nuclear regulatory mechanism(s) controlling TFEB/TFE3 nuclear translocation and activation.



# **CHAPTER 1**

## **Translation Inhibitors Activate Autophagy Master Regulators TFE3 and TFE3**

## **Abstract**

The autophagy-lysosome pathway is a major protein degradation pathway stimulated by multiple cellular stresses, including nutrient or growth factor deprivation, hypoxia, misfolded proteins, damaged organelles, and intracellular pathogens. Recent studies have revealed that transcription factor EB (TFEB) and transcription factor E3 (TFE3) play a pivotal role in the biogenesis and functions of autophagosome and lysosome. Here I report that three translation inhibitors (cycloheximide, lactimidomycin, and rocaglamide A) can facilitate the nuclear translocation of TFEB/TFE3 via dephosphorylation and 14-3-3 dissociation. In addition, the inhibitor-mediated TFEB/TFE3 nuclear translocation significantly increases the transcriptional expression of their downstream genes involved in the biogenesis and function of autophagosome and lysosome. Furthermore, I demonstrated that translation inhibition increased autophagosome biogenesis but impaired the degradative autolysosome formation because of lysosomal dysfunction. These results highlight the previously unrecognized function of the translation inhibitors as activators of TFEB/TFE3, suggesting a novel biological role of translation inhibition in autophagy regulation.

## Introduction

Macroautophagy, hereafter referred to as autophagy, is a normal degradative pathway that exists in all eukaryotic cells [1,2]. Autophagy involves sequestration of cytoplasmic contents, including organelles, by double membranes, to form a unique nascent autophagic vacuole (hereafter autophagosome) and their delivery to lysosomes for digestion [3–5]. A number of autophagy-related proteins are implicated in the formation of the autophagosome, such as microtubule-associated proteins 1A/1B light chain 3B (LC3B). LC3B produced as a precursor (pro-LC3B) is cleaved by the ATG4 protease into a cytosolic form referred to as LC3B(I). LC3B(I) is subsequently conjugated with phosphatidylethanolamine (PE) to LC3B(II) via a ubiquitination-like enzymatic reaction, followed by insertion into both inner and outer membranes of the growing vesicular sac (also called phagophore). Consequently, increased LC3B(II) is routinely used as a marker of autophagy activation. In addition, LC3B is widely used as a microscopic marker of phagophores and autophagosomes [6,7].

The progression and resolution of autophagy critically depends on the lysosomal function, as lysosomes play a role in the breakdown and recycling of cellular compartments. Lysosome is a single membrane-bound compartment that is filled with more than 60 resident acid hydrolases: proteases, phosphatases, lipases, nucleases, and glycosidases [8,9]. Most of these enzymes are functionally optimized at a low pH, which is maintained by the vacuolar H<sup>+</sup>-ATPase (V-ATPase), an ATP-driven proton pump located on the lysosomal transmembrane [10,11]. Lysosome mainly contains various acidic proteases, including cathepsins representing a major class of lysosomal proteases, which contribute to the degradation of proteins or organelles. The cathepsin family consists of three different protease families including aspartic proteases (cathepsin D and E), serine proteases (cathepsins A and G), and cysteine cathepsins (cathepsins B, C, F, H, K, L, O, S, V, X, and W) [12,13]. Cathepsins are synthesized as inactive pro-cathepsins in the endoplasmic reticulum (ER) and transported into the endosome/lysosome compartment. Inside lysosomes, the cleavage of propeptide converts pro-cathepsins to mature active cathepsins [13]. Most lysosomal cathepsins are functionally optimized at a low pH, as cathepsins are stable and active at an acidic pH. The most abundant lysosomal membrane proteins include the lysosome-associated membrane protein (LAMP)1 and LAMP2, which together constitute ~50% of lysosomal membrane proteins [14,15]. Therefore, those proteins are used as markers of the lysosome level and integrity.

The induction and formation of autophagosome during autophagy are followed by late stages such as autophagosome-lysosome fusion and cargo degradation for completion of autophagy [4,5,11]. The fusion of nascent autophagosome with late endosome or lysosome generates autolysosome, a process also known as autophagosome maturation, which is

mediated by ATG8 family members, membrane tethering complexes, Rab GTPases, soluble N-ethylmaleimide-sensitive factor attachment protein receptors (SNAREs), and a voltage-gated calcium channel [4,5,16,17]. The lysosomal V-ATPase is responsible for lysosome acidification and is indispensable for lysosomal acid enzyme activation and cargo degradation. However, V-ATPase-deficient lysosomes can fuse with autophagosomes and endosomes [18]. In addition, Niemann–Pick type C disease (NPC) cells and CtsB/L inhibition or genetic depletion can impair autolysosome clearance but preserve intact autophagosome-lysosome fusion [19,20]. Thus, the studies suggest that intact lysosomal acidification and protease activity are not required for autolysosome formation although lysosomal impairment can lead to an accumulation of cargo in inactive autolysosomes.

Autophagy was considered as a pathway exclusively regulated by cellular processes in enucleated cells forming autophagosomes [21]. However, increasing evidence indicates that autophagy is regulated at the transcription level by several transcriptional factors including [transcription factor EB (TFEB), transcription factor E3 (TFE3), E2 transcription factor1 (E2F1), and Forkhead box O (FOXO)] [22–24]. TFEB is a member of the microphthalmia-associated transcription factor (MiTF) that also includes MITF, TFE3, and TFEC proteins [25]. It is believed that TFEB and TFE3 are master regulators of the autophagy-lysosome pathway (ALP) controlling the expression of genes required for autophagosome formation, lysosome biogenesis, and lysosome function [26–28]. Activities of TFEB and TFE3 are regulated by post-translational modification, especially phosphorylation [29–32]. To date, several kinases that phosphorylate TFEB and TFE3 have been identified. Among them, mTOR, as part of the protein complex Torin-2-mediated mechanistic target of rapamycin complex 1 (mTORC1), represents the main kinase responsible for TFEB and TFE3 phosphorylation [33–36]. Under nutrient-rich conditions, the lysosome-localized mTOR phosphorylates TFEB (at Ser142 and Ser211) and TFE3 (at Ser321). The phosphorylated TFEB and TFE3 subsequently interact with the cytosolic chaperone 14-3-3 proteins, which results in sequestration of these transcription factors as an inactive form in the cytosol [33,35–37]. Under nutrient deprivation and metabolic stress, mTOR activity is inhibited and/or Ca<sup>2+</sup>-calmodulin-dependent protein phosphatase calcineurin is activated, without further phosphorylation of TFEB and TFE3, resulting in the prevention of binding to 14-3-3 and rapid accumulation of TFEB and TFE3 in the nucleus [30,38–40]. However, recent studies have shown that mTOR-independent phosphorylation (S138 and S134) and calcineurin-independent dephosphorylation also play a role in the modulation of TFEB localization, indicating that other kinases and phosphatases can regulate TFEB activity [41–43]. Thus, the mechanisms governing TFEB/TFE3 localization in response to multiple signals are still not fully understood. Subsequently, nuclear TFEB promotes the transcription of genes required for autophagosome formation, lysosome

biogenesis and lysosome function by direct binding to promoters of the coordinated lysosomal expression and regulation (CLEAR) element [26–28].

Protein biosynthesis is one of the major metabolic processes, which are crucial for maintaining cellular functions including autophagy. Therefore, eukaryotic translation is an attractive target to destroy fast-growing tumor cells and impair and/or delay the spread of fast-replicating viral pathogens [44–48]. In addition, growing evidence indicates that autophagy modulation is also important for anti-cancer [49,50] and anti-viral therapies [51,52]. The mTORC1 not only regulates autophagy via TFEB/TFE3 phosphorylation [33–36], but also stimulates mRNA translation via phosphorylation of several translational regulatory proteins such as eukaryotic translation initiation factor 4E (eIF4E)-binding proteins 1 and 2 (4E-BP), ribosomal protein S6 kinases 1 and 2 (S6K1/2), and RNA-binding protein La-related protein 1 (LARP1) [53]. It is known that mTORC1 inhibitors such as Torin1 and 2 can inhibit mRNA translation [47,54] but induce autophagy [29,30,33–36]. Therefore, I investigated whether other translation inhibitors can also affect TFEB/TFE3 phosphorylation, localization, and further autophagic pathways. In this report, I analyzed three different translation inhibitors with different mechanisms of action. First, I used cycloheximide (CHX), a well-known translation inhibitor that can bind to the E-site of the 60S ribosome together with deacylated tRNA, followed by ribosome arrest on the next codon in the mRNAs anywhere [47,55,56]. The next inhibitor was another 60S tRNA E-site inhibitor lactimidomycin (LTM), which can preferentially arrest ribosome at the first peptide bond [47,55,56]. The last one was a natural product rocaglamide A (RocA) isolated from plants belonging to genus *Aglaia*. It is an inhibitor of eukaryotic initiation factor 4A (eIF4A), an ATP-dependent DEAD-box RNA helicase. It preferentially represses translation by clamping eIF4A onto purine-rich regions within mRNA 5' leaders, followed by inhibition of 43S pre-initiation complexes (PICs), leading to the premature translation from uORF and the inhibition of downstream ORF translation [47,57,58]. Further, a recent study suggested that rocaglates including RocA can interfere with the heterotrimeric (eIF4A, 4E, and 4G) eIF4F complex release from the cap (7-methylguanosine) structure, resulting in direct inhibition of translation of the target mRNA and a bystander effect that leads to trans-inhibition of translation on otherwise normally unresponsive mRNAs [59]. Among these inhibitors, it has been reported that CHX pretreatment under starvation conditions cannot inhibit the formation of autophagosomes, but can prevent their conversion to degradative autolysosomes [60], although conflicting reports of its effect on autophagy exist [61,62]. However, whether these translation inhibitors can modulate the localization of autophagy master regulators TFEB/TFE3 and whether translation inhibition can affect autophagic pathways require further investigation.

In the present study, I analyzed the impact of translation inhibition using three chemicals (CHX, LTM, RocA) on TFEB localization and autophagy pathways. Such chemical-mediated translation inhibition promoted TFEB dephosphorylation and nuclear translocation. TFEB nuclear localization was modulated by a phosphatase calcineurin but not a kinase mTORC1. In addition, LTM and RocA significantly increased the expression of a number of genes downstream of TFEB required for autophagosome formation, lysosome biogenesis, and lysosome function. Further, I demonstrated that treatment with LTM and RocA facilitated autophagosome biogenesis but prevented degradative autolysosome formation.

## Materials and Methods

### Antibodies and Reagent

The following antibodies were used in this study: rabbit polyclonal anti-GFP (A-11122, Invitrogen, Carlsbad, CA, USA); mouse monoclonal anti-GFP (B-2) (sc-9996), mouse monoclonal anti-pan 14-3-3 (sc-133232) (Santa Cruz Biotechnology, Dallas, TX, USA), rabbit polyclonal anti-TFEB (A303-673A, Bethyl Laboratories, Montgomery, TX, USA), rabbit polyclonal anti-TFEB (MBS9125929, MyBioSource, San Diego, CA, USA), mouse monoclonal anti-phospho-(Ser) 14-3-3 binding motif (#9606), rabbit polyclonal anti-LC3A/B (#4108), rabbit monoclonal anti-mTOR (#2983), rabbit polyclonal anti-phosphoSer2448-mTOR (#2971), rabbit polyclonal anti-p70 S6 kinase (#2971), mouse monoclonal anti-phospho Thr389-p70 S6 kinase (#9206) (Cell Signaling Technology, Danvers, MA, USA), rabbit polyclonal anti-LC3B (L7543), rat monoclonal anti-LAMP1 (1D4B-C), rat monoclonal anti-LAMP2 (ABL-93-C) (Developmental Studies Hybridoma Bank, Iowa City, IA, USA), goat polyclonal anti-Cathepsin B (AF965), goat polyclonal anti-Cathepsin L (AF1515) (R&D Systems, Minneapolis, MN, USA), mouse monoclonal anti- $\beta$ -Actin (A5441) (Sigma-Aldrich, St. Louis, MO, USA), rabbit polyclonal anti-histone H3 (ab1791, Abcam, Cambridge, UK), mouse monoclonal anti-puromycin (MABE343, Merck Millipore, Burlington, MA, USA), peroxidase-conjugated AffiniPure goat anti-rabbit IgG (H + L) (111-035-003), peroxidase-conjugated AffiniPure F(ab')<sub>2</sub> fragment donkey anti-mouse IgG H + L (751-036-151), peroxidase-conjugated AffiniPure rabbit anti-goat IgG (H + L) (305-035-003), peroxidase AffiniPure goat anti-rat IgG (H + L) (112-035-003), Alexa Fluor 594-conjugated AffiniPure F(ab')<sub>2</sub> fragment donkey anti-rabbit IgG (H + L) (711-586-152), Alexa Fluor 594-conjugated AffiniPure F(ab')<sub>2</sub> fragment goat anti-mouse IgG (H + L) (115-586-003), Alexa Fluor 647 AffiniPure F(ab')<sub>2</sub> fragment goat anti-mouse IgG (H + L) (115-606-146) (Jackson Immuno Research Laboratories, Inc, West Grove, PA, USA), goat anti-rabbit Alexa Fluor 488 (A-11034), and goat anti-rat Alexa Fluor 647 (A-21247) (Invitrogen, Carlsbad, CA, USA). Rabbit polyclonal anti-TFE3 was a gift from Professor Hiderou Yoshida, Department of Molecular Biochemistry, Graduate school of Life Science, University of Hyogo, Hyogo, Japan.

The following chemicals were used in this study: cycloheximide (CHX, C-7698, Sigma-Aldrich), rocaglamide A (RocA, 14841) and bafilomycin A1 (Baf A1, 11038) (Cayman Chemical, Michigan, USA), lactimidomycin (LTM, 5.06291.0001, Merck Millipore, Burlington, MA, USA), LysoTracker Red DND-99 (L7528, Thermo Fisher Scientific, Waltham, MA, USA), puromycin (sc-108071) and cyclosporin A (CsA, sc-3503) (Santa Cruz Biotechnology, Dallas, TX, USA), Torin2 (4248, Tocris Bioscience, Bristol, UK), FK506 (Tlr-FK5, InvivoGen, San Diego, CA, USA), 4',6-diamidino-2-phenylindole dihydrochloride (DAPI, D1306), and blasticidin S HCl (R210-01) (Invitrogen, Carlsbad, CA, USA).

### **Construction of Expression Plasmids**

For TFEB-EGFP or EGFP expression, human TFEB fused with the enhanced green fluorescent protein (EGFP) expressing pLUB-hTFEB-EGFP-IRES-Bla or EGFP expressing pLUB-EGFP-IRES-Bla plasmids was constructed. The pLUB-IRES-Bla plasmid was constructed by changing the CMV promoter of pLVX-IRES-Bla with the ubiquitin C promoter of pUB-EGFP (11155, Addgene, Watertown, MA, USA). The Ssp1-EcoRI fragment containing ubiquitin C promoter from pUB-EGFP was inserted into pLVX-IRES-Bla treated with ClaI-Klenow-EcoRI. To construct pLUB-hTFEB-EGFP-IRES-Bla, the NotI-Klenow-EcoRI fragment containing hTFEB-EGFP from pEGFP-N1-TFEB (38119, Addgene, Watertown, MA, USA) was inserted into pLUB-IRES-Bla treated with SmaI-EcoRI. To construct pLUB-EGFP-IRES-Bla, the NotI-Klenow-EcoRI fragment containing EGFP of pEGFP-N1 (#6085-1, Clontech, Takara Bio USA, Inc., San Jose, CA, USA) was inserted into pLUB-IRES-Bla treated with BamHI-Klenow-EcoRI.

To generate a tandem fluorescent reporter expressing mRFP-EGFP-LC3B, pEGFP-LC3B was constructed by inserting the cDNA fragment encoding LC3B from pmRFP-LC3B (21075, Addgene, Watertown, MA, USA) treated with BglII and BamHI into the pEGFP-C1 (6084-1, Clontech Laboratories, San Jose, CA, USA) treated with the same restriction enzymes. The coding sequence fragment of mRFP was amplified from pmRFP-LC3B vector via polymerase chain reaction (PCR) with the following primers: 5'-GAGAGCTAGCGGCCACCATGGCCTCCTCCGAGGAC-3' and 5'-GAGAACCGGTCCACCGCGCCGGTGGAGTGGCG-3'. The tandem fluorescent reporter pmRFP-EGFP-LC3B was constructed by inserting the PCR product of the mRFP sequence treated with NheI and AgeI into pEGFP-LC3B treated with the same restriction enzymes.

### **Establishment of Cell Culture and Cell Line**

Mouse embryonic fibroblast (MEF) cells were described previously [91] and cultured in Dulbecco's modified Eagle's medium (DMEM) supplemented with 10% fetal bovine serum (FBS) (WelGENE, Gyongsan, Korea), 1% penicillin-streptomycin (WelGENE) and 1% non-essential amino acids (WelGENE), as previously described [91]. Immortalized hepatocytes were described previously [64] and grown in Medium 199 (WelGENE) supplemented with 10% FBS (WelGENE) and 1% penicillin-streptomycin (WelGENE). The HeLa cell line was purchased from Korean cell line bank and cultured in MEM Alpha medium (M0894, Sigma-Aldrich, St. Louis, MO, USA) supplemented with 4.4 mg/mL sodium bicarbonate, 10% FBS (WelGENE), and 1% penicillin-streptomycin (WelGENE). All cells were incubated at 37 °C with 5% CO<sub>2</sub>.



To generate TFEB-EGFP or EGFP stably expressing MEF cell lines, lentiviral particles containing pLUB-hTFEB-EGFP-IRES-Bla or pLUB-EGFP-IRES-Bla constructs were produced in Lenti-X-293T cells using LentiX packaging Single Shot Protocol-At-A-Glance Kit (Clontech). Lentivirus production was verified using Lenti-X GoStix™ (Takara Korea Biomedical Inc, Seoul, Korea). MEF cells were transduced with each virus supernatant for 48 h. These infected cells were layered at one cell per well into 96-well cell culture plates via serial dilutions. These cells were cultured in the culture media containing 5 µg/mL blasticidin S HCl (Invitrogen, Carlsbad, CA, USA) for 10 days. The expression of TFEB-EGFP or EGFP was monitored by western blot with anti-GFP antibody and anti-TFEB. Green fluorescence-positive colonies were examined under confocal microscopy using an FV1200-OSR microscope (Olympus, Shinjuku, Japan) as described in the next section. Among several positive clones identified, I selected those that showed high expression of TFEB-EGFP or EGFP and regulated nuclear translocation of TFEB-EGFP upon treatment with well-known autophagy inducers such as Earle's balanced salt solution (EBSS) or Torin2.

### **Immunofluorescences Staining and Confocal Microscopy**

Cells were plated on collagen-coated glass coverslips in 6-well dishes and cultured overnight. These cells were treated with the indicated chemicals for indicated times, followed by rinsing twice with phosphate-buffered saline (PBS). Cells were then fixed with 4% paraformaldehyde in PBS for 15 min, and permeabilized with 0.1% Triton X-100 in PBS for 5 min. For puromycin, TFEB or TFE3 staining, cells were blocked with 3% bovine serum albumin (BSA) in PBS for 1 h and incubated with the indicated primary antibodies overnight at 4 °C. Especially, for TFE3 staining in immortalized hepatocytes, cells were blocked with 2.5% normal horse serum (S-2012, Vector Laboratories, Burlingame, CA, USA) for 1 h and incubated with the primary antibody against TFE3 overnight at 4 °C.

To visualize LC3A/B puncta or the colocalization of punctate LC3A/B and LAMP1, the cells on the coverslip were fixed with 100% methanol for 10 min at -20 °C. These cells were blocked with 3% BSA in PBS containing 0.05% Tween-20 for 1 h and incubated with the indicated primary antibodies overnight at 4 °C.

Cells incubated with the indicated primary antibodies were further incubated with fluorescence-conjugated secondary antibodies for 1 h at room temperature, followed by nuclear staining with DAPI (Invitrogen). Finally, coverslips were mounted on ProLong Gold mounting medium (Invitrogen) and cells were visualized via confocal laser microscopy using a FV1200-OSR microscope (Olympus, Shinjuku, Japan). The puromycin intensity was measured using the mean fluorescence intensity tool in FV10-ASW-4.2 software (Olympus, Shinjuku, Japan). The colocalization of LC3A/B and LAMP1 was measured using Pearson's

correlation coefficient calculator tool in the FV10-ASW-4.2 software (Olympus, Shinjuku, Japan).

For lysosome staining, MEF TFEB-EGFP cells and HeLa cells were plated on collagen-coated 35-mm glass bottom confocal dishes (101,350, SPL Life Science, Pocheon-si, Gyeonggi-do, Korea) at a density of  $1.2 \times 10^5$  cells. On the next day, the cells were treated with the indicated chemicals in a phenol-red free culture medium (DMEM or MEM, GIBCO, Carlsbad, CA, USA) for the indicated times. In the last 30 min of the chemical treatment, 100 nM LysoTracker Red DND-99 (L7528) (Invitrogen, Carlsbad, CA, USA) was added to the cell culture media. The live images of lysosomes were visualized under an FV1200-OSR microscope (Olympus, Shinjuku, Japan). The LysoTracker Red intensity was measured using the mean fluorescence intensity tool in FV10-ASW-4.2 software (Olympus, Shinjuku, Japan).

For the autophagic flux assay using a tandem fluorescent probe, the pmRFP-EGFP-LC3B was transfected into the HeLa cells using Mirus Bio *TransIT*-LT1 transfection reagent (MIR2306, Thermo Fisher Scientific, Waltham, MA, USA) according to the manufacturer's instructions for 30 h, followed by treatment with Torin2, LTM or RocA for the indicated times. These cells were additionally incubated with puromycin (10  $\mu$ g/mL for 10 min) to label actively translating peptides. Cells were then prepared as described above.

### **Immunoblot Analysis**

Cells were lysed in Nondiet P40 lysis buffer (1% NP40, 50 mM Tris-Cl pH 7.5, 150 mM NaCl, 0.05% SDS, 0.5 mM Na-vanadate, 100 mM NaF, 50 mM  $\beta$ -glycerophosphate, and Halt Protease Inhibitor Cocktail (Thermo Fisher Scientific, Waltham, MA, USA). Cell lysates were centrifuged at 13,000 $\times$  *g* for 15 min at 4 °C and supernatants were collected. The protein concentration was determined using Pierce™ BCA Protein Assay Kit (Thermo Fisher Scientific, Waltham, MA, USA). Next, the same amount of protein lysate was subjected to sodium dodecyl sulfate-polyacrylamide gel electrophoresis (SDS-PAGE), followed by transfer to polyvinylidene difluoride or nitrocellulose membranes. The membranes were blocked with 5% non-fat skim milk in 1 $\times$  Tris-Buffered Saline-Tween 20 (0.1% Tween 20, 20 mM Tris-HCl, pH 7.5, and 150 mM NaCl) at room temperature for 1 h. Membranes were incubated with the indicated primary antibodies at 4 °C overnight and then with horseradish peroxidase-conjugated secondary antibodies for 1 h at room temperature. Targeted proteins were visualized with SuperSignal™ West Pico PLUS Chemiluminescent substrate (Thermo Fisher Scientific, Waltham, MA, USA) and detected using an Azure Biosystems C300 (Azure Biosystems, Inc., Dublin, CA, USA).

### **Co-Immunoprecipitation Assay**

TFEB-EGFP expressing MEF (MEF-TFEB-EGFP) cells were plated onto 100 mm culture dishes at a density of  $7 \times 10^5$  cells. The next day, cells were treated with CHX, LTM or RocA for the indicated times. These cells were collected in completed growth media and then washed once with PBS. Cell pellets were dissolved in 250  $\mu$ L immunoprecipitation (IP) lysis buffer (50 mM Tris HCl, pH 7.5, 150 mM NaCl, 1% Triton X-100, 1 mM EDTA) supplemented with half protease and phosphatase inhibitor cocktail at 1 $\times$  final concentration (Thermo Fisher Scientific, Waltham, MA, USA). Lysed cells were passed through a 26 G needle eight times. Cell lysates were incubated on ice for 20 min and centrifuged at 13,000 $\times$  g for 15 min at 4  $^{\circ}$ C to collect soluble fractions. To prepare the antibody-bead complex, 2  $\mu$ g/mL of GFP antibody (Invitrogen, Carlsbad, CA, USA) was rotated with 30  $\mu$ L of slurry containing protein A/G agarose plus beads (Thermo Fisher Scientific, Waltham, MA, USA) in 1 mL of IP binding buffer (50 mM Tris HCl, pH 7.5, 100 mM NaCl, 1 mM EDTA) supplemented with half protease and phosphatase inhibitor cocktail at 1 $\times$  final concentration (Thermo Fisher Scientific, Waltham, MA, USA) for 3 h at 4  $^{\circ}$ C. Then, 1 mg protein lysate was diluted in 1 mL of the IP binding buffer and transferred to the GFP antibody-protein A/G agarose bead complex and incubated under rotation for an additional 3 h at 4  $^{\circ}$ C. After incubation, beads were washed twice in 1 mL of the IP binding buffer. Samples were eluted with 45  $\mu$ L of 1.5 $\times$  SDS sample loading buffer, boiled at 100  $^{\circ}$ C for 5 min, and separated by SDS-PAGE.

### **Subcellular Fractionation**

The MEF-TFEB-EGFP cells were plated on 100 mm culture dishes at a density of  $7 \times 10^5$  cells. The next day, cells were treated with CHX, LTM, or RocA for the indicated times. Cells were collected in the completed growth media, followed by washing once with cold PBS. Cell pellets were lysed in ice-cold hypotonic buffer (10 mM HEPES, 10 mM KCl, 0.1 mM EDTA, 0.5% NP-40, 1 mM DTT, half protease and phosphatase inhibitor cocktail, pH 7.4) for 40 min on ice. Cell lysates were centrifuged at 13,000 $\times$  g for 15 min. Supernatants were collected as cytoplasmic fractions. Cell pellets obtained as nuclear fractions were washed with the hypotonic buffer to completely remove the residual cytoplasmic fractions. The cell pellets were resuspended in nuclear extraction buffer (20 mM HEPES, 400 mM NaCl, 1 mM EDTA, 1 mM DTT, half protease and phosphatase inhibitor cocktail). The protein concentration was measured, and the lysate samples were analyzed using western blot.

### **RNA Isolation and Quantitative Real-Time Polymerase Chain Reaction (qRT-PCR) Analysis**

The total RNAs were isolated from MEF-TFEB-EGFP cells treated with indicated chemicals for indicated time using a QIAzol lysis reagent (QIAGEN, Hilden, Germany). The cDNAs were synthesized with a high-capacity cDNA RT kit (Applied Biosystems, Waltham, CA, USA) for

quantitative polymerase chain reaction (qPCR). The qPCRs were carried out with a TOPreal™ qPCR 2X PreMIX (SYBR Green with High ROX) (RT501M, Enzynomics, Daejeon, Korea) using a StepOnePlus Real Time System (Applied Biosystems, Waltham, CA, USA). The specificity of each primer pair was confirmed using the melting curve analysis. The copy number relative to  $\beta$ -actin mRNA was calculated as previously described [92]. Primer sequences are presented in Table 1.

### **Statistical Analysis**

All data are presented as means  $\pm$  SEM. The data were analyzed using GraphPad Prism 5 (GraphPad Software, San Diego, CA, USA). The statistical significance of differences between groups was evaluated via the unpaired two-tailed Student's *t*-tests and  $p < 0.05$  was considered statistically significant.

**Table 1. List of primers for qPCR**

<b>Gene</b>	<b>Species</b>	<b>Forward primer (5' to 3')</b>	<b>Reverse primer (5' to 3')</b>
<b>ATG5</b>	<b>Mouse</b>	CCAGGTGATGATTCACGG	GGCTGGGGGACAATGCTAA
<b>ATG12</b>	<b>Mouse</b>	GGAGACACTCCTATAATGAAA	ATAAATAAACAACTGTTCCGA
<b>LC3B</b>	<b>Mouse</b>	CGTCCTGGACAAGACCAAGT	ACCATCTACAGGAAGCCGTC
<b>P62</b>	<b>Mouse</b>	GCTGCCCTATACCCACATCT	CGCCTTCATCCGAGAAAC
<b>ATP6V1H</b>	<b>Mouse</b>	GGATGCTGCTGTCCCAACTAA	TCTCTTGCTTGCTCCTCGGAAC
<b>Cathepsin B (CTB)</b>	<b>Mouse</b>	ACAGTGCCACACAGCTTCTTC	TCCTTGATCCTTCTTTCTTGCC
<b>HEXAB</b>	<b>Mouse</b>	CTGGTGTGCTAGTGTGCGC	CAGGGCCATGATGTCTCTTGT
<b>LAMP1</b>	<b>Mouse</b>	ACCTGTGCGAGTGGCAACTTCA	GGGCACAAGTGGTGGTGAG
<b>MCOLN1</b>	<b>Mouse</b>	GCTGGGTTACTCTGATGGGTC	CCACCACGGACATAGGCATAC
<b>TPP1</b>	<b>Mouse</b>	CCCCTCATGTGGATTTTGTGG	TGGTTCTGGACGTTGTCTTGG
<b>UVRAG</b>	<b>Mouse</b>	CAAGCTGACAGAAAAGGAGCGAG	GGAAGAGTTTGCCTCAAGTCTGG
<b>mTFEB</b>	<b>Mouse</b>	CCTGCCGACCTGACTCAGA	CTCAATTAGGTTGTGATTGTCTTTCTTC
<b>hTFEB</b>	<b>Human</b>	ACCTGTCCGAGACCTATGGG	CGTCCAGACGCATAATGTTGTC
<b>mTFE3</b>	<b>Mouse</b>	CCTGAAGGCATCTGTGGATT	TGTAGGTCCAGAAGGGCATC
<b><math>\beta</math>-actin</b>	<b>Mouse</b>	GATCTGGCACCACACCTTCT	GGGGTGTGAAGGTCTCAA

## Results

### **Glutarimide-Containing Ribosome Inhibitors and eIF4A Helicase Inhibitor-Mediated Translation Inhibition Induce Transcription Factor EB (TFEB) and Transcription Factor E3 (TFE3) Nuclear Translocation**

To analyze changes in TFEB cellular localization under diverse experimental conditions, I established a mouse embryonic fibroblast (MEF) cell line expressing a human TFEB-fused enhanced green fluorescent protein (EGFP) at the C-terminal and a control MEF cell line expressing EGFP only (Figure 1A,B). As it is known that most endogenous TFEB is observed in the cytoplasm before activation [23,24]. The results showed that TFEB-EGFP was mainly localized in the cytoplasm, whereas EGFP alone was distributed in the cell under basal conditions (Figure 1A). Next, I determined whether TFEB-EGFP nuclear translocation can be induced by starvation or mechanistic target of rapamycin complex 1 (mTORC1) inhibition in the established MEF-TFEB-EGFP cell line. As reported previously [23,24,28,36], most cells carried nuclear translocated TFEB-EGFP in both EBSS-mediated starvation (Figure 1C,D) and Torin-2-mediated mTORC1 inhibition (Figure 1F,G) conditions. In addition, this change in subcellular localization under starvation or mTORC1 inhibition is paralleled by TFEB dephosphorylation [33–35]. Therefore, similar to previous reports [33–35], inhibition of mTORC1 by treatment with starvation or Torin2 altered the electrophoretic mobility of TFEB-EGFP including endogenous TFEB, which appeared as fast-migrating forms (Figure 1E,H). Based on these results, the established MEF-TFEB-EGFP cell line can be used as a reporter cell line to monitor TFEB subcellular localization.

Next, I determined whether the inhibition of protein synthesis induced TFEB nuclear translocation in the MEF cell line, by treating MEF-TFEB-EGFP cell lines with glutarimide-containing natural products cycloheximide (CHX) and lactimidomycin (LTM) in a dose (Figure 2A–D) and time (Figure 3A,B,D,E) dependent manner, respectively. To assess the impact of the inhibitors on translation, I performed puromycin labeling, followed by immunofluorescence using an antibody against puromycin in cells treated with or without inhibitors (Figure 3A,D and Figure 2A,C). Fluorescence intensities of puromycylated nascent peptides were strong in cells treated without CHX. The intensity was significantly reduced by CHX in a dose-dependent manner. It declined eventually to ~20% by treatment with 50 µg/ml CHX, suggesting that the working concentration range of CHX was sufficient to observe its inhibitory effect on cellular translation (Figure 2A,B). Under similar treatment conditions of CHX, a green fluorescence signal of EGFP was observed to determine the subcellular localization of TFEB-EGFP. The CHX treatment at the lowest concentration (2 µg/mL) for 4 h even induced nuclear translocation of TFEB-EGFP in almost 80% of cells (Figure 2A,B) although a minor fluorescence signal of TFEB-EGFP was still observed in the cytoplasm. However, the increase

in CHX concentration to 50  $\mu\text{g}/\text{mL}$  resulted in the nuclear translocation of almost all TFEB-EGFP proteins (Figure 2A,B). Next, in a time-course experiment, the nuclear translocation of TFEB-EGFP in approximately 55% of MEF-TFEB-EGFP cells occurred at 1 h after treatment with CHX 50  $\mu\text{g}/\text{mL}$  (Figure 3A). The percentage of MEF-TFEB-EGFP cells carrying nuclear TFEB-EGFP reached nearly 100% at 8 h after treatment (Figure 3A,D). To validate these results, I performed a subcellular fractionation analysis using MEF-TFEB-EGFP cells. As expected, I found that the amount of TFEB-EGFP in the nuclear fraction increased upon treatment with CHX (Figure 3G). Furthermore, I observed the augmented nuclear accumulation of endogenous TFEB in response to the CHX treatment (Figure 3G). CHX can bind to the E-site of the 60S ribosome together with deacylated tRNA, resulting in the freezing of all translating ribosomes in the mRNAs [47,56,63]. Therefore, I tested another translocation inhibitor lactimidomycin (LTM). It is known to preferentially act on initiating ribosomes, but not on elongating ribosomes. Thus, its addition to cells can lead to polysome disassembly [47,56,63]. Different doses (100, 250, 500, and 1000 nM for 4 h) of LTM clearly showed its translational inhibitory effects (Figure 2C,D). In addition, LTM treatment induced the nuclear translocation of TFEB-EGFP in more than 90% of the cells under all tested concentrations (Figure 2C,D). Next, similar to the time-dependent experiment of CHX, the maximal nuclear translocation of TFEB-EGFP (around 100%) occurred at 8 h after MEF-TFEB-EGFP cells were treated with LTM 500 nM (Figure 3B,E). Finally, the subcellular fractionation analysis confirmed the augmented nuclear accumulation of TFEB-EGFP and endogenous TFEB following the LTM treatment (Figure 3H).

Although CHX and LTM are specific inhibitors of protein synthesis blocking the ribosome at the translocation stage, this study cannot exclude the possibility that TFEB and TFE3 nuclear translocation might be induced as an unknown side effect. Therefore, a different type of translation inhibitor RocA with distinct mechanism of action was selected to reproduce that observation. RocA, an inhibitor of eukaryotic initiation factor 4A (eIF4A), preferentially represses translation by clamping eIF4A onto purine-rich regions within mRNA 5' leaders. It then interferes with the scanning of 43S pre-initiation complexes (PICs) [57,58]. Furthermore, a recent report suggested that RocA can interfere with the release eIF4F complex from the cap structure to inhibit the translation of the target mRNA. It exerts a bystander effect on translation initiation by sequestering eIF4F, leading to trans-inhibition of translation on otherwise normally unresponsive mRNAs [59]. Therefore, RocA also acts as a general translation inhibitor similar to CHX and LTM.

First, in dose-dependent experiments (0.5, 1, and 3  $\mu\text{M}$  for 4 h) RocA clearly showed its translational inhibitory effect (Figure 2E,F). As expected, RocA treatment gradually increased the nuclear translocation of TFEB-EGFP in a dose-dependent manner. RocA treatment (3  $\mu\text{M}$  for 4 h) induced TFEB-EGFP nuclear translocation of  $\sim 77\%$  of cells (Figure 2E,F). Next, a time

course experiment showed that RocA treatment (3  $\mu$ M for 16 h) induced nuclear translocation of TFEB-EGFP in almost 100% of cells (Figure 3C,F), suggesting that RocA was also a strong inducer of TFEB nuclear translocation although additional time was needed to attain the maximal level of TFEB nuclear translocation compared with CHX or LTM. Finally, a subcellular fractionation analysis confirmed augmented nuclear accumulation of TFEB-EGFP and endogenous TFEB following RocA treatment (Figure 3I). These results indicate that translation inhibition may induce nuclear translocation of TFEB, a master regulator of lysosome biogenesis and autophagy.

To exclude the nuclear translocation of TFEB in response to three translation inhibitors as a cell type-specific event, I assessed endogenous TFEB nuclear translocation in both mouse immortalized hepatocytes and human HeLa cells [64]. In agreement with results of the MEF-TFEB-EGFP cell line, both immortalized hepatocytes and human HeLa cells showed almost 100% of nuclear translocation upon treatment with CHX, LTM or RocA for 8 h, whereas less than 30% of cells showed accumulation of TFEB in the nucleus under normal conditions (Figure 4A,B). TFEB belongs to the MiT family of helix-loop-helix leucine zipper transcription factors, together with TFE3, MITF and TFEC [23,24]. Therefore, the regulatory mechanism of TFEB is shared by TFE3 [23,24,32] and TFEB and TFE3 play a cooperative role as needed [65,66]. Therefore, I asked whether TFE3 can also be translocated to the nucleus in both immortalized hepatocytes and human HeLa cells treated with a translation inhibitor CHX, LTM, or RocA. As expected, similar to TFEB, TFE3 was also efficiently translocated into the nucleus in both immortalized hepatocytes and human HeLa cells treated with CHX, LTM or RocA for 8 h (Figure 4C,D). Together, these results suggest that translation inhibition might induce the nuclear translocation of both TFEB and TFE3 via a common regulatory mechanism conserved in different cell types and species.

### **Translation Inhibitors Induce TFEB Dephosphorylation and 14-3-3 Dissociation**

It has been proposed that the cellular localization and activity of TFEB are mainly controlled by its phosphorylation status [23,29,31] although other phosphorylation-independent mechanisms (such as SUMOylation, acetylation, and glucosylation) have also been reported [67–70]. Multiple studies have reported that TFEB migration on the protein gel is affected by its phosphorylation status [29,34,42]. Therefore, to assess the TFEB phosphorylation level indirectly, I analyzed changes in the electrophoretic mobility of both TFEB-EGFP and endogenous TFEB in CHX-, LTM-, RocA-, or Torin2-treated MEF-TFEB-EGFP cells. Torin2 treatment resulted in a rapid downshift in both TFEB-EGFP and TFEB migration. They were predominantly found in a fast-migrating form(s) in MEF-TFEB-EGFP cell lysates (Figure 5A). Treatment with CHX, LTM, or RocA led to a progressive shift in both TFEB-EGFP and



endogenous TFEB bands to fast-migrating forms (arrows at left and right sides of the figures) in cell lysates under increased treatment times (Figure 5A–C). During the last time point (16 h) of inhibitor treatment, the fast-migrating TFEB-EGFP and endogenous TFEB bands (arrows) appeared to carry similar molecular weight compared with bands of Torin2 treatment, suggesting that CHX, LTM, and RocA induced TFEB activation via dephosphorylation, an effect analogous to that caused by Torin1 [29,42]. To substantiate these observations, I investigated whether TFEB phosphorylation at a specific site was affected by treatment with CHX, LTM, or RocA. Among 11 known phosphorylation sites of human TFEB [31,71], under normal nutrient conditions, mTORC1 phosphorylates TFEB at serine 211. This phosphorylation promotes the binding of TFEB to the chaperone 14-3-3 and retention of the transcription factor in the cytosol [23,31]. Therefore, I tested whether treatment with CHX, LTM, and RocA decreased the phosphorylation of TFEB-EGFP at Ser211 leading to the dissociation of 14-3-3 from the TFEB-EGFP/14-3-3 complex in MEF-TFEB-EGFP cells. TFEB-EGFP was immunoprecipitated with an anti-GFP antibody. TFEB-EGFP immunoprecipitates were used to determine the phosphorylation level of TFEB-EGFP at Ser211 and the TFEB-EGFP/14-3-3 complex. As expected, band intensities of p-TFEB-EGFP at Ser211 identified by immunoblotting with anti-phospho-(Ser) 14-3-3 binding motif antibody in TFEB-EGFP immunoprecipitates was markedly reduced by treatment with CHX, LTM, or RocA although these changes were not stronger than those induced by Torin2 (Figure 5D–F). Consistently, the band intensities of 14-3-3 proteins identified by immunoblotting with anti-14-3-3 antibody in TFEB immunoprecipitates were also markedly reduced by CHX, LTM, or RocA treatment, although these changes were not stronger than those induced by Torin2 (Figure 5D–F). Thus, the increased nuclear translocation of TFEB and TFE3 illustrated in Figures 3 and 5 was likely due to dephosphorylation and dissociation of the 14-3-3 from the TFEB (or TFE3)/14-3-3 complex upon treatment with translation inhibitors.

### **Translation Inhibition-Mediated TFEB Nuclear Localization Is Modulated by Calcineurin, not mTORC1**

The phosphorylation status of TFEB is regulated by multiple kinases including mTORC1 and phosphatase calcineurin [23,31,38,42,71]. As shown in Figure 6D–F, inhibitor treatments reduced TFEB phosphorylation at serine 211, a target site of mTORC1 [5,33,72]. Therefore, I first investigated mTOR activation and its level. However, levels of mTOR phosphorylation (S2448) and mTOR were unchanged at all time points in cell lysates exposed to translation inhibitors, whereas the Torin2 treatment strongly reduced mTOR phosphorylation (Figure 6A–C). By contrast, phosphorylation (T389) of the mTOR target p70/S6 kinase was increased by CHX, LTM, or RocA treatment at all time points, whereas its phosphorylation was drastically inhibited by Torin2 treatment (Figure 6A–C). These results suggest that dephosphorylation-

mediated TFEB and TFE3 nuclear translocation in cells treated with translation inhibitors might not involve mTOR. Next, I assessed whether inhibition of the phosphatase calcineurin can block TFEB nuclear translocation in translation inhibitor-treated MEF-TFEB-EGFP cells. For this, cells treated with CHX, LTM, or RocA were co-treated with both calcineurin inhibitors FK506 and cyclosporin A (CsA) for 4 h. As seen in Figure 6D–F, the translocation of TFEB-EGFP to the nucleus upon treatment with translation inhibitors was significantly reduced in the presence of calcineurin inhibitors, indicating that calcineurin may play an important role in the regulation of TFEB dephosphorylation and nuclear translocation in response to translation inhibition. However, it is important to note that inhibition of calcineurin did not completely abrogate the nuclear translocation of TFEB although it was significantly reduced by calcineurin inhibitors. Therefore, additional and unidentified factors might mediate TFEB dephosphorylation and nuclear translocation following treatment with translation inhibitors.

### **Translation Inhibition-Mediated TFEB Nuclear Localization Stimulates Autophagy-Related Gene Expression and Autophagosome Formation without New Protein Synthesis**

I next assessed whether LTM and RocA-induced TFEB/TFE3 nuclear translocation upregulated the transcription of autophagy-related genes. MEF-TFEB-EGFP cells were treated with LTM for 8 h or RocA for 8 and 16 h. Following 8 h of treatment, both inhibitors induced nuclear translocation of more than 80% TFEB and drastic translation inhibition (Figure 3B,C,E,F). Under the same conditions, LTM and RocA significantly increased the transcription of several autophagy genes and lysosomal genes downstream of TFEB/TFE3 in MEF-TFEB-EGFP cells (Figure 7A,B), suggesting that translation inhibition induces transcription of autophagy-related genes without new protein synthesis.

Although the results were observed a significant transcriptional increase in translation inhibition-mediated autophagy-related genes in LTM and RocA-treated cells, it did not indicate activation of autophagic pathways, such as autophagosome formation. Therefore, to assess whether translation inhibition can promote autophagy, an autophagosome marker protein microtubule-associated proteins 1 light chain 3B (hereafter referred to as LC3B) was analyzed. The conversion of LC3B(I) to LC3B(II), a key molecule involved in autophagosome, is a key event in autophagosome formation [6]. As shown in Figure 7C,D, in line with dephosphorylation (arrows at left and right sides of the figures) of TFEB and TFEB-EGFP, following conversion of LC3B(I) to LC3B(II) in cells treated with LTM or RocA, levels of LC3B(II) were significantly increased in a time-dependent manner. Further, to directly monitor the possible impact of translation inhibitors on autophagosome formation, I visualized the presence of LC3A/B-positive puncta in LTM or RocA-treated cells (Figure 7E,F). As shown in

Figure 7E,F, a marked increase in the number of LC3A/B-positive autophagic puncta in cells treated with LTM or RocA was observed. Together, these results indicate that translation inhibition may not only activate TFEB/TFE3, but also may stimulate autophagosome formation without new protein synthesis.

### **Translation Inhibitors Prevent Degradative Autolysosome Formation**

Increased levels of LC3B(II) proteins and LC3A/B-positive autophagosomes following LTM and RocA treatment represent either autophagy activation or suppression of late steps in the autophagy pathway [5,72]. To ascertain whether the changes were caused by an increasing autophagic flux, I investigated the LC3B(II) and p62(SQSTM1) accumulation in cells incubated with bafilomycin A1 (Baf A1, 200 nM for 3 h before harvest), a specific inhibitor of vacuolar H<sup>+</sup>-ATPases and a blocker of autophagosome-lysosome fusion [18,72]. During autophagic flux, active LC3B(II) and p62 proteins accumulate upon Baf A1 treatment [73]. In the absence of treatment with translation inhibitors, the levels of both LC3(II) and p62 proteins were increased by Baf A1 as expected (Figure 8A,B, lanes 1 vs. 4), indicating an active autophagic flux. However, with LTM treatment, Baf A1 failed to induce LC3B(II) and p62 accumulation (Figure 8A, lanes 2, 3 vs. 5, 6), whereas RocA treatment induced their accumulation except for LC3B(II) at 16 h (Figure 8B, lanes 2, 3 vs. 5, 6). Thus, the autophagic flux assay using Baf A1 did not clearly indicate whether LTM or RocA-induced translation inhibition increased autophagic flux. In addition, it is possible that strong translation inhibition and ubiquitin-proteasome pathway-mediated degradation [74,75] may prevent accumulation of both LC3(II) and p62 proteins in the assay conditions using the combination of both translation inhibitors and Baf A1.

Therefore, I next performed a different autophagic flux assay using an mRFP-GFP-LC3 tandem fluorescent probe [72,73]. HeLa cells were transfected with the mRFP-EGFP-LC3 construct and then treated with indicated compounds. At first, LTM and RocA-mediated translation inhibition was monitored by immunofluorescence of puromycylated proteins. A tandem fluorescent-tagged reporter was then used to monitor the autophagic flux, including the autophagosome synthesis and autophagosome-lysosome fusion. Autophagosomes appeared yellow (with green and red) and autolysosomes appeared as red vesicles since EGFP was quenched in acidic environments. However, mRFP is relatively stable. It can show fluorescence even in an acidic pH found in lysosomes [76,77]. As expected, Torin2 treatment increased the number of autolysosomes (mRFP<sup>+</sup>EGFP<sup>-</sup> LC3B puncta) but reduced autophagosomes (mRFP<sup>+</sup>EGFP<sup>+</sup> LC3B puncta) (left panels and graph in Figure 8C), suggesting that the autophagic flux was significantly activated by mTORC1 inhibition. However, following LTM or RocA treatment, which induced strong translation inhibition at 8 and 16 h (puromycin of Figure 8C), the number of autolysosomes (mRFP<sup>+</sup>EGFP<sup>-</sup> LC3B

puncta) was not increased although the number of autophagosomes (mRFP<sup>+</sup>EGFP<sup>+</sup> LC3B puncta) was increased (right panels and graphs of Figure 8C), indicating possible defects in the autophagic flux.

To determine which step in the autophagic flux was inhibited upon treatment with LTM or RocA, I first evaluated the fusion of autophagosomes with lysosomes, which is an important stage in the autophagic flux. Autophagosome-lysosome fusion can be detected via colocalization of LC3 and lysosomal-associated membrane protein 1 (LAMP1) [5,72]. I performed immunostaining of LC3A/B and LAMP1 and quantified the colocalization of LC3A/B and LAMP1 in LTM- or RocA-treated MEF-TFEB-EGFP cells. However, intriguingly, I found that the colocalization of LC3A/B and LAMP1 was significantly increased in LTM- or RocA-treated cells following the nuclear translocation of TFEB-EGFP when incubation time was increased (Figure 9A,B), indicating the fusion of autophagosomes with endosomes and/or lysosomes at least. However, the late steps of the autophagic process to maintain the functional autophagic flux includes autolysosome acidification as well as autophagosome-lysosome fusion to form degradative autolysosomes [5,18]. Autolysosome acidification requires active lysosomes independent of autophagosome-lysosome fusion [18]. In addition, the results of autophagic flux assay using tandem fluorescent-tagged LC3 (mRFP-EGFP-LC3) suggested that LTM or RocA treatment did not increase the number of acidic autolysosomes (Figure 8C). Therefore, I asked whether LTM or RocA treatment affected lysosomal acidification and lysosomal protein levels. In Torin2-treated cells, the induction of autophagy resulted in the nuclear translocation of TFEB-EGFP and increased autophagic vesicles strongly labeled with LysoTracker, a dye known to accumulate in acidic vesicles (Figure 9C and Figure 8D). However, LTM or RocA treatment significantly reduced the number and intensity of LysoTracker-positive structures in both MEF-TFEB-EGFP cells (Figure 9C) and HeLa cells (Figure 8D), suggesting that the translation inhibition disrupted lysosomal acidity and reduced the number of functional lysosomes. Further, I found that LTM or RocA treatment strongly reduced the expression of cysteine cathepsins B and L (CtsB/L) known to be major lysosomal proteases, whereas LAMP1 and LAMP2 as major protein constituents of the lysosomal membrane, were not significantly changed (Figure 9D,E). Thus, these findings suggest that LTM- or RocA-mediated translation inhibition induces autophagic vesicle (AV) formation but prevents degradative autolysosome formation.

Here I analyzed the effects of three different translation inhibitors on the activation of the autophagy master transcriptional regulators TFEB/TFE3 and autophagic pathways. The translation inhibitors induced the nuclear translocation of both TFEB and TFE3 in human and mouse cells. Their translocation was related to translation inhibition-mediated dephosphorylation and 14-3-3 dissociation. However, TFEB dephosphorylation did not occur

via mTORC1 inhibition, but via activation of calcineurin and/or other phosphatases in cells treated with translation inhibitors. Surprisingly, LTM and RocA strongly stimulated the expression of several autophagic and lysosomal genes without a new protein synthesis. In addition, I observed that LTM and RocA promoted autophagosome formation. However, the translation inhibition prevented the degradative autolysosome formation and induced lysosomal dysfunction. Therefore, translation inhibition might be one of the components of TFEB/TFE3 activation although it eventually induces dysfunction of autophagosome maturation probably because of inhibition of protein synthesis (Figure 10).

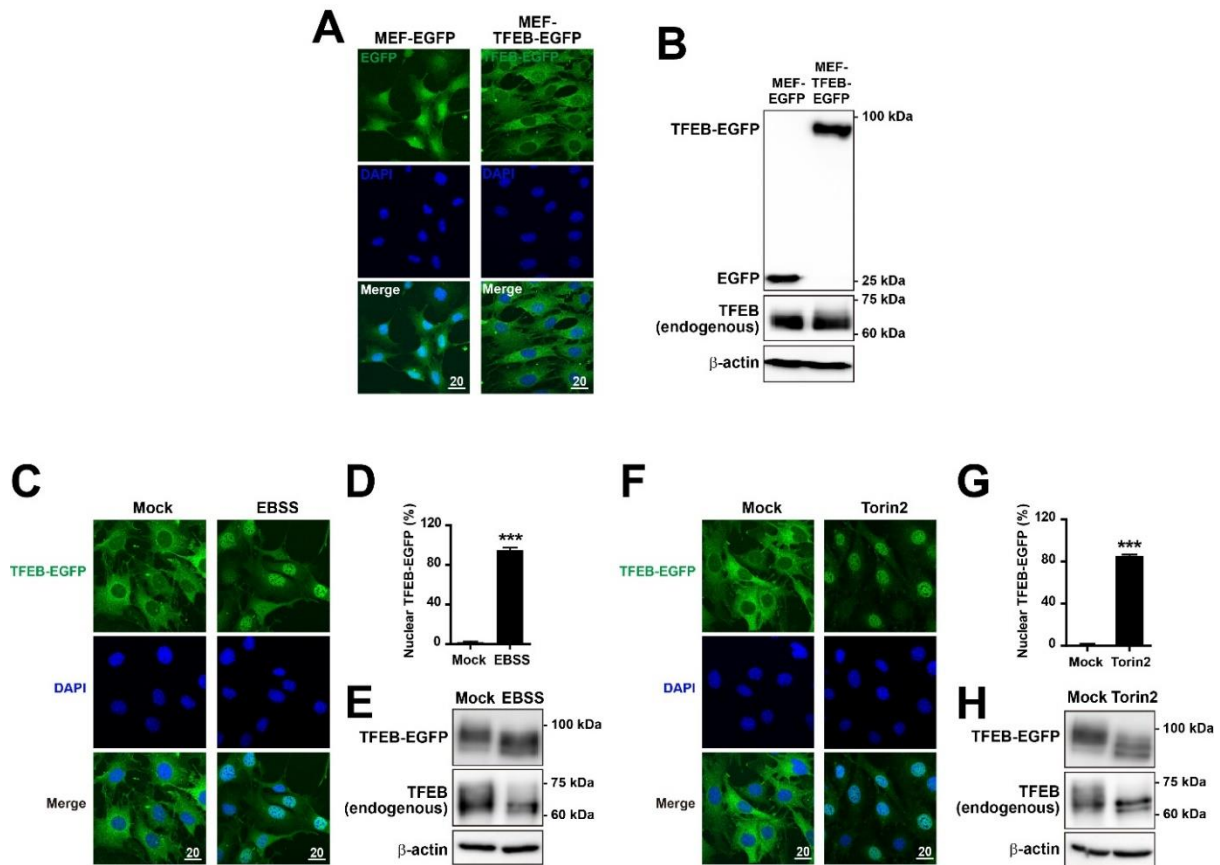
## Discussion

Among 370 inhibitors of eukaryotic protein synthesis have been reported [47], I used three translation inhibitors (CHX, LTM, and RocA) with distinct inhibitory mechanisms to analyze the effect of translation inhibition on the regulation of TFEB activity and autophagy. All three translation inhibitors acted similarly on TFEB and TFE3 activation and autophagic processes. Inhibitor treatments triggered TFEB nuclear translocation at 1 h when translation inhibition was less than 60%, indicating a rapid molecular mechanism(s) without new protein synthesis. I thought that calcium, a ubiquitous second messenger, was a candidate mediator because its level can be rapidly changed to regulate the activities of multiple enzymes including calcineurin phosphatase [82]. In addition, the activation of calcineurin can promote the nuclear translocation of TFEB and TFE3 [38,80,81]. As expected, the results showed that calcineurin inhibitors (FK506 and CsA) reduced translation inhibitor-mediated TFEB nuclear translocation, although their inhibitory effect was not complete, whereas no mTOR inhibition was observed (Figure 7A–F). However, the mechanism of the activation of calcium-dependent calcineurin upon translation inhibition is unknown. Several studies have suggested that the ER, lysosome, and mitochondria are sources of calcium, which can activate phosphatases including calcineurin responsible for TFEB/TFE3 activation [38,40,80,81]. Interestingly, previous studies have reported that puromycin, another translation inhibitor, can inhibit peptidyl transfer on ribosomes, causing ER calcium leakage via Sec61 translocon [78,79]. In addition, I observed that puromycin also promoted the nuclear translocation of TFEB [83]. Overall, these findings suggest that calcium is an important mediator of translation inhibition-mediated TFEB/TFE3 activation. However, further studies are needed to determine the cellular organelles and molecular mechanism involved in calcium release and to identify phosphatases including calcineurin responsible for TFEB/TFE3 activation upon translation inhibition.

Recent studies have suggested that subcellular localization of TFEB can be determined via regulation of the TFEB nuclear export, because it continuously shuttles between the cytosol and nucleus via the CRM1-dependent nuclear export under normal conditions [29,30,32]. Among those studies, Yin et al. [32] suggested that cyclin D-dependent kinases 4/6 (CDK4/6) can interact with and phosphorylate TFEB on serine 142 and TFE3 on serine 246 in the nucleus, resulting in their inactivation and cytoplasmic translocation. Therefore, CDK4/6 inhibition can induce TFEB/TFE3 nuclear translocation, thereby activating TFEB/TFE3-dependent autophagic pathways including autophagic gene expression and lysosome biogenesis [32]. Interestingly, multiple reports have shown that CHX treatment can reduce the expression of cyclin D1 [84–86], a well-known cell cycle regulator which dimerizes with CDK4/6 and facilitates to pass through the G1 phase by inhibiting the retinoblastoma protein [87,88]. The cyclin D level can be reduced by inhibiting its transcription and translation,

and even inducing proteasome- and autophagy-mediated degradation [84,85,89,90]. However, under my experimental conditions, translational inhibition and proteasome-mediated degradation were the most plausible mechanisms underlying decreased cyclin D because the inhibition of protein synthesis disrupted the last step (degradative autolysosome formation) of autophagy and pre-emptively nullified the possible effect of reduced cyclin D1 transcription. Therefore, it is possible that translation inhibition-mediated cyclin D reduction inhibits CDK4/6 activity in the nucleus, thereby activating TFEB/TFE3 (Figure 10). These possible mechanisms are under investigation now.

In previous studies investigating the effect of CHX pre-treatment on autophagic pathways, no nascent autophagic vesicles has been found to be cathepsin-D positive, suggesting that the CHX-mediated inhibition of protein synthesis does not inhibit the initial formation of autophagosomes, but interferes with a later stage in autophagosome maturation such as autophagosome-lysosome fusion [60]. In this study, I observed that LTM and RocA treatments increased LC3B(II) protein level and LC3A/B-positive autophagic puncta, indicating that LTM and RocA activated the formation of autophagosomes. However, similar to the CHX effect [59], LTM or RocA-mediated translation inhibition impaired the autophagic flux. LTM or RocA treatment resulted in an increase in LC3A/B and LAMP1-double positive autophagic puncta, without increasing mRFP positive and EGFP negative LC3B autophagic puncta, indicating that LTM and RocA-mediated translation inhibition prevented degradative autolysosome formation in autophagosome maturation. Accordingly, treatment with LTM and RocA reduced the number of functional lysosomes by disrupting lysosomal acidity and substantially reducing the expression of major lysosomal proteases CtsB and CtsL. In addition, Mauvezin et al. suggested that, although non-functional lysosomes such as V-ATPase-deficient lysosomes can fuse with autophagosomes, they prevent degradative autolysosome formation [18]. Therefore, it is possible to generate non-functional autolysosomes via fusion between autophagosomes and non-functional lysosomes in LTM or RocA-treated cells (Figure 10).

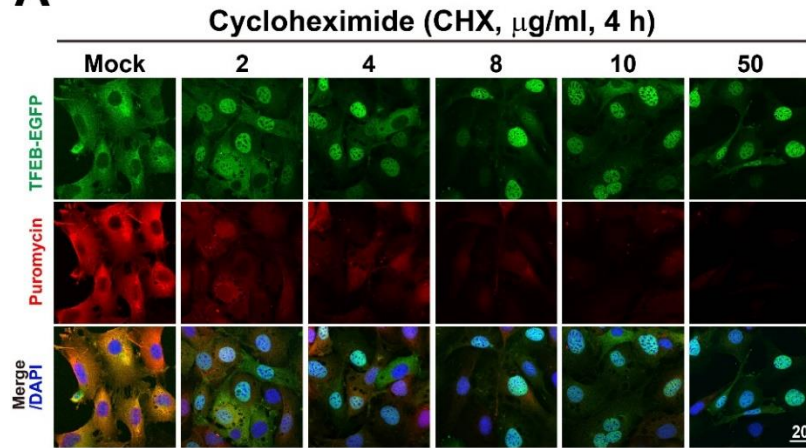
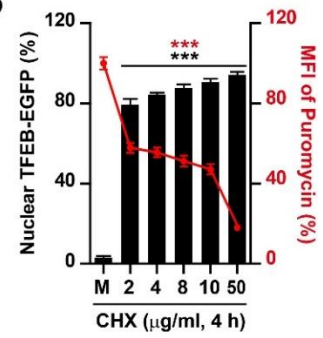
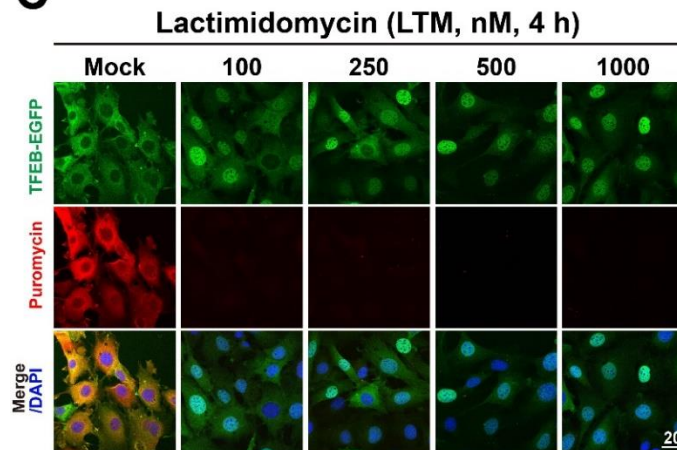
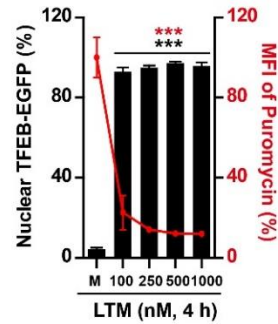
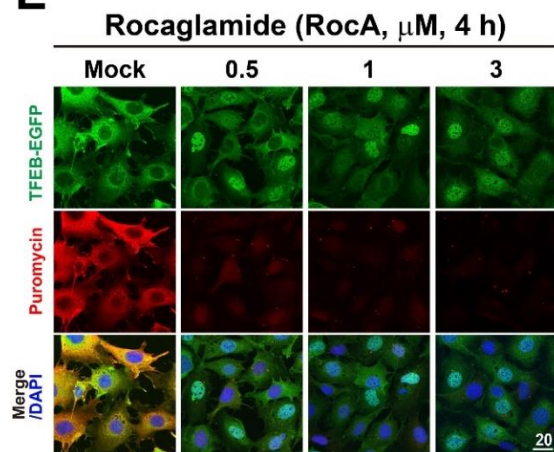
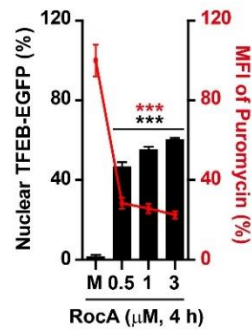


**Figure 1. Establishment of an MEF cell line stably expressing TFEB-EGFP.**

**(A)** EGFP or TFEB-EGFP expressing MEF cells were transduced with lentiviral particles containing pLUB-EGFP-IRES-Bla or pLUB-hTFEB-EGFP-IRES-Bla constructs, followed by blasticidin selection. From the selected cell lines, cells were fixed and stained with DAPI (blue) for nucleus DNA. Cellular localization of EGFP or TFEB-EGFP was indicated by green fluorescence in the cells. Scale bar, 20  $\mu$ m. **(B)** Immunoblot analysis of total cellular lysates from MEF cells stably expressing EGFP or TFEB-EGFP using the antibodies against GFP to detect TFEB-EGFP and EGFP combined, TFEB (used to detect endogenous TFEB), or  $\beta$ -actin. **(C,F)** Representative images of confocal microscopic analysis. TFEB-EGFP-expressing MEF (MEF-TFEB-EGFP) cells were starved with Earle's balanced salt solution (EBSS) (C) or treated with Torin2 (100 nM) (F) for 4 h. Cells were fixed and stained with DAPI (blue) for DNA. Cellular localization of TFEB-EGFP was indicated by green fluorescence signals in the cells. Scale bar, 20  $\mu$ m. **(D,G)** Quantification of the percentage of MEF-TFEB-EGFP cells with nuclear TFEB-EGFP treated with EBSS or Torin2 as indicated in (C) and (F). Data are expressed as mean  $\pm$  SEM of at least 150 cells from six random fields in each group. \*\*\* $p < 0.001$ ; Mock vs. EBSS or Torin2. **(E,H)** MEF-TFEB-EGFP cells were treated with EBSS (C), Torin2 (F) for 4 h. Total cellular lysates were separated via 6% SDS-PAGE and then analyzed

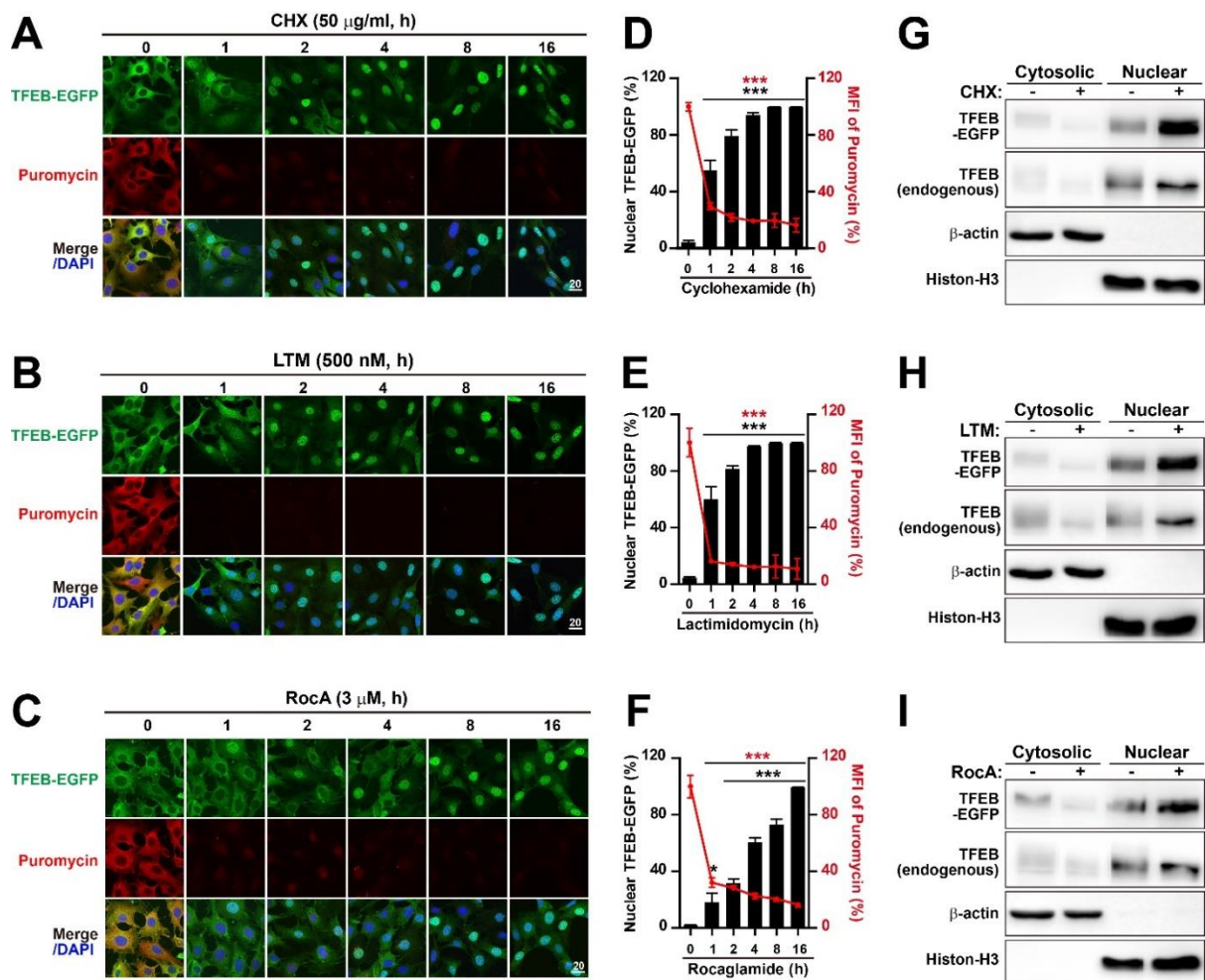


by immunoblotting with antibodies against GFP (for TFEB-EGFP), TFEB (for endogenous TFEB), or  $\beta$ -actin.

**A****B****C****D****E****F**

**Figure 2. Translation inhibition by cycloheximide (CHX), lactimidomycin (LTM) and rocaglamide A (RocA) induces TFEB nuclear translocation in a dose-dependent manner.**

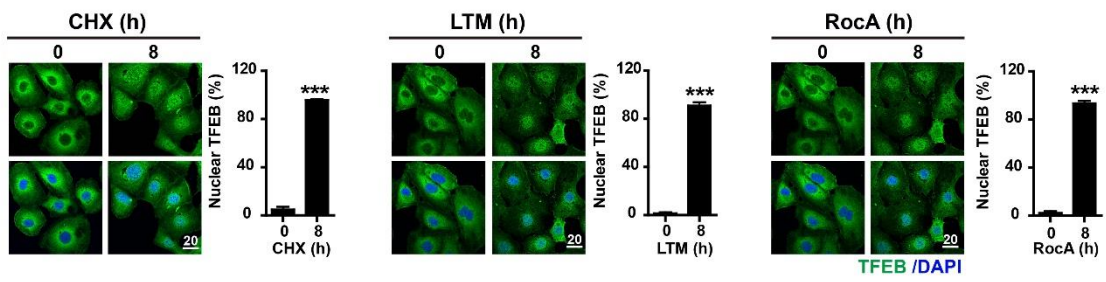
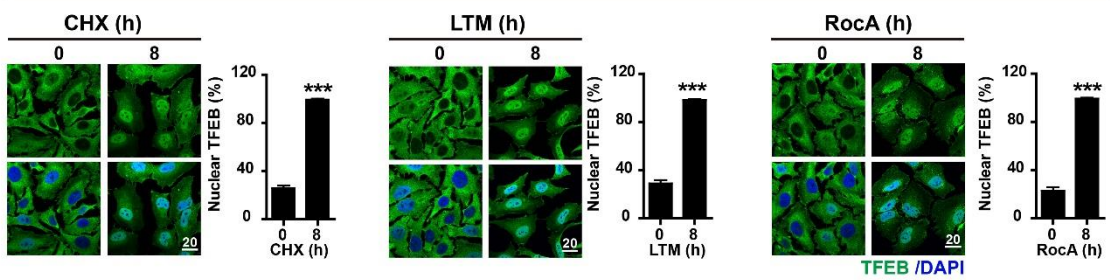
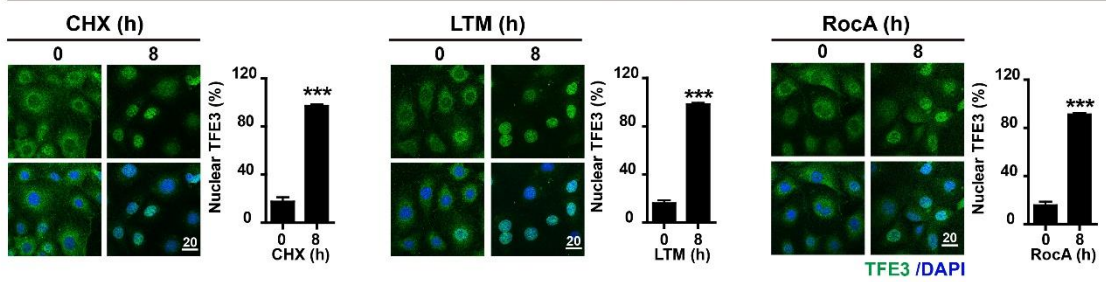
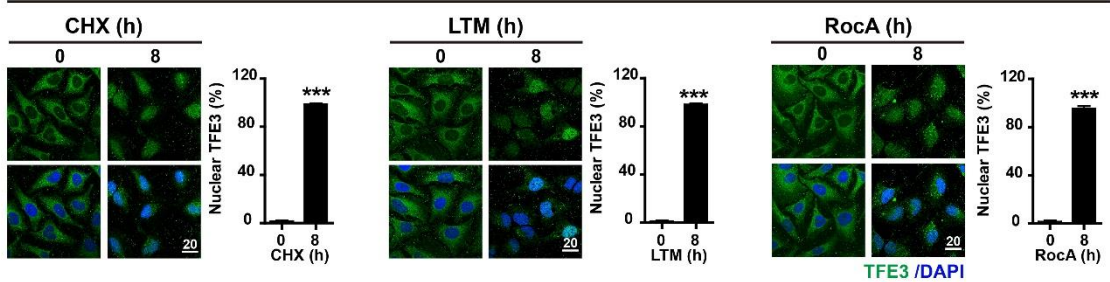
**(A,C,E)** Representative images of confocal microscopic analysis. TFEB-EGFP-expressing MEF (MEF-TFEB-EGFP) cells were treated with CHX (A), LTM (C), or RocA (E) at the indicated concentrations for 4 h. Before harvesting, cells were additionally incubated with puromycin (10  $\mu$ g/mL for 10 min) to label actively translating peptides. Cells were stained with anti-puromycin antibody (red) against puromycin-labeled proteins and DAPI (blue) for DNA. Cellular localization of TFEB-EGFP was indicated by green fluorescence in the cells. Scale bar, 20  $\mu$ m. **(B,D,F)** Quantification of the percentage of MEF-TFEB-EGFP cells with nuclear TFEB-EGFP (left y axis) and the mean fluorescent intensity (MFI) of puromycin (right y axis) in (A), (C), or (E) images. Data are expressed as mean  $\pm$  SEM of at least 150 cells from six random fields in each group. \*\*\*p < 0.001; 0 h vs. other concentrations.



**Figure 3. Translation inhibition induces nuclear translocation of TFEB in a time-dependent manner.**

(A–C) Representative images of confocal analysis. TFEB-EGFP expressing MEF (MEF-TFEB-EGFP) cells were treated with cycloheximide (CHX, 50  $\mu$ g/mL) (A), lactimidomycin (LTM, 500 nM) (B) rocaglamide A (RocA, 3  $\mu$ M) for the indicated times. Before harvesting, cells were additionally incubated with puromycin (10  $\mu$ g/mL for 10 min) to label actively translating peptides. Cells were stained with anti-puromycin antibody (red) against puromycin-labeled proteins and DAPI (blue) for nucleus DNA. Cellular localization of TFEB-EGFP was indicated by green fluorescence signals in the cells. Scale bar, 20  $\mu$ m. (D–F) Quantification of the percentage of MEF-TFEB-EGFP cells with nuclear TFEB-EGFP (left y axis) and the mean fluorescent intensity (MFI) of puromycin (right y axis) following CHX, LTM or RocA treatment as indicated in (A–C). Data are expressed as mean  $\pm$  SEM of at least 150 cells from 6 random fields in each group. \*\*\*  $p < 0.001$ ; 0 h vs. other times. (G–I) Immunoblot analysis of subcellular distribution of TFEB-EGFP and endogenous TFEB in MEF-TFEB-EGFP cells treated with or without CHX (50  $\mu$ g/mL) (G), LTM (500 nM) (H) or RocA (3  $\mu$ M) (I) for 8 h was performed,

using antibodies against GFP and TFEB.  $\beta$ -actin and Histon-H3 were used as loading controls of cytoplasmic and nuclear fractions, respectively.

**A****Immortalized hepatocyte****B****HeLa****C****Immortalized hepatocyte****D****HeLa**

**Figure 4. Translation inhibition induces TFEB and TFE3 nuclear translocation in immortalized hepatocytes or HeLa cells.**

**(A-D)** Representative images of the confocal analysis of TFEB (A,B) or TFE3 (C,D) subcellular distribution in different cell lines. Immortalized hepatocytes (A,C) or HeLa cells (B,D) were treated CHX (50 µg/mL), LTM (500 nM) or RocA (3 µM) for 0 and 8 h. Cells were fixed, permeabilized, and stained with anti-TFEB (A,B) (green) or anti-TFE3 (C,D) (green). DAPI (blue) indicated for nucleus in merged images (lower panels). Scale bar, 20 µm. The graphs represent quantification of the percentage of hepatocytes and HeLa with nuclear TFEB or TFE3 upon CHX, LTM or treatment. Data are expressed as mean ± SEM of at least 150 cells from six random fields in each group. \*\*\*p < 0.001; 0 h vs. 8 h.

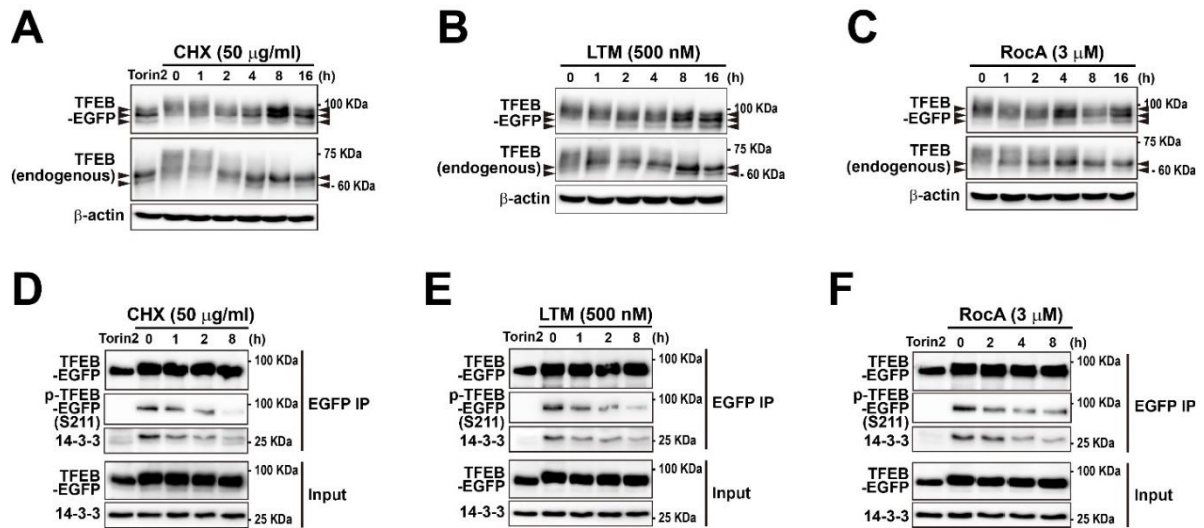


**Figure 5. Translation inhibition promotes TFEB dephosphorylation and 14-3-3 dissociation.**

(A–C) MEF-TFEB-EGFP cells were treated with CHX (50 μg/mL) (A), LTM (500 nM) (B), or RocA (3 μM) (C) for indicated times and Torin2 (mTOR inhibitor, 100 nM) for 3 h as a positive control. Total cellular lysates were separated on 6% SDS-PAGE, followed by immunoblotting with antibodies against GFP, TFEB (used to detect TFEB-EGFP and endogenous TFEB together), or β-actin. Arrows at left and right sides of each panel indicate fast-migrating forms of TFEB-EGFP and TFEB proteins in chemical treated samples, compared with untreated samples (0 h). (D–F) Immunoblot analysis of immunoprecipitated TFEB-EGFP and 14-3-3 in MEF-TFEB-EGFP cells treated with translation inhibitors. The cells were treated with CHX (50 μg/mL) (D), LTM (500 nM) (E), or RocA (3 μM) (F) for indicated time and Torin2 (mTOR inhibitor, 100 nM) for 3 h as a positive control. Cells were lysed and subjected to immunoprecipitation with anti-GFP antibody. Immunoprecipitates were analyzed by immunoblotting with antibodies against GFP (for detecting TFEB-EGFP) and phospho-(Ser) 14-3-3 binding motif (known to bind phosphorylated TFEB-EGFP at Ser 211), or 14-3-3.



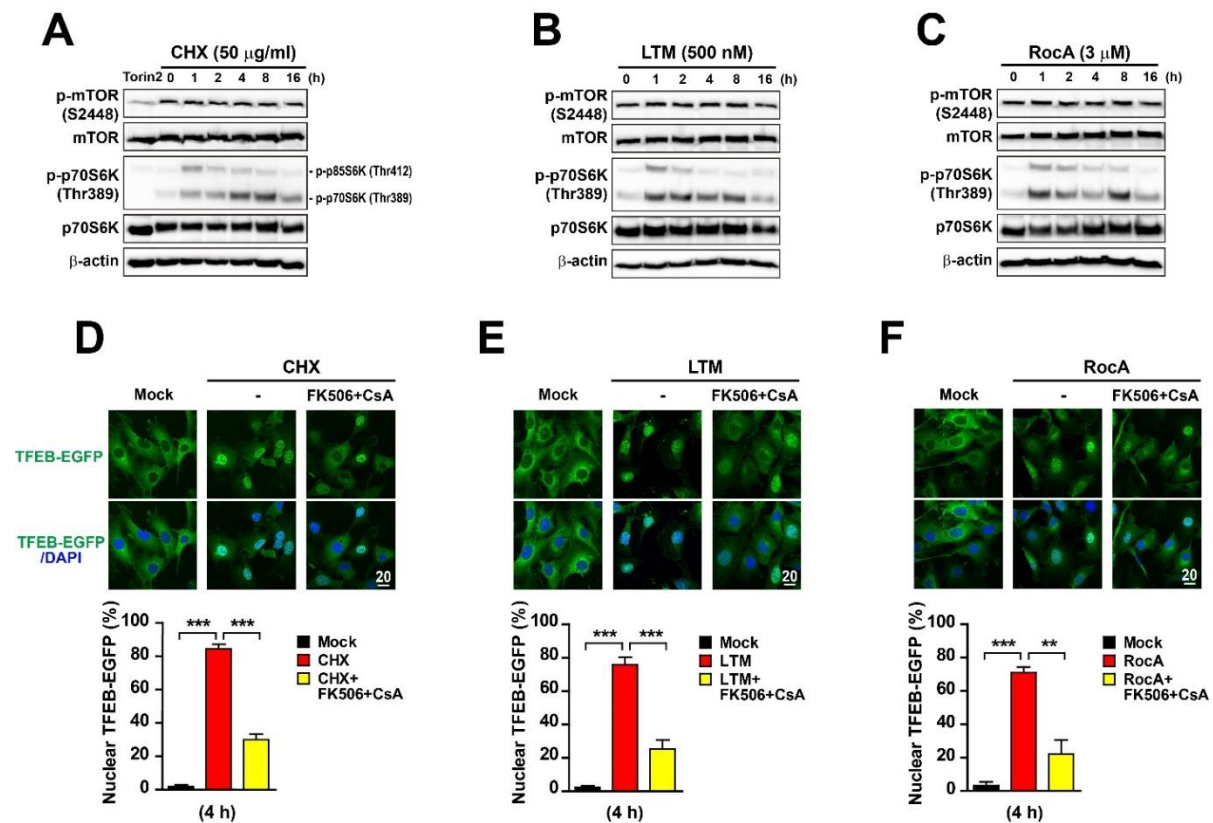


**Figure 6. Calcineurin inhibition prevents translation inhibitor-induced TFEB nuclear translocation.**

(A–C) Immunoblot analysis of protein lysates obtained from MEF-TFEB-EGFP cells treated with CHX (50  $\mu\text{g/ml}$ ) (A), LTM (500 nM) (B), or RocA (3  $\mu\text{M}$ ) (C) for indicated time and Torin2 (mTOR inhibitor, 250 nM) for 3 h as a positive control. Total cellular lysates were analyzed by immunoblotting with indicated antibodies. (D–F) Representative images of confocal microscopic analysis. MEF-TFEB-EGFP cells were treated with Mock (DMSO), CHX (50  $\mu\text{g/ml}$ ) (D), LTM (500 nM) (E), or RocA (3  $\mu\text{M}$ ) (F) with or without calcineurin inhibitors [FK506 (10  $\mu\text{M}$ ) and cyclosporin A (CsA, 20  $\mu\text{M}$ )] for 4 h. Cellular localization of TFEB-EGFP was indicated by green fluorescence in cells. DAPI (blue) staining indicates nucleus in merged images (lower panels). Scale bar, 20  $\mu\text{m}$ . Graphs (lower panels) represent quantified results of the percentage of MEF-TFEB-EGFP cells with nuclear TFEB-EGFP upon chemical treatment. Data are expressed as mean  $\pm$  SEM of at least 150 cells from 6 random fields in each group. \*\*  $p < 0.01$  and \*\*\*  $p < 0.001$ ; Mock vs. translation inhibitors or translation inhibitors vs. translation inhibitors + FK506 + CsA.

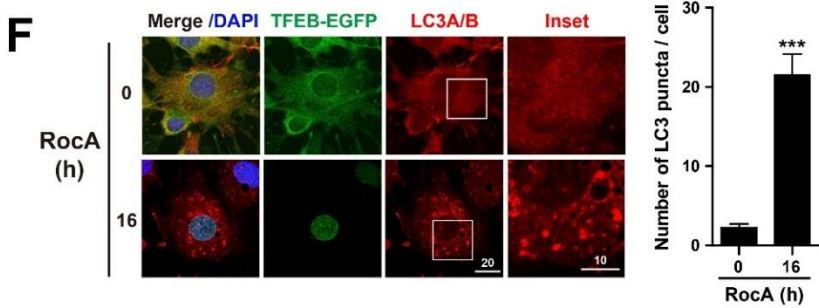
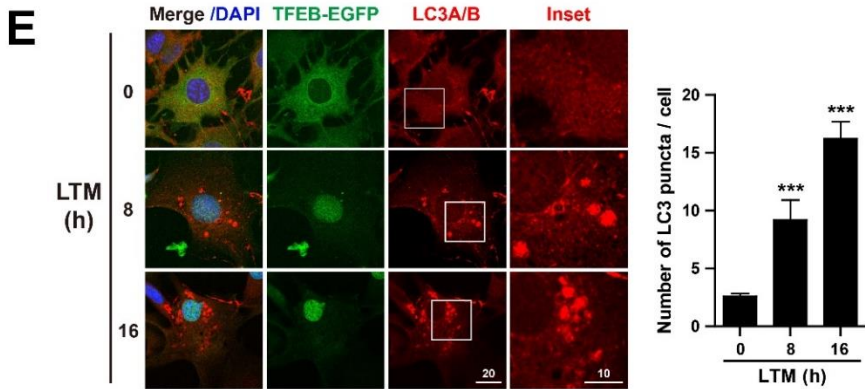
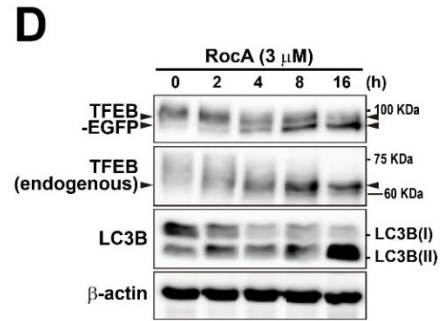
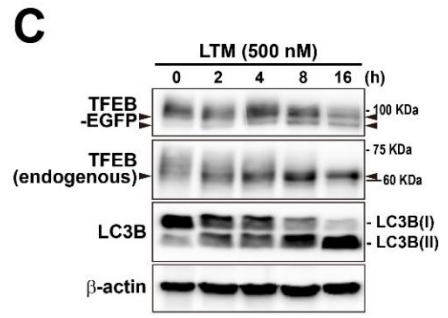
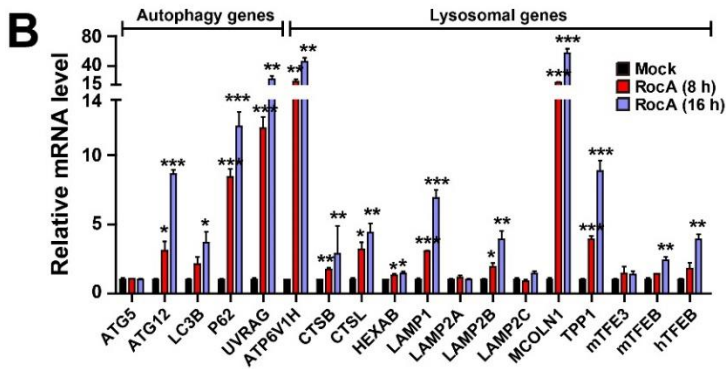
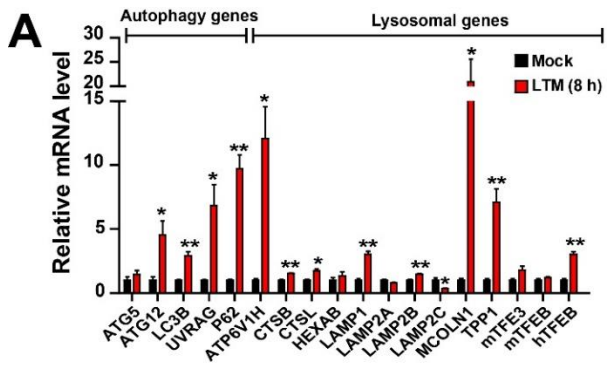


**Figure 7. Translation inhibition induces autophagy-related gene expression and promotes autophagosome formation.**

(A,B) Quantitative RT-PCR analysis of mRNA expression of autophagy and lysosomal genes in MEF-TFEB-EGFP cells treated with LTM (Mock and 500 nM for 8 h) (A) or RocA (Mock and 3  $\mu$ M for 8 h and 16 h) (B). Data are expressed as mean  $\pm$  SEM from three independent experiments. \*  $p < 0.05$ , \*\*  $p < 0.01$ , \*\*\*  $p < 0.001$ ; Mock vs. Translation inhibitors. (C,D) Immunoblot analysis of protein lysates derived from MEF-TFEB-EGFP cells treated with LTM (500 nM) (C) or RocA (3  $\mu$ M) (D) for indicated times. Total cellular lysates were analyzed by immunoblotting with antibodies against GFP, TFEB, LC3B, or  $\beta$ -actin. Arrows at left and right sides of each panel indicate fast-migrating forms of TFEB-EGFP and TFEB proteins in chemical treated samples, compared with untreated samples (0 h). (E,F) Immunofluorescence analysis of LC3/B-positive autophagosomes in MEF-TFEB-EGFP cells treated with LTM (500 nM for 0 h, 8 h, or 16 h) (E) or RocA (3  $\mu$ M for 0 or 16 h) (F). Cells were fixed and stained with anti-LC3A/B (red). DAPI (blue) staining indicates nucleus in the merged images (the first column). Cellular localization of TFEB-EGFP is indicated by green fluorescence in the cells. Insets show a magnified view of the area outlined in the white lined box, Scale bar, 20  $\mu$ m. Graphs represent results of quantification of LC3A/B puncta in each cell in left panel images. Data are expressed as mean  $\pm$  SEM of at least 30 cells derived from 6 random fields in each group. \*\*\*  $p < 0.001$ ; 0 h vs. 8 h or 16 h.

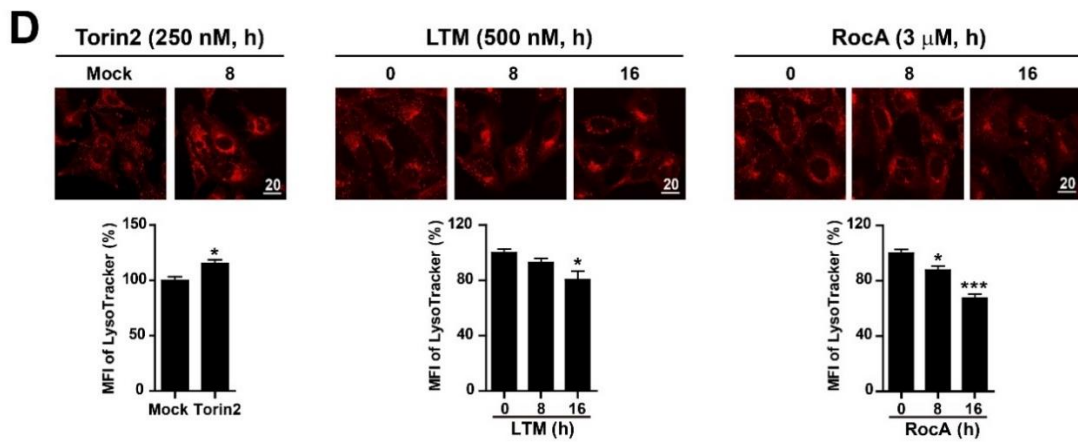
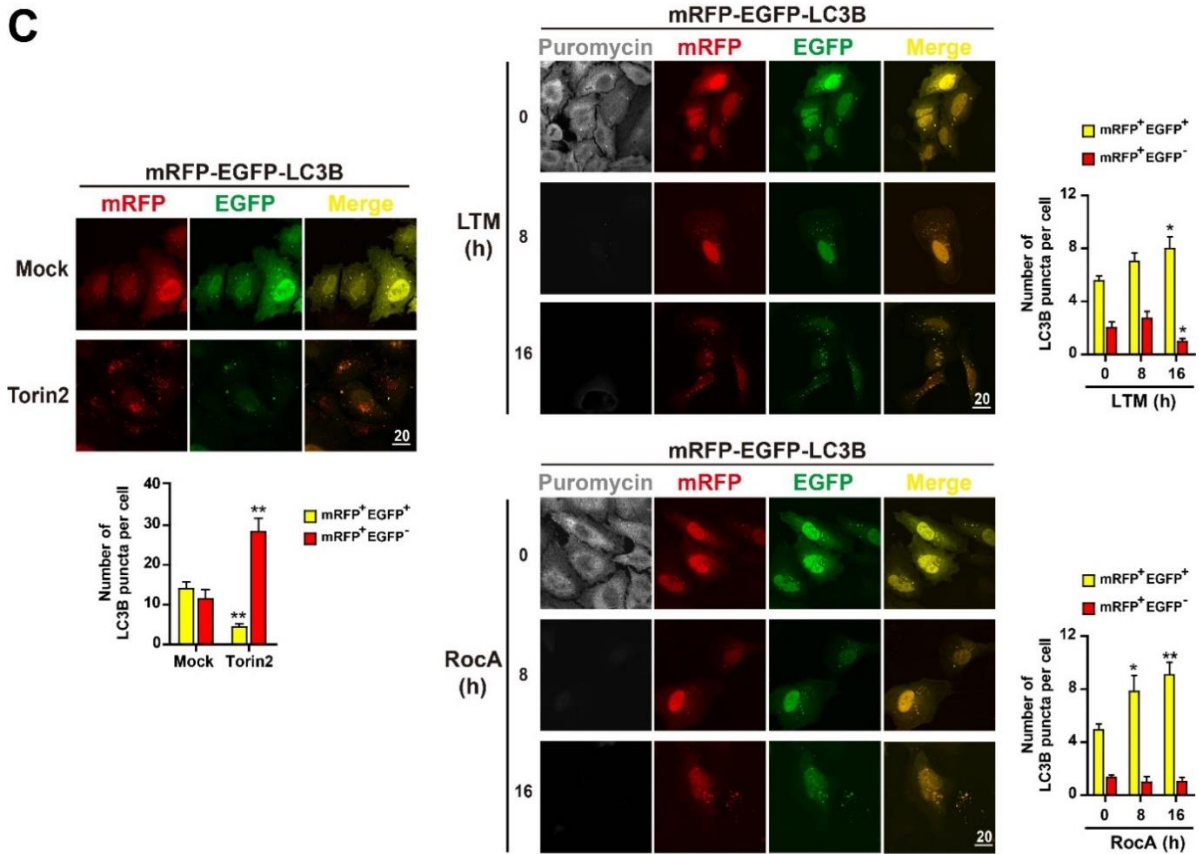
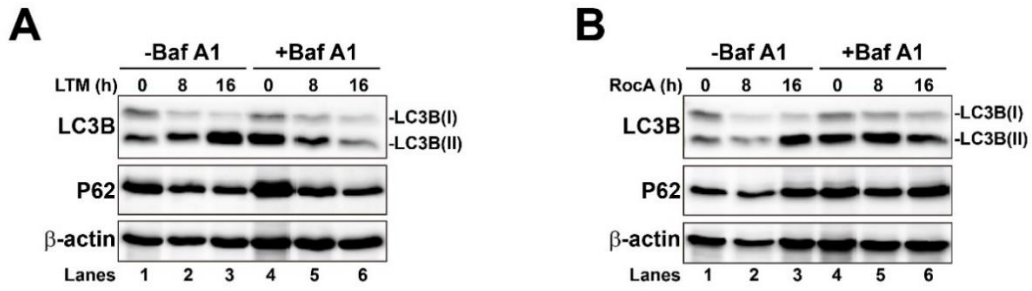


**Figure 8. Translation inhibitors inhibit autophagic flux and induce lysosomal dysfunction.**

**(A,B)** Immunoblot analysis of protein lysates obtained from MEF-TFEB-EGFP cells treated with LTM (500 nM) (A) or RocA (3  $\mu$ M) (B) for indicated times in the absence or presence of lysosomal inhibitor bafilomycin A1 (Baf A1, 200 nM) for 3 h before harvest. The total cellular lysates were analyzed by immunoblotting with antibodies against LC3B, p62 or  $\beta$ -actin. **(C)** HeLa cells were transfected with a tandem fluorescent reporter pmRFP-EGFP-LC3B plasmid for 30 h and treated with LTM (500 nM) or RocA (3  $\mu$ M) for indicated times and Torin2 (mTOR inhibitor, 250 nM) for 6 h as a positive control. Before harvesting, cells were additionally incubated with puromycin (10  $\mu$ g/mL) for 10 min to label actively translating peptides. Cells were then stained with anti-puromycin antibody (gray) against puromycin-labeled proteins. Scale bar, 20  $\mu$ m. Autophagic flux was analyzed graphically by quantifying the number of mRFP<sup>+</sup>EGFP<sup>+</sup> (yellow LC3B puncta) as autophagosomes and mRFP<sup>+</sup>EGFP<sup>-</sup> (red LC3B puncta) as autolysosomes. Data are expressed as mean  $\pm$  SEM of at least 30 cells from six random fields in each group. \*p < 0.05, \*\*p < 0.01, and \*\*\*p < 0.001; 0 h vs. 8 h or 16 h. **(D)** HeLa cells were treated with LTM (500 nM) or RocA (3  $\mu$ M) for indicated times and Torin2 (mTOR inhibitor, 250 nM) for 8 h as a positive control. Acidic vesicles were stained with LysoTracker Red (100 nM, 40 min) and the mean fluorescent intensity (MFI) was quantified and presented graphically. Scale bar, 20  $\mu$ m. Data are expressed as mean  $\pm$  SEM of at least 30 cells from six random fields in each group. \*p < 0.05 and \*\*\*p < 0.001; 0 h vs. 8 h or 16 h.

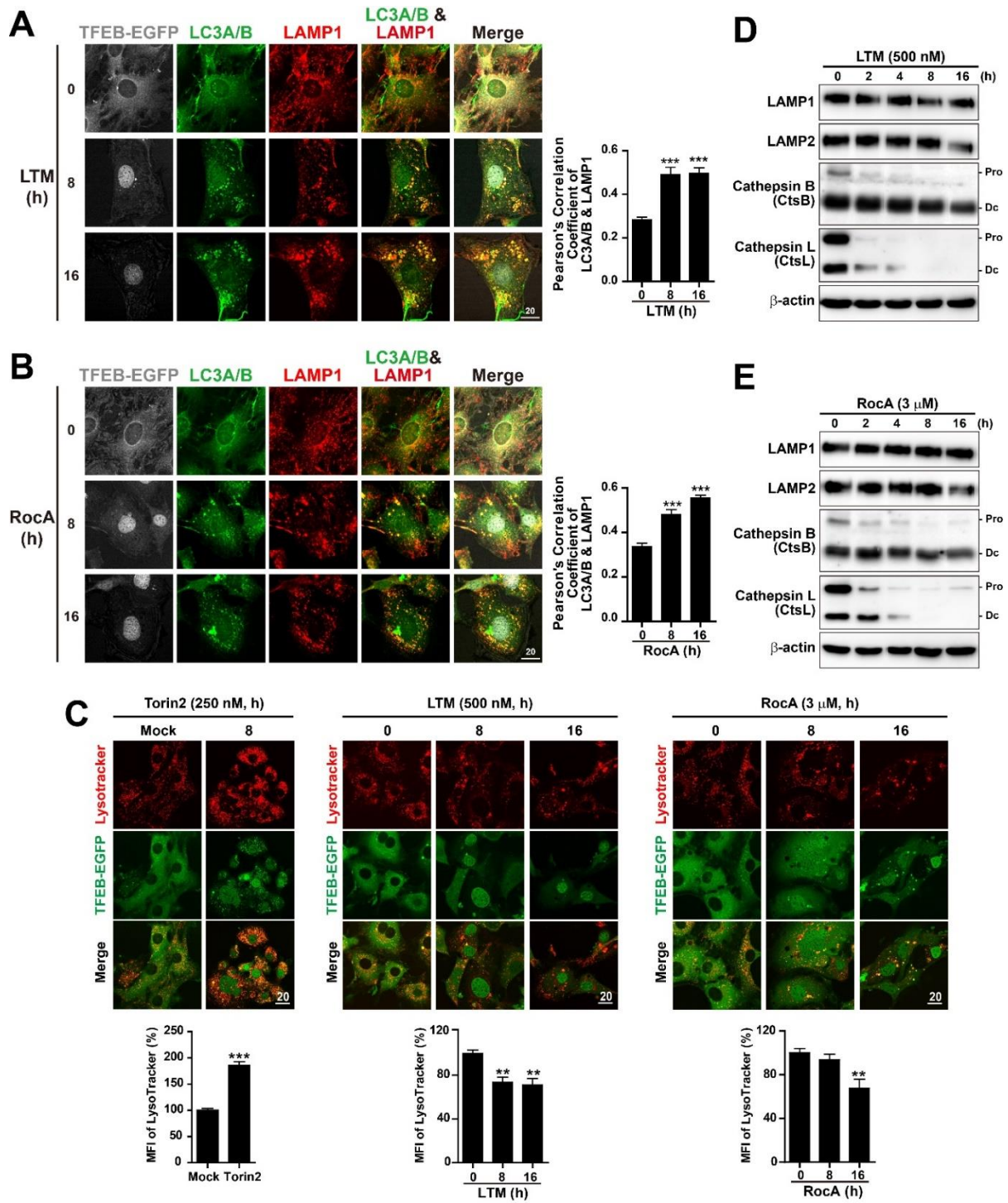


**Figure 9. Translation inhibition induces autolysosome formation but lysosomal dysfunction.**

(A,B) MEF-TFEB-EGFP cells were treated with LTM (500 nM) (A) or RocA (3  $\mu$ M) (B) for the indicated time. Cells were fixed and co-stained with anti-LC3A/B (green) and anti-LAMP1 (red). Green fluorescence of TFEB-EGFP was converted to gray. Scale bar, 20  $\mu$ m. Graphs represent results of quantification of LC3A/B and LAMP1-double positive puncta per cell in the left panel of images. Data are expressed as mean  $\pm$  SEM of at least 30 cells from 6 random fields in each group. \*\*\*  $p < 0.001$ ; 0 h vs. 8 h or 16 h. (C) MEF-TFEB-EGFP cells were treated with LTM (500 nM) or RocA (3  $\mu$ M) for indicated times and Torin2 (mTOR inhibitor, 250 nM) for 8 h as a positive control. Acidic vesicles were visualized with LysoTracker Red (100 nM, 15 min) (red) and cellular localization of TFEB-EGFP is indicated by green fluorescence signal in cells. Scale bar, 20  $\mu$ m. Mean fluorescent intensity (MFI) of LysoTracker Red was quantified and presented in the graphs. Data are expressed as mean  $\pm$  SEM of at least 30 cells derived from 6 random fields in each group. \*\*  $p < 0.01$  and \*\*\*  $p < 0.001$ ; 0 h vs. 8 h or 16 h. (D,E) Immunoblot analysis of protein lysates from MEF-TFEB-EGFP cells treated with LTM (500 nM) (C) or RocA (3  $\mu$ M) (D) for indicated times. The total cellular lysates were analyzed by immunoblotting with indicated antibodies. Pro: procathepsin form. Dc: heavy chain of the double-chain form.

**Figure 10.**

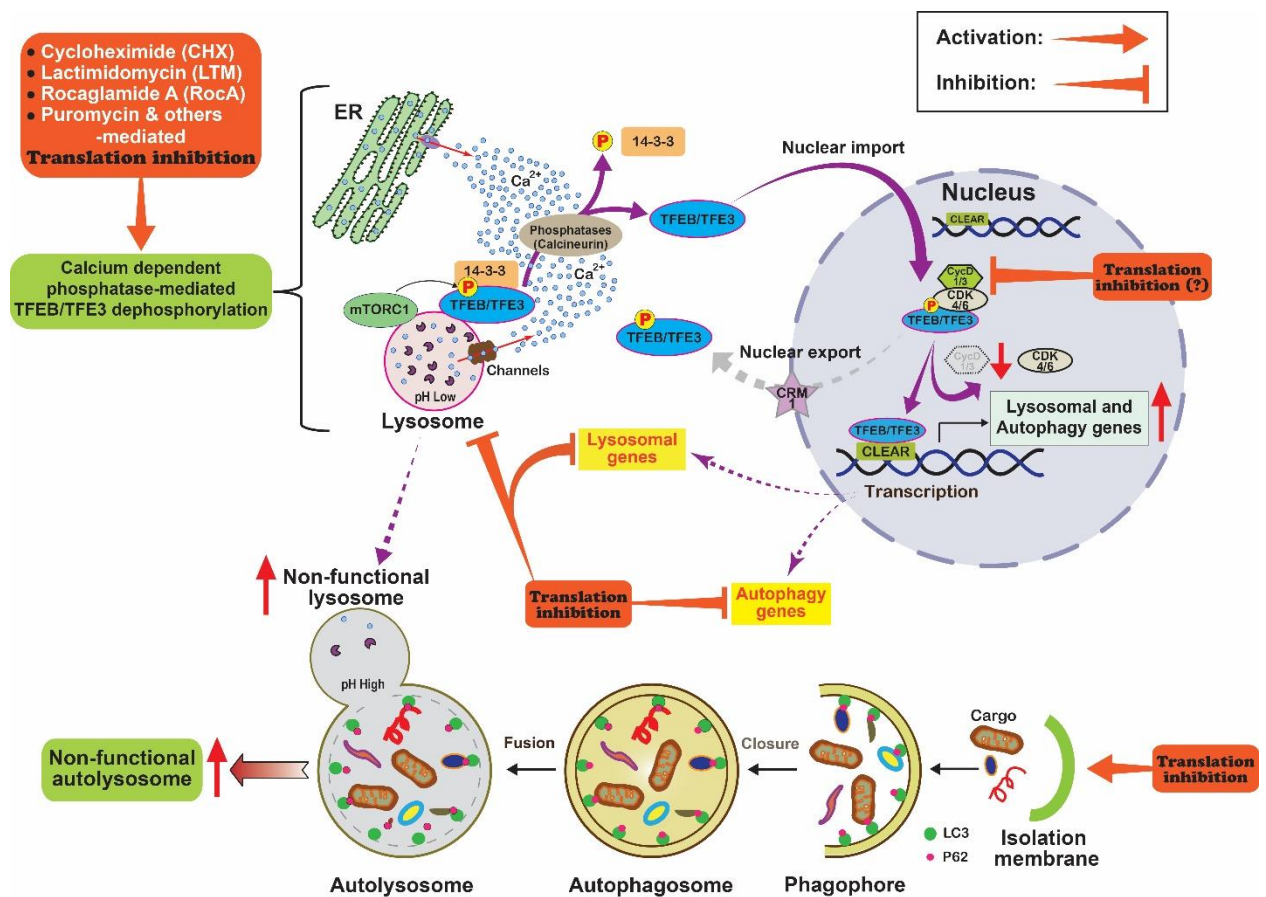


**Figure 10. Model to explain translation inhibition-mediated regulation of TFEB/TFE3 nuclear localization and autophagy.**

Chemical translation inhibitors (CHX, LTM, puromycin and others)-mediated translation inhibition may induce cytosolic release of  $\text{Ca}^{2+}$  from the ER or lysosome [78,79]. Higher cytosolic  $\text{Ca}^{2+}$  concentration then activates phosphatases including calcineurin, which can then dephosphorylate TFEB and TFE3 [38,40,80,81]. These dephosphorylated TFEB and TFE3 are released from 14-3-3 proteins and can translocate to the nucleus [33,35–37]. Under normal conditions, CDK4/6 are activated by cyclin Ds in the nucleus. These activated kinases can then interact with and phosphorylate TFEB and TFE3, promoting their CRM1-dependent nuclear export and inactivation [32]. However, CDK4/6 might be inactivated owing to reduced levels of cyclin Ds when translation is inhibited. TFEB and TFE3 are not phosphorylated by CDK4/6 and thus are retained in the nucleus, where they can induce transcription of lysosomal and autophagy genes. In addition, translation inhibition can promote autophagosome formation and autophagosome-lysosome fusion. However, it ends up inducing lysosomal dysfunction and preventing degradative autolysosome formation owing to protein synthesis inhibition on lysosomal and autophagy gene expression.



## References

1. Klionsky, D.J.; Emr, S.D. Autophagy as a regulated pathway of cellular degradation. *Science* **2000**, *290*, 1717–1721.
2. Mizushima, N.; Ohsumi, Y.; Yoshimori, T. Autophagosome formation in mammalian cells. *Cell Struct. Funct.* **2002**, *27*, 421–429.
3. Kim, K.H.; Lee, M.S. Autophagy—A key player in cellular and body metabolism. *Nat. Rev. Endocrinol.* **2014**, *10*, 322–337.
4. Nakamura, S.; Yoshimori, T. New insights into autophagosome-lysosome fusion. *J. Cell Sci.* **2017**, *130*, 1209–1216.
5. Zhao, Y.G.; Zhang, H. Autophagosome maturation: An epic journey from the ER to lysosomes. *J. Cell Biol.* **2019**, *218*, 757–770.
6. Kabeya, Y.; Mizushima, N.; Ueno, T.; Yamamoto, A.; Kirisako, T.; Noda, T.; Kominami, E.; Ohsumi, Y.; Yoshimori, T. LC3, a mammalian homologue of yeast Apg8p, is localized in autophagosome membranes after processing. *EMBO J.* **2000**, *19*, 5720–5728.
7. Ohsumi, Y. Historical landmarks of autophagy research. *Cell Res.* **2014**, *24*, 9–23.
8. Huotari, J.; Helenius, A. Endosome maturation. *EMBO J.* **2011**, *30*, 3481–3500.
9. Luzio, J.P.; Pryor, P.R.; Bright, N.A. Lysosomes: Fusion and function. *Nat. Rev. Mol. Cell Biol.* **2007**, *8*, 622–632.
10. Mindell, J.A. Lysosomal acidification mechanisms. *Annu. Rev. Physiol.* **2012**, *74*, 69–86.
11. Perera, R.M.; Zoncu, R. The Lysosome as a Regulatory Hub. *Annu. Rev. Cell Dev. Biol.* **2016**, *32*, 223–253.
12. Kaminsky, V.; Zhivotovsky, B. Proteases in autophagy. *Biochim. Biophys. Acta* **2012**, *1824*, 44–50.
13. Yadati, T.; Houben, T.; Bitorina, A.; Shiri-Sverdlov, R. The Ins and Outs of Cathepsins: Physiological Function and Role in Disease Management. *Cells* **2020**, *9*.
14. Saftig, P.; Klumperman, J. Lysosome biogenesis and lysosomal membrane proteins: Trafficking meets function. *Nat. Rev. Mol. Cell Biol.* **2009**, *10*, 623–635.
15. Yang, C.; Wang, X. Lysosome biogenesis: Regulation and functions. *J. Cell Biol.* **2021**, *220*.
16. Lorincz, P.; Juhasz, G. Autophagosome-Lysosome Fusion. *J. Mol. Biol.* **2020**, *432*, 2462–2482.
17. Tian, X.; Gala, U.; Zhang, Y.; Shang, W.; Nagarkar Jaiswal, S.; di Ronza, A.; Jaiswal, M.; Yamamoto, S.; Sandoval, H.; Duraine, L.; et al. A voltage-gated calcium channel regulates lysosomal fusion with endosomes and autophagosomes and is required for neuronal homeostasis. *PLoS Biol.* **2015**, *13*, e1002103.

18. Mauvezin, C.; Nagy, P.; Juhasz, G.; Neufeld, T.P. Autophagosome-lysosome fusion is independent of V-ATPase-mediated acidification. *Nat. Commun.* **2015**, *6*, 7007.
19. Cermak, S.; Kosicek, M.; Mladenovic-Djordjevic, A.; Smiljanic, K.; Kanazir, S.; Hecimovic, S. Loss of Cathepsin B and L Leads to Lysosomal Dysfunction, NPC-Like Cholesterol Sequestration and Accumulation of the Key Alzheimer2019s Proteins. *PLoS ONE* **2016**, *11*, e0167428.
20. Elrick, M.J.; Yu, T.; Chung, C.; Lieberman, A.P. Impaired proteolysis underlies autophagic dysfunction in Niemann-Pick type C disease. *Hum. Mol. Genet.* **2012**, *21*, 4876–4887.
21. Morselli, E.; Marino, G.; Bennetzen, M.V.; Eisenberg, T.; Megalou, E.; Schroeder, S.; Cabrera, S.; Benit, P.; Rustin, P.; Criollo, A.; et al. Spermidine and resveratrol induce autophagy by distinct pathways converging on the acetylproteome. *J. Cell Biol.* **2011**, *192*, 615–629.
22. Di Malta, C.; Cinque, L.; Settembre, C. Transcriptional Regulation of Autophagy: Mechanisms and Diseases. *Front. Cell Dev. Biol.* **2019**, *7*, 114.
23. Napolitano, G.; Ballabio, A. TFEB at a glance. *J. Cell Sci.* **2016**, *129*, 2475–2481.
24. Raben, N.; Puertollano, R. TFEB and TFE3: Linking Lysosomes to Cellular Adaptation to Stress. *Annu. Rev. Cell Dev. Biol.* **2016**, *32*, 255–278.
25. Steingrimsson, E.; Copeland, N.G.; Jenkins, N.A. Melanocytes and the microphthalmia transcription factor network. *Annu. Rev. Genet.* **2004**, *38*, 365–411.
26. Palmieri, M.; Impey, S.; Kang, H.; di Ronza, A.; Pelz, C.; Sardiello, M.; Ballabio, A. Characterization of the CLEAR network reveals an integrated control of cellular clearance pathways. *Hum. Mol. Genet.* **2011**, *20*, 3852–3866.
27. Sardiello, M.; Palmieri, M.; di Ronza, A.; Medina, D.L.; Valenza, M.; Gennarino, V.A.; Di Malta, C.; Donaudy, F.; Embrione, V.; Polishchuk, R.S.; et al. A gene network regulating lysosomal biogenesis and function. *Science* **2009**, *325*, 473–477.
28. Settembre, C.; Di Malta, C.; Polito, V.A.; Garcia Arencibia, M.; Vetrini, F.; Erdin, S.; Erdin, S.U.; Huynh, T.; Medina, D.; Colella, P.; et al. TFEB links autophagy to lysosomal biogenesis. *Science* **2011**, *332*, 1429–1433.
29. Li, L.; Friedrichsen, H.J.; Andrews, S.; Picaud, S.; Volpon, L.; Ngeow, K.; Berridge, G.; Fischer, R.; Borden, K.L.B.; Filippakopoulos, P.; et al. A TFEB nuclear export signal integrates amino acid supply and glucose availability. *Nat. Commun.* **2018**, *9*, 2685.
30. Napolitano, G.; Esposito, A.; Choi, H.; Matarese, M.; Benedetti, V.; Di Malta, C.; Monfregola, J.; Medina, D.L.; Lippincott-Schwartz, J.; Ballabio, A. mTOR-dependent phosphorylation controls TFEB nuclear export. *Nat. Commun.* **2018**, *9*, 3312.
31. Puertollano, R.; Ferguson, S.M.; Brugarolas, J.; Ballabio, A. The complex relationship between TFEB transcription factor phosphorylation and subcellular localization. *EMBO J.* **2018**, *37*.

32. Yin, Q.; Jian, Y.; Xu, M.; Huang, X.; Wang, N.; Liu, Z.; Li, Q.; Li, J.; Zhou, H.; Xu, L.; et al. CDK4/6 regulate lysosome biogenesis through TFEB/TFE3. *J. Cell Biol.* **2020**, 219.
33. Martina, J.A.; Chen, Y.; Gucek, M.; Puertollano, R. mTORC1 functions as a transcriptional regulator of autophagy by preventing nuclear transport of TFEB. *Autophagy* **2012**, 8, 903–914.
34. Pena-Llopis, S.; Vega-Rubin-de-Celis, S.; Schwartz, J.C.; Wolff, N.C.; Tran, T.A.; Zou, L.; Xie, X.J.; Corey, D.R.; Brugarolas, J. Regulation of TFEB and V-ATPases by mTORC1. *EMBO J.* **2011**, 30, 3242–3258.
35. Rocznik-Ferguson, A.; Petit, C.S.; Froehlich, F.; Qian, S.; Ky, J.; Angarola, B.; Walther, T.C.; Ferguson, S.M. The transcription factor TFEB links mTORC1 signaling to transcriptional control of lysosome homeostasis. *Sci. Signal.* **2012**, 5, ra42.
36. Settembre, C.; Zoncu, R.; Medina, D.L.; Vetrini, F.; Erdin, S.; Erdin, S.; Huynh, T.; Ferron, M.; Karsenty, G.; Vellard, M.C.; et al. A lysosome-to-nucleus signalling mechanism senses and regulates the lysosome via mTOR and TFEB. *EMBO J.* **2012**, 31, 1095–1108.
37. Martina, J.A.; Diab, H.I.; Lishu, L.; Jeong, A.L.; Patange, S.; Raben, N.; Puertollano, R. The nutrient-responsive transcription factor TFE3 promotes autophagy, lysosomal biogenesis, and clearance of cellular debris. *Sci. Signal.* **2014**, 7, ra9.
38. Medina, D.L.; Di Paola, S.; Peluso, I.; Armani, A.; De Stefani, D.; Venditti, R.; Montefusco, S.; Scotto-Rosato, A.; Prezioso, C.; Forrester, A.; et al. Lysosomal calcium signalling regulates autophagy through calcineurin and TFEB. *Nat. Cell Biol.* **2015**, 17, 288–299.
39. Vega-Rubin-de-Celis, S.; Pena-Llopis, S.; Konda, M.; Brugarolas, J. Multistep regulation of TFEB by mTORC1. *Autophagy* **2017**, 13, 464–472.
40. Wang, W.; Gao, Q.; Yang, M.; Zhang, X.; Yu, L.; Lawas, M.; Li, X.; Bryant-Geneviev, M.; Southall, N.T.; Marugan, J.; et al. Up-regulation of lysosomal TRPML1 channels is essential for lysosomal adaptation to nutrient starvation. *Proc. Natl. Acad. Sci. USA* **2015**, 112, E1373–E1381.
41. Chen, L.; Wang, K.; Long, A.; Jia, L.; Zhang, Y.; Deng, H.; Li, Y.; Han, J.; Wang, Y. Fasting-induced hormonal regulation of lysosomal function. *Cell Res.* **2017**, 27, 748–763.
42. Li, Y.; Xu, M.; Ding, X.; Yan, C.; Song, Z.; Chen, L.; Huang, X.; Wang, X.; Jian, Y.; Tang, G.; et al. Protein kinase C controls lysosome biogenesis independently of mTORC1. *Nat. Cell Biol.* **2016**, 18, 1065–1077.
43. Martina, J.A.; Puertollano, R. Protein phosphatase 2A stimulates activation of TFEB and TFE3 transcription factors in response to oxidative stress. *J. Biol. Chem.* **2018**, 293, 12525–12534.
44. Bordeleau, M.E.; Robert, F.; Gerard, B.; Lindqvist, L.; Chen, S.M.; Wendel, H.G.; Brem, B.; Greger, H.; Lowe, S.W.; Porco, J.A., Jr.; et al. Therapeutic suppression of translation

- initiation modulates chemosensitivity in a mouse lymphoma model. *J. Clin. Investig.* **2008**, *118*, 2651–2660.
45. Carocci, M.; Yang, P.L. Lactimidomycin is a broad-spectrum inhibitor of dengue and other RNA viruses. *Antivir. Res.* **2016**, *128*, 57–62.
  46. Cencic, R.; Carrier, M.; Galicia-Vazquez, G.; Bordeleau, M.E.; Sukarieh, R.; Bourdeau, A.; Brem, B.; Teodoro, J.G.; Greger, H.; Tremblay, M.L.; et al. Antitumor activity and mechanism of action of the cyclopenta[b]benzofuran, silvestrol. *PLoS ONE* **2009**, *4*, e5223.
  47. Dmitriev, S.E.; Vladimirov, D.O.; Lashkevich, K.A. A Quick Guide to Small-Molecule Inhibitors of Eukaryotic Protein Synthesis. *Biochemistry (Mosc)* **2020**, *85*, 1389–1421.
  48. Pelletier, J.; Graff, J.; Ruggero, D.; Sonenberg, N. Targeting the eIF4F translation initiation complex: A critical nexus for cancer development. *Cancer Res.* **2015**, *75*, 250–263.
  49. Levy, J.M.M.; Towers, C.G.; Thorburn, A. Targeting autophagy in cancer. *Nat. Rev. Cancer* **2017**, *17*, 528–542.
  50. Perez-Hernandez, M.; Arias, A.; Martinez-Garcia, D.; Perez-Tomas, R.; Quesada, R.; Soto-Cerrato, V. Targeting Autophagy for Cancer Treatment and Tumor Chemosensitization. *Cancers* **2019**, *11*.
  51. Choi, Y.; Bowman, J.W.; Jung, J.U. Autophagy during viral infection—A double-edged sword. *Nat. Rev. Microbiol.* **2018**, *16*, 341–354.
  52. Maity, S.; Saha, A. Therapeutic Potential of Exploiting Autophagy Cascade Against Coronavirus Infection. *Front. Microbiol.* **2021**, *12*, 675419.
  53. Valvezan, A.J.; Manning, B.D. Molecular logic of mTORC1 signalling as a metabolic rheostat. *Nat. Metab.* **2019**, *1*, 321–333.
  54. Thoreen, C.C.; Chantranupong, L.; Keys, H.R.; Wang, T.; Gray, N.S.; Sabatini, D.M. A unifying model for mTORC1-mediated regulation of mRNA translation. *Nature* **2012**, *485*, 109–113.
  55. Garreau de Loubresse, N.; Prokhorova, I.; Holtkamp, W.; Rodnina, M.V.; Yusupova, G.; Yusupov, M. Structural basis for the inhibition of the eukaryotic ribosome. *Nature* **2014**, *513*, 517–522.
  56. Schneider-Poetsch, T.; Ju, J.; Eyler, D.E.; Dang, Y.; Bhat, S.; Merrick, W.C.; Green, R.; Shen, B.; Liu, J.O. Inhibition of eukaryotic translation elongation by cycloheximide and lactimidomycin. *Nat. Chem. Biol.* **2010**, *6*, 209–217.
  57. Iwasaki, S.; Floor, S.N.; Ingolia, N.T. Rocaglates convert DEAD-box protein eIF4A into a sequence-selective translational repressor. *Nature* **2016**, *534*, 558–561.
  58. Iwasaki, S.; Iwasaki, W.; Takahashi, M.; Sakamoto, A.; Watanabe, C.; Shichino, Y.; Floor, S.N.; Fujiwara, K.; Mito, M.; Dodo, K.; et al. The Translation Inhibitor Rocaglamide Targets

- a Bimolecular Cavity between eIF4A and Polypurine RNA. *Mol. Cell* **2019**, *73*, 738–748 e739.
59. Chu, J.; Zhang, W.; Cencic, R.; O'Connor, P.B.F.; Robert, F.; Devine, W.G.; Selznick, A.; Henkel, T.; Merrick, W.C.; Brown, L.E.; et al. Rocaglates Induce Gain-of-Function Alterations to eIF4A and eIF4F. *Cell Rep.* **2020**, *30*, 2481–2488.
  60. Lawrence, B.P.; Brown, W.J. Inhibition of protein synthesis separates autophagic sequestration from the delivery of lysosomal enzymes. *J. Cell Sci.* **1993**, *105*, 473–480.
  61. Amenta, J.S.; Brocher, S.C. Mechanisms of protein turnover in cultured cells. *Life Sci.* **1981**, *28*, 1195–1208.
  62. Shelburne, J.D.; Arstila, A.U.; Trump, B.F. Studies on cellular autophagocytosis. The relationship of autophagocytosis to protein synthesis and to energy metabolism in rat liver and flounder kidney tubules in vitro. *Am. J. Pathol.* **1973**, *73*, 641–670.
  63. Lee, S.; Liu, B.; Lee, S.; Huang, S.X.; Shen, B.; Qian, S.B. Global mapping of translation initiation sites in mammalian cells at single-nucleotide resolution. *Proc. Natl. Acad. Sci. USA* **2012**, *109*, E2424–E2432.
  64. Choi, W.G.; Han, J.; Kim, J.H.; Kim, M.J.; Park, J.W.; Song, B.; Cha, H.J.; Choi, H.S.; Chung, H.T.; Lee, I.K.; et al. eIF2alpha phosphorylation is required to prevent hepatocyte death and liver fibrosis in mice challenged with a high fructose diet. *Nutr. Metab.* **2017**, *14*, 48.
  65. Pastore, N.; Brady, O.A.; Diab, H.I.; Martina, J.A.; Sun, L.; Huynh, T.; Lim, J.A.; Zare, H.; Raben, N.; Ballabio, A.; et al. TFEB and TFE3 cooperate in the regulation of the innate immune response in activated macrophages. *Autophagy* **2016**, *12*, 1240–1258.
  66. Pastore, N.; Vainshtein, A.; Klisch, T.J.; Armani, A.; Huynh, T.; Herz, N.J.; Polishchuk, E.V.; Sandri, M.; Ballabio, A. TFE3 regulates whole-body energy metabolism in cooperation with TFEB. *EMBO Mol. Med.* **2017**, *9*, 605–621.
  67. Bao, J.; Zheng, L.; Zhang, Q.; Li, X.; Zhang, X.; Li, Z.; Bai, X.; Zhang, Z.; Huo, W.; Zhao, X.; et al. Deacetylation of TFEB promotes fibrillar Abeta degradation by upregulating lysosomal biogenesis in microglia. *Protein Cell* **2016**, *7*, 417–433.
  68. Beck, W.H.J.; Kim, D.; Das, J.; Yu, H.; Smolka, M.B.; Mao, Y. Glucosylation by the Legionella Effector SetA Promotes the Nuclear Localization of the Transcription Factor TFEB. *iScience* **2020**, *23*, 101300.
  69. Miller, A.J.; Levy, C.; Davis, I.J.; Razin, E.; Fisher, D.E. Sumoylation of MITF and its related family members TFE3 and TFEB. *J. Biol. Chem.* **2005**, *280*, 146–155.
  70. Zhang, J.; Wang, J.; Zhou, Z.; Park, J.E.; Wang, L.; Wu, S.; Sun, X.; Lu, L.; Wang, T.; Lin, Q.; et al. Importance of TFEB acetylation in control of its transcriptional activity and lysosomal function in response to histone deacetylase inhibitors. *Autophagy* **2018**, *14*, 1043–1059.

71. Hsu, C.L.; Lee, E.X.; Gordon, K.L.; Paz, E.A.; Shen, W.C.; Ohnishi, K.; Meisenhelder, J.; Hunter, T.; La Spada, A.R. MAP4K3 mediates amino acid-dependent regulation of autophagy via phosphorylation of TFEB. *Nat. Commun.* **2018**, *9*, 942.
72. Yoshii, S.R.; Mizushima, N. Monitoring and Measuring Autophagy. *Int. J. Mol. Sci.* **2017**, *18*.
73. Klionsky, D.J.; Abdel-Aziz, A.K.; Abdelfatah, S.; Abdellatif, M.; Abdoli, A.; Abel, S.; Abeliovich, H.; Abildgaard, M.H.; Abudu, Y.P.; Acevedo-Arozena, A.; et al. Guidelines for the use and interpretation of assays for monitoring autophagy (4th edition). *Autophagy* **2021**, *17*, 1–382.
74. Jia, R.; Bonifacino, J.S. Negative regulation of autophagy by UBA6-BIRC6-mediated ubiquitination of LC3. *Elife* **2019**, *8*.
75. Kocaturk, N.M.; Gozuacik, D. Crosstalk Between Mammalian Autophagy and the Ubiquitin-Proteasome System. *Front. Cell Dev. Biol.* **2018**, *6*, 128.
76. Kimura, S.; Noda, T.; Yoshimori, T. Dissection of the autophagosome maturation process by a novel reporter protein, tandem fluorescent-tagged LC3. *Autophagy* **2007**, *3*, 452–460.
77. N'Diaye, E.N.; Kajihara, K.K.; Hsieh, I.; Morisaki, H.; Debnath, J.; Brown, E.J. PLIC proteins or ubiquilins regulate autophagy-dependent cell survival during nutrient starvation. *EMBO Rep.* **2009**, *10*, 173–179.
78. Cassel, R.; Ducreux, S.; Alam, M.R.; Dingreville, F.; Berle, C.; Burda-Jacob, K.; Chauvin, M.A.; Chikh, K.; Païta, L.; Al-Mawla, R.; et al. Protection of Human Pancreatic Islets from Lipotoxicity by Modulation of the Translocon. *PLoS ONE* **2016**, *11*, e0148686.
79. Lang, S.; Erdmann, F.; Jung, M.; Wagner, R.; Cavalie, A.; Zimmermann, R. Sec61 complexes form ubiquitous ER Ca<sup>2+</sup> leak channels. *Channels (Austin)* **2011**, *5*, 228–235.
80. Martina, J.A.; Diab, H.I.; Brady, O.A.; Puertollano, R. TFEB and TFE3 are novel components of the integrated stress response. *EMBO J.* **2016**, *35*, 479–495.
81. Wang, C.; Niederstrasser, H.; Douglas, P.M.; Lin, R.; Jaramillo, J.; Li, Y.; Oswald, N.W.; Zhou, A.; McMillan, E.A.; Mendiratta, S.; et al. Small-molecule TFEB pathway agonists that ameliorate metabolic syndrome in mice and extend *C. elegans* lifespan. *Nat. Commun.* **2017**, *8*, 2270.
82. Creamer, T.P. Calcineurin. *Cell Commun. Signal.* **2020**, *18*, 137.
83. Dang, T.T.; Kim, M.J.; Kim, K.H.; Lee, Y.Y.; Hien, L.T.; Nam, S.; Chung, S.W.; Chung, H.T.; Yoshida, H.; Kim, K.; et al. eIF2alpha phosphorylation is responsible for TFEB and TFE3 nuclear localization during ER stress. **2021**, In press.
84. Chen, G.; Ding, X.F.; Bouamar, H.; Pressley, K.; Sun, L.Z. Everolimus induces G1 cell cycle arrest through autophagy-mediated protein degradation of cyclin D1 in breast cancer cells. *Am. J. Physiol. Cell Physiol.* **2019**, *317*, C244–C252.

85. Raven, J.F.; Baltzis, D.; Wang, S.; Mounir, Z.; Papadakis, A.I.; Gao, H.Q.; Koromilas, A.E. PKR and PKR-like endoplasmic reticulum kinase induce the proteasome-dependent degradation of cyclin D1 via a mechanism requiring eukaryotic initiation factor 2alpha phosphorylation. *J. Biol. Chem.* **2008**, *283*, 3097–3108.
86. Thomas, S.E.; Malzer, E.; Ordonez, A.; Dalton, L.E.; van, T.W.E.F.A.; Liniker, E.; Crowther, D.C.; Lomas, D.A.; Marciniak, S.J. p53 and translation attenuation regulate distinct cell cycle checkpoints during endoplasmic reticulum (ER) stress. *J. Biol. Chem.* **2013**, *288*, 7606–7617.
87. Dick, F.A.; Rubin, S.M. Molecular mechanisms underlying RB protein function. *Nat. Rev. Mol. Cell Biol.* **2013**, *14*, 297–306.
88. Morgan, D.O. Cyclin-dependent kinases: Engines, clocks, and microprocessors. *Annu. Rev. Cell Dev. Biol.* **1997**, *13*, 261–291. <https://doi.org/10.1146/annurev.cellbio.13.1.261>.
89. Diehl, J.A.; Zindy, F.; Sherr, C.J. Inhibition of cyclin D1 phosphorylation on threonine-286 prevents its rapid degradation via the ubiquitin-proteasome pathway. *Genes Dev.* **1997**, *11*, 957–972.
90. Hashemolhosseini, S.; Nagamine, Y.; Morley, S.J.; Desrivieres, S.; Mercep, L.; Ferrari, S. Rapamycin inhibition of the G1 to S transition is mediated by effects on cyclin D1 mRNA and protein stability. *J. Biol. Chem.* **1998**, *273*, 14424–14429.
91. Han, J.; Back, S.H.; Hur, J.; Lin, Y.H.; Gildersleeve, R.; Shan, J.; Yuan, C.L.; Krokowski, D.; Wang, S.; Hatzoglou, M.; et al. ER-stress-induced transcriptional regulation increases protein synthesis leading to cell death. *Nat. Cell Biol.* **2013**, *15*, 481–490.
92. Lee, H.Y.; Nam, S.; Kim, M.J.; Kim, S.J.; Back, S.H.; Yoo, H.J. Butyrate Prevents TGF-beta1-Induced Alveolar Myofibroblast Differentiation and Modulates Energy Metabolism. *Metabolites* **2021**, *11*.

## **CHAPTER 2**

**Phosphorylation of eukaryotic translation initiation factor 2 $\alpha$  is  
indispensable for nuclear translocation of TFEB and TFE3  
during ER stress**



## Abstract

There are diverse links between autophagy pathways and unfolded protein response (UPR) pathways under endoplasmic reticulum (ER) stress conditions to restore ER homeostasis. Phosphorylation of eukaryotic translation initiation factor 2 $\alpha$  (eIF2 $\alpha$ ) is an important mechanism that can regulate all three UPR pathways through transcriptional and translational reprogramming to maintain cellular homeostasis and overcome cellular stresses. In this study, to investigate the roles of eIF2 $\alpha$  phosphorylation in regulation of autophagy during ER stress, I used eIF2 $\alpha$  phosphorylation-deficient (*A/A*) cells in which residue 51 was mutated from serine to alanine. *A/A* cells exhibited defects in multiple steps of autophagic processes (such as autophagosome and autolysosome formation, and autophagic flux) that are regulated by the transcriptional activities of the autophagy master transcription factors TFEB and TFE3 under ER stress conditions. eIF2 $\alpha$  phosphorylation was required for nuclear translocation of TFEB and TFE3 during ER stress. In addition, calcineurin-mediated dephosphorylation of TFEB and TFE3 and 14-3-3 dissociation were required for their nuclear translocation, but were insufficient to induce their nuclear retention during ER stress. Overexpression of the activated ATF6 $\alpha$  form was necessary and sufficient to induce both dephosphorylation and nuclear translocation of TFEB in *A/A* cells during ER stress. Consequently, overexpression of the activated ATF6 $\alpha$  or TFEB form rescued autophagic defects in *A/A* cells during ER stress. These results suggest that eIF2 $\alpha$  phosphorylation is important for autophagy and UPR pathways, to restore ER homeostasis and reveal how eIF2 $\alpha$  phosphorylation connects UPR pathways to autophagy.

## Introduction

Eukaryotic translation initiation factor 2 $\alpha$  (eIF2 $\alpha$ ) is a subunit of the eIF2 complex, which facilitates the placement of an initiator tRNA (methionyl-tRNA<sub>i</sub>) onto the P site of the 40S ribosomal subunit during the translation initiation of cytoplasmic mRNAs in eukaryotic cells [1]. eIF2 complex activity is regulated by eIF2 $\alpha$  phosphorylation, which occurs on serine 51 (S51) and is mediated by four kinases (EIF2AK1/HRI, EIF2AK2/PKR, EIF2AK3/PERK, and EIF2AK4/GCN2) in response to diverse cellular stresses including heme deficiency, oxidative stress, viral infection, endoplasmic reticulum (ER) stress, and amino acid deficiency [2-4]. eIF2 $\alpha$  phosphorylation transiently attenuates the translation of most mRNAs and promotes the translation of selected mRNAs, including the transcripts of transcription factor (TF) genes (*Atf4*, *Chop*, *Atf5*, and *C/ebp $\alpha$ / $\beta$* ), nutrient metabolism-related genes (*Cat1*, *Slc35a4*, and *Eprs*), a phosphatase regulatory subunit gene (*Gadd34*), and cellular adaptation-related genes (*Ibtk4* and *Cpeb4*) [5, 6]. These signaling programs allow cells to conserve resources and initiate adaptive gene expression to restore cellular homeostasis, referred to as the integrated stress response [3, 7, 8].

Eukaryotic cells cope with ER stress by activating the unfolded protein response (UPR), which is initiated by three main UPR sensors [IRE1 $\alpha$  (inositol-requiring 1 $\alpha$ ), ATF6 (activating transcription factor 6), and PERK (PKR-like ER kinase)] [9, 10]. IRE1 $\alpha$  has ER stress-regulated kinase and endonuclease activities that can initiate unconventional splicing of *Xbp1* mRNA to remove a 26 nucleotide intron and then introduce a translational frameshift. Spliced *Xbp1* (*Xbp1s*) mRNA encodes a potent TF (XBP1s) that induces transcription of genes encoding proteins that facilitate protein folding, secretion, and degradation in response to ER stress [9, 10]. ATF6 is a TF encoded by two related genes, *Atf6 $\alpha$*  and *Atf6 $\beta$*  [11]. Upon ER stress, it translocates to the Golgi apparatus, where it is cleaved by site-1 protease and site-2 protease. The cleaved N-terminal cytosolic domain of ATF6 (hereafter referred to as “the activated ATF6 form”) then translocates into the nucleus, where it binds to ER stress-response elements and thereby activates target genes that encode proteins with functions in ER protein folding, endoplasmic reticulum-associated degradation (ERAD), protein secretion, and ER biogenesis [11, 12]. PERK is the major protein responsible for attenuation of mRNA translation via eIF2 $\alpha$  phosphorylation, reducing the protein burden within the ER. Paradoxically, PERK-mediated eIF2 $\alpha$  phosphorylation upregulates the translation of several mRNAs as described above. Among them, translation of *Atf4* mRNA is crucial for upregulation of genes involved in redox homeostasis, amino acid metabolism, protein folding, and protein synthesis [5, 9]. In addition, crosstalk can occur between the PERK-eIF2 $\alpha$  phosphorylation-ATF4 pathway and other UPR pathways (IRE1 $\alpha$ /XBP1- and ATF6-mediated UPR pathways). Phosphorylation of eIF2 $\alpha$  is required for maximal induction of XBP1s protein by stabilizing its mRNA [13], and for

activation of ATF6 by facilitating its trafficking from the ER to the Golgi in response to ER stress [14]. Thus, phosphorylation of eIF2 $\alpha$  affecting activation of all three UPR pathways is responsible for transcriptional as well as translational reprogramming to help cells maintain cellular homeostasis and overcome cellular stresses.

Macroautophagy (hereafter referred to as “autophagy”) is an evolutionarily conserved cellular process by which accumulating aberrant proteins or damaged subcellular organelles undergo lysosomal degradation [15, 16]. In brief, autophagy includes five steps: initiation and phagophore nucleation, phagophore expansion, autophagosome maturation, autophagosome-lysosome fusion, and cargo degradation by lysosomal enzymes [17, 18]. Numerous genes are required to perform these processes [19-21]. Increasing evidence indicates that autophagy is regulated at the transcriptional level by several TFs, including transcription factor EB (TFEB), transcription factor E3 (TFE3), Forkhead box O, and E2 transcription factor1 [22-24]. TFEB is a member of the microphthalmia-associated TF family, which also includes MITF, TFE3, and TFEC [25]. TFEB and TFE3 are believed to be the master regulators of the autolysosome pathway, and to control expression of genes required for autophagosome formation, lysosome biogenesis, and lysosome function by directly binding to promoters of the coordinated lysosomal expression and regulation (CLEAR) element [20, 26, 27]. Diverse post-translational modifications (PTMs), including phosphorylation, regulate the activities of these TFs [28-32]. Several kinases that phosphorylate TFEB and TFE3 have been identified. Among them, mammalian target of rapamycin complex 1 (mTORC1) is the best-studied [33-36]. Under normal conditions, lysosomal mTORC1 phosphorylates TFEB (at S142 and S211) and TFE3 (at S321). Phosphorylated TFEB and TFE3 interact with 14-3-3 (also known as YWHA), which results in sequestration of these TFs as inactive forms in the cytosol [35-38]. Under starvation and other conditions when mTORC1 is inhibited and/or the Ca<sup>2+</sup>-calmodulin-dependent protein phosphatase calcineurin is activated, further phosphorylation of TFEB/TFE3 does not occur. This prevents binding to 14-3-3 and induces rapid accumulation of TFEB and TFE3 in the nucleus [31, 39, 40]. However, recent reports suggest that nuclear translocation of TFEB/TFE3 is more complex than generally appreciated. For example, TFEB continuously shuttles between the cytosol and nucleus via nuclear export dependent on the nuclear exportin chromosomal maintenance 1 (CRM1) [29, 30, 41]. CRM1 is an export receptor for leucine-rich nuclear export signals (NESs) [29, 30, 42]. Therefore, whether TFEB is retained in the nucleus has been proposed to depend on the phosphorylation statuses of S142 and S138, which are localized in the proximity of a NES. Nuclear export is promoted by phosphorylation of S142 via mTORC1 and extracellular signal-regulated kinase 2 (under nutrient-rich conditions) [29, 30] or cyclin-dependent kinases 4/6 (CDK4/6, during G1 phase) [41]. Moreover, phosphorylation of S142 primes TFEB for phosphorylation of S138 by glycogen synthase kinase-3 $\beta$  (GSK3 $\beta$ ) [30]. Therefore, the absence of S142 phosphorylation

may lead to nuclear retention of TFEB/TFE3. Thus, the mechanisms governing the localization of TFEB/TFE3 in response to multiple signals are not fully understood.

Several studies have shown that the UPR induces autophagy to degrade unfolded and aggregated proteins and thereby restore ER homeostasis [43-46], although excessive and prolonged ER stress may inhibit autophagy by impairing lysosomes [47]. Several components of UPR signaling pathways transcriptionally upregulate genes encoding autophagy machinery, indicating a high level of crosstalk between ER stress and autophagy [43-46]. Several lines of evidence suggest that eIF2 $\alpha$  phosphorylation plays a key role in regulation of autophagy. PERK/eIF2 $\alpha$  phosphorylation is reportedly involved in polyglutamine 72 repeat aggregate-induced autophagy [48]. A nonphosphorylatable knock-in mutation (S51A) of eIF2 $\alpha$  and dominant-negative PERK inhibit polyglutamine 72 repeat-induced LC3 conversion. Induction of autophagic puncta by diverse pharmacological autophagy enhancers is also partially inhibited in homozygous S51A eIF2 $\alpha$  knock-in (*A/A*) mutant human osteosarcoma U2OS cells [49]. Furthermore, the TFs ATF4 and CHOP, which are downstream targets of phosphorylated eIF2 $\alpha$  are reportedly required to increase transcription of a set of autophagy genes (autophagosome formation, elongation, and function) under amino acid starvation or ER stress conditions [50]. Thus, eIF2 $\alpha$  phosphorylation may play a central role in autophagy in response to ER stress. Nevertheless, the molecular mechanisms involved in activation and regulation of autophagy through eIF2 $\alpha$  phosphorylation remain unclear.

In the present study, I revealed that eIF2 $\alpha$  phosphorylation plays an essential role in nuclear translocation of TFEB and TFE3. Dephosphorylation (at both S211 and S142) of TFEB and its dissociation from 14-3-3 were insufficient for its nuclear translocation in eIF2 $\alpha$  phosphorylation-deficient (*A/A*) cells during ER stress. Instead, overexpression of the activated ATF6 $\alpha$  form was necessary and sufficient to induce both dephosphorylation and nuclear translocation of TFEB in *A/A* cells during ER stress. Consequently, overexpression of the activated ATF6 $\alpha$  or TFEB form restored autophagy in *A/A* cells during ER stress. These data highlight a new mechanism controlling the subcellular localization and activity of TFEB via an eIF2 $\alpha$  phosphorylation-dependent component of UPR signaling pathways under ER stress conditions.

## Materials and Methods

### Reagents and antibodies

The following reagents were used: Tm (Sigma-Aldrich, 654380), Tg (Merck Millipore, 586005), Torin2 (Tocris Bioscience, 4248), DTT (Promega, V3151), FK506 (InvivoGen, Tlrl-FK5), Hoechst 33258 solution (Sigma-Aldrich, 94403), LPS from *Escherichia coli* O55:B5 (Sigma-Aldrich, L2880), CHX (Sigma-Aldrich, C7698), LMB (Santa Cruz Biotechnology, sc-358688), LysoTracker™ Red DND-99 (Thermo Fisher Scientific, L7528), 4',6-diamidino-2-phenylindole dihydrochloride (DAPI; Invitrogen, D1306), MG132 (CSNpharm, CSN11436), and Baf A1 (Cayman Chemical, 11038). To induce starvation, cells were incubated in EBSS (1.8 mM CaCl<sub>2</sub> [Junsei Chemical, 18230-1201], 5.3 mM KCl [USB Corporation, 20598], 0.8 mM MgSO<sub>4</sub> [Sigma-Aldrich, M7506], 117 mM NaCl [Biosesang, SR1009-250-00], 26 mM NaHCO<sub>3</sub> [Sigma-Aldrich, S6014], 1 mM NaH<sub>2</sub>PO<sub>4</sub> [Sigma-Aldrich, ]8282], and 5.6 mM D(+)-glucose [Junsei Chemical, 64220-0]01]) for the indicated durations.

The following antibodies were used for western blot (WB), immunofluorescence (IF) staining, or immunoprecipitation (IP): anti-eIF2 $\alpha$  (D-3) (Santa Cruz Biotechnology, sc-133132 [WB]), anti-GFP (B-2) (Santa Cruz Biotechnology, sc-9996 [WB]), anti-HA (Santa Cruz Biotechnology, sc-7392 [WB]), anti-lamin A/C (Santa Cruz Biotechnology, sc-6215 [WB]), anti-pan 14-3-3 (Santa Cruz Biotechnology, sc-133232 [WB]), anti-Beclin1 (Cell Signaling Technology, 3495S [WB]), anti-CHOP (Cell Signaling Technology, 2895S [WB]), anti-IRE1 $\alpha$  (Cell Signaling Technology, 3294S [WB]), anti-phospho-14-3-3 binding motif (Cell Signaling Technology, 9601S [WB]), anti-LC3A/B (Cell Signaling Technology, 4108S [IF]), anti-GSK3 $\beta$  (Cell Signaling Technology, 9832S [IF]), anti-PERK (Cell Signaling Technology, 3192S [WB]), anti-p70S6K (#2971S, WB), anti-phospho-Thr389-p70S6K (Cell Signaling Technology #9206S, WB), anti-mTOR (Cell Signaling Technology, 2983S [WB]), anti-phospho-Ser2448-mTOR (Cell Signaling Technology, 2971S [WB]), anti-phospho-TFEB (S211) (E9S8N) (Cell Signaling Technology, 37681S [WB]), anti-Histone H3 (Abcam, ab1791 [WB]), anti-phospho-eIF2 $\alpha$  (Abcam, ab32157 [WB]), anti- $\beta$ -actin (Sigma-Aldrich, A5441 [WB]), anti-FLAG (Sigma-Aldrich, F1804 [WB]), anti-LC3B (Sigma-Aldrich, L7543 [WB]), anti-TFEB (Sigma-Aldrich, HPA023881 [WB and IF]), anti-ATF4 (Proteintech, 10835-1-AP [WB]), anti-TFEB (Proteintech, 13372-1-AP [WB]), anti-ATF6 $\alpha$  (Proteintech, 24169-1-AP [WB]), anti-LAMP1 (Developmental Studies Hybridoma Bank, 1D4B-C [WB and IF]), anti-LAMP2 (Developmental Studies Hybridoma Bank, ABL-93-C [WB]), anti-cathepsin B (R&D Systems, AF965 [WB]), anti-cathepsin L (R&D Systems, AF1515 [WB]), anti-GFP (Clontech Laboratories, 632381 [WB]), anti-GFP (Invitrogen, A-11122 [IP]), anti-TFEB (Bethyl Laboratories, A303-673A [WB]), anti-TFEB (MyBioSource, MBS9125929 [IF]), anti-TFEB-phospho-Ser142 (Merck Millipore, ABE1971 [WB]), anti-XBP1s (BioLegend, 619502 [WB]), anti-ATF6 $\beta$  (BioLegend, 853201

[WB]), anti-HA.11 epitope tag (BioLegend, 901514 [WB and IF]), anti-KDEL (Enzo Life Sciences, ADI-SPA-827 [WB]), anti-p62 (Abnova, H00008878-M01 [WB]), and anti- $\alpha$ 1-antitrypsin (Dako, A0012 [WB]). The anti-TFE3 antibody was a gift from Professor Hiderou Yoshida (Department of Molecular Biochemistry, Graduate School of Life Science, University of Hyogo, Japan). The following secondary peroxidase- and fluorescence-conjugated antibodies were used: peroxidase-conjugated AffiniPure goat antirabbit IgG (H + L) (Jackson ImmunoResearch Laboratories, 111-035-003), peroxidase-conjugated AffiniPure F(ab')<sub>2</sub> fragment donkey antimouse IgG (H + L) (Jackson ImmunoResearch Laboratories, 751-036-151), peroxidase-conjugated AffiniPure rabbit antigoat IgG (H + L) (Jackson ImmunoResearch Laboratories, 305-035-003), peroxidase-conjugated AffiniPure goat antirat IgG (H + L) (Jackson ImmunoResearch Laboratories, 112-035-003), Alexa Fluor 594-conjugated AffiniPure F(ab')<sub>2</sub> fragment donkey antirabbit IgG (H + L) (Jackson ImmunoResearch Laboratories, 711-586-152), Alexa Fluor 594-conjugated AffiniPure F(ab')<sub>2</sub> fragment goat antimouse IgG (H + L) (Jackson ImmunoResearch Laboratories, 115-586-003), Alexa Fluor 647-conjugated AffiniPure F(ab')<sub>2</sub> fragment goat antimouse IgG (H + L) (Jackson ImmunoResearch Laboratories, 115-606-146), Alexa Fluor 488-conjugated goat antirabbit (Invitrogen, A-11034), Alexa Fluor 594-conjugated donkey antirat (Invitrogen, A-21209), and Alexa Fluor 647-conjugated goat antirat (Invitrogen, A-21247).

### Expression vectors

The plasmid (pcDNA3.1- $\alpha$ 1-antitrypsin mutant Z (ATZ)) expressing human ATZ carrying a missense mutation (substitution of lysine for glutamate at amino acid 342) was provided by Professor Randal J. Kaufman (Degenerative Diseases Program, Sanford Burnham Prebys Medical Discovery Institute, La Jolla, CA, USA).

The pGL4.14-5XCLEAR-Firefly luciferase plasmid (named 5xCLEAR luciferase reporter) used to measure the transcriptional activity of TFEB was constructed by inserting the nucleotide sequence of 5XCLEAR-CMVmini-TATA into the NheI- and XhoI-digested pGL4.14 vector (Promega, E669A). The nucleotide sequence of 5XCLEAR-CMVmini-TATA was GCTAGCCCGGCCACGTGGCCGCAGGGTCACGTGACCCTGCGCACCAGGTGGTGCTG CCCGTCACCTGACGGTGCGGCTCAGCTGAGCCCGTAGGCGTGACGGTGGGAGGCC TATATAAGCAGAGCTCGTTTAGTGAACCGTCAGATCGCCTGGACTCGAG (underlined sequences indicate the five CLEAR motifs and one TATA sequence).

To generate wild-type eIF2 $\alpha$ - and EGFP-expressing lentiviral vectors, pLEF-eIF2 $\alpha$ (WT)-IRES-Bla and pLEF-EGFP-IRES-Bla plasmids were constructed, respectively. pLEF-IRES-Bla was constructed by replacing the CMV promoter of pLVX-IRES-Bla [51] with the EF-1 $\alpha$  promoter of pEF-EGFP (Addgene, 11154). The Ssp1-EcoRI fragment containing the EF-1 $\alpha$  promoter from pEF-EGFP was inserted into pLVX-IRES-Bla treated with ClaI-

Klenow-EcoRI. To construct pLEF-eIF2 $\alpha$ (WT)-IRES-Bla, the Eco47III-EcoRI fragment containing eIF2 $\alpha$ (WT) from pBabe-eIF2 $\alpha$ (WT) [52] was inserted into pLEF-IRES-Bla treated with BamHI-Klenow-EcoRI. To construct pLEF-EGFP-IRES-Bla, the NotI-Klenow-EcoRI fragment containing EGFP from pEGFP-N1 (Clontech, 6085-1) was inserted into pLEF-IRES-Bla treated with BamHI-Klenow-EcoRI.

To construct pLEF-HA-Cas9-IRES-Bla, the HA-Cas9 fragment from p3s-Cas9-HN [53] treated with SacI-T4 DNA polymerase was inserted into pLEF-IRES-Bla treated with SmaI.

To express eIF2 $\alpha$ (S51A) (substitution of alanine for serine at amino acid 51), the 3xFLAG-fused eIF2 $\alpha$ (S51A)-expressing pLUB-3xFlag-eIF2 $\alpha$ (S51A)-IRES-Puro plasmid was constructed. First, pLUB-IRES-Puro was constructed by replacing the blasticidin S deaminase gene of pLUB-IRES-Bla [51] with the puromycin N-acetyltransferase gene of pLVX-AcGFP-N1 (Clontech, 632154). The cDNA fragment encoding puromycin N-acetyltransferase was amplified from the pLVX-AcGFP-N1 vector via PCR with the following primers: 5'-TTTAAACCACAACCATGGCCGAGTACAAGCCC-3' and 5'-TTTAAAGCTTAGCTCAGGCACCGGGCTTGCG-3'. The PCR product treated with BstXI and BlnI was inserted into pLUB-IRES-Bla treated with the same restriction enzymes to construct pLUB-IRES-Puro. To generate the eIF2 $\alpha$ (S51A) sequence of the pLUB-3xFlag-eIF2 $\alpha$ (S51A)-IRES-Puro plasmid, pShuttle-CMV-eIF2 $\alpha$ (S51A) was first constructed. The coding sequence of eIF2 $\alpha$ (S51A) was amplified from pBabe-eIF2 $\alpha$ (S51A) [52] via PCR with the following primers: 5'-TTTCTCGGTACCACCATGCCGGGGCTAAG-3' and 5'-TTTATCCTCGAGCGTTAATCTTCAGCTTTGGC-3'. The PCR product treated with KpnI and XhoI was inserted into pShuttle-CMV (Addgene, 16403) treated with the same restriction enzymes to construct pShuttle-CMV-eIF2 $\alpha$ (S51A). Next, the cDNA fragment encoding eIF2 $\alpha$ (S51A) was transferred into p3xFlag-CMV-10 (Sigma-Aldrich, 32190102) to add an N-terminal 3xFLAG tag. The cDNA fragment encoding eIF2 $\alpha$ (S51A) was amplified from pShuttle-CMV-eIF2 $\alpha$ (S51A) via PCR with the following primers: 5'-TTTTTTAAGCTTCCGGGGCTAAGTTGTAGATT-3' and 5'-TTTAAAGAATTCTTAATCTTCAGCTTTGGCTTCC-3'. The PCR product treated with HindIII and EcoRI was inserted into p3xFlag-CMV treated with the same restriction enzymes to construct p3xFlag-CMV-eIF2 $\alpha$ (S51A). Finally, the cDNA fragment encoding 3xFLAG-eIF2 $\alpha$ (S51A) was amplified from p3xFlag-CMV-eIF2 $\alpha$ (S51A) via PCR with the following primers: 5'-AAAGGGTTCGAAATGGACTACAAAGACCATGACG-3' and 5'-TTTGGGGGATCCTTAATCTTCAGCTTTGGCTTCC-3'. The PCR product treated with BstBI and BamHI was inserted into pLUB-IRES-Puro treated with the same restriction enzymes to construct the pLUB-3xFlag-eIF2 $\alpha$ (S51A)-IRES-Puro plasmid.

To generate wild-type eIF2 $\alpha$ - and mutant eIF2 $\alpha$ (S51A)-expressing adenoviral vectors, pShuttle-CMV-eIF2 $\alpha$ (WT) and pShuttle-CMV-eIF2 $\alpha$ (S51A) plasmids were constructed,

respectively. The construction strategy for the pShuttle-CMV-eIF2 $\alpha$ (S51A) plasmid was described above. To construct pShuttle-CMV-eIF2 $\alpha$ (WT), the cDNA fragment encoding wild-type eIF2 $\alpha$  was amplified from pBabe-eIF2 $\alpha$ (WT) via PCR with the following primers: 5'-AAATTTAAGCTTATGCCGGGGCTAAGTTGTAG-3' and 5'-AAATTTGAATTCTTAATCTTCAGCTTTGGCTTCC-3'. The PCR product treated with KpnI and XhoI was inserted into pShuttle-CMV treated with the same restriction enzymes to construct the pShuttle-CMV-eIF2 $\alpha$ (WT) plasmid.

The human TFEB fused with EGFP-expressing pLUB-TFEB-EGFP-IRES-Bla and EGFP-expressing pLUB-EGFP-IRES-Bla plasmids were described elsewhere [51].

To generate human C-terminally 3xFLAG-tagged wild-type TFEB- and mutant TFEB(S211A)-expressing adenoviral vectors, pShuttle-CMV-TFEB-3xFlag and pShuttle-CMV-TFEB(S211A)-3xFlag plasmids were constructed, respectively. pCMV-TFEB-3xFlag was constructed by inserting the cDNA fragment encoding human TFEB from pEGFP-N1-TFEB (Addgene, 38119) treated with BglII and KpnI into p3xFlag-CMV-14 (Sigma-Aldrich, E7908) treated with the same restriction enzymes. To construct pShuttle-CMV-TFEB-3xFlag, the cDNA fragment encoding TFEB-3xFLAG was amplified from pCMV-TFEB-3xFlag via PCR with the following primers: 5'-TTAGTAAGATCTCGAGCTCAAGCTTG-3' and 5'-TTAGTAGCGGCCGCTACTTGTTCATCGTCATCCTT-3'. The PCR product treated with BglII and NotI was inserted into pShuttle-CMV treated with the same restriction enzymes to construct pShuttle-CMV-TFEB-3xFlag. pShuttle-CMV-TFEB(S211A)-3xFlag was constructed by inserting the cDNA fragment encoding TFEB(S211A) from pcDNA3.1-TFEB(S211A)-MYC (Addgene, 805) treated with EcoRI-HindIII-Klenow into pShuttle-CMV-TFEB-3xFlag treated with BglII-Sall-Klenow.

To express UPR TFs (ATF4, XBP1s, ATF6 $\alpha$ (1-373) and ATF6 $\beta$ (1-393)), pCGN-vector, pCGN-ATF6 $\alpha$ (1-373), pCGN-IRES-DsRed2, pCGN-ATF4-IRES-DsRed2, pCGN-XBP1s-IRES-DsRed2, pCGN-ATF6 $\alpha$ (1-373)-IRES-DsRed2, and pCGN-ATF6 $\beta$ (1-393)-IRES-DsRed2 were used. The pCGN-ATF6 $\alpha$ (1-373) plasmid encoding the N-terminal domain of human ATF6 $\alpha$  (aa 1–373) with an haemagglutinin (HA) epitope tag at the N-terminus was described previously [54]. To generate the pCGN-vector, the pCGN-ATF6 $\alpha$ (1-373) plasmid was treated with XbaI and BamHI to remove the ATF6 $\alpha$  (aa 1–373) coding sequence, and the linearized empty vector was self-ligated. The internal ribosome entry site (IRES)-driven *Discosoma Sp.* red fluorescent protein (DsRed2)-expressing plasmid (pCGN-IRES-DsRed2) was constructed by replacing EGFP of pCGN-IRES-EGFP [54] with DsRed2 of pDsRed2-Nuc (Clontech, 632408). To construct pCGN-IRES-DsRed2, the cDNA fragment encoding DsRed2 was amplified from pDsRed2-Nuc via PCR with the following primers: 5'-TTTTTTCCACAACCATGGCCTCCTCCGAGAACG-3' and 5'-TTTTTTTCGGCCGTACAGGAACAGGTGGTGGCGG-3'. The PCR product treated with BstXI



and EagI was inserted into pCGN-IRES-EGFP treated with the same restriction enzymes to construct pCGN-IRES-DsRed2. pCGN-ATF4-IRES-DsRed2, pCGN-XBP1s-IRES-DsRed2, pCGN-ATF6 $\alpha$ (1-373)-IRES-DsRed2, and pCGN-ATF6 $\beta$ (1-393)-IRES-DsRed2 were constructed by replacing the IRES-EGFP of pCGN-ATF4-IRES-EGFP, pCGN-XBP1s-IRES-EGFP, pCGN-ATF6 $\alpha$ (1-373)-IRES-EGFP, and pCGN-ATF6 $\beta$ (1-393)-IRES-EGFP [54] with IRES-DsRed2 of pCGN-IRES-DsRed2, respectively. The IRES-DsRed2 fragment obtained from pCGN-IRES-DsRed2 treated with EagI-Klenow-Sall was inserted into vectors treated with the same enzymes.

To generate the HA-ATF6 $\alpha$ (1-373)-expressing adenoviral vector (named pShuttle-CMV-HA-ATF6 $\alpha$ (1-373)), the BamHI-Klenow-NdeI fragment containing CMV-HA-ATF6 $\alpha$ (1-373) from pCGN-ATF6 $\alpha$ (1-373) was inserted into pShuttle-CMV treated with XhoI-Klenow-NdeI.

The HA-tagged 14-3-3-expressing plasmid (pcDNA3.1-HA-14-3-3) was obtained from Professor Eek-Hoon Jho (Department of Life Science, University of Seoul, Seoul, Korea) [55].

### **Transfection and virus production**

Cells were transfected with plasmids using Mirus Bio™ TransIT™-LT1 transfection reagent (Fisher Scientific, MIR2306) according to the manufacturer's instructions for 24–36 h (as described in each figure legend).

Recombinant adenoviruses expressing wild-type eIF2 $\alpha$ , mutant eIF2 $\alpha$ (S51A), TFEB-3xFLAG, TFEB(S211A)-3xFLAG, and HA-ATF6 $\alpha$ (1-373) were generated using the AdEasy vector system according to the manufacturer's instructions (Agilent Technologies, 240009). In brief, BJ5183 cells were cotransformed with the shuttle vector (pShuttle-CMV-eIF2 $\alpha$ (WT), pShuttle-CMV-eIF2 $\alpha$ (S51A), pShuttle-CMV-TFEB-3xFlag, pShuttle-CMV-TFEB(S211A)-3xFlag, or pShuttle-CMV-HA-ATF6 $\alpha$ (1-373)) and the viral DNA plasmid pAdEasy-1 to generate a recombinant adenoviral plasmid. Then, HEK-293A cells were transfected with the recombinant adenoviral plasmids using the calcium phosphate technique to produce viral particles, which were purified using CsCl (Sigma-Aldrich, 3032) gradient centrifugation. The viral titer was determined using an AdEasy Viral Titer Kit (Aligent Technologies, 972500) according to the manufacturer's instructions.

To produce lentiviral particles expressing eIF2 $\alpha$ (WT), EGFP, HA-Cas9, or 3xFLAG-eIF2 $\alpha$ (S51A), Lenti-X-293T cells (Clontech Laboratories, 632180) were cotransfected with each lentiviral construct (pLEF-eIF2 $\alpha$ (WT)-IRES-Bla, pLEF-EGFP-IRES-Bla, pLEF-HA-Cas9-IRES-Bla, or pLUB-3xFlag-eIF2 $\alpha$ (S51A)-IRES-Puro) and a third-generation lentiviral packaging system (pRSV-Rev, pMD2-VSVG, and pMDLg/pRRE plasmids) using Mirus Bio™ TransIT™-LT1 transfection reagent. On the third day after transfection, lentiviruses were

collected from the supernatant of Lenti-X-293T cells, diluted in complete medium containing 8 µg/mL polybrene, and infected into cells for 48 h.

### Cell lines and cell culture

All cell lines were incubated at 37°C in a humidified incubator containing 5% CO<sub>2</sub>. Immortalized hepatocytes (*S/S<sup>Hep</sup>* and *A/A<sup>Hep</sup>*) were cultured in Medium 199 (WeiGENE, LM 006-01) supplemented with 10% fetal bovine serum (FBS; WeiGENE, S 001-07) and 1% penicillin-streptomycin (WeiGENE, LS 202-02) as previously described [56]. MEFs (*S/S<sup>MEF</sup>*, *A/A<sup>MEF</sup>*, *perk<sup>+/+</sup>*, and *perk<sup>-/-</sup>*) were grown in Dulbecco's modified Eagle's medium (DMEM; WeiGENE, LM 001-05) supplemented with 10% FBS, 1% penicillin-streptomycin, 2% MEM amino acids (WeiGENE, LS 004-01), and 1% MEM nonessential amino acids (WeiGENE, LS 005-01) [57]. The HeLa cell line (Korean Cell Line Bank, 10002) was cultured in MEM Alpha medium (Sigma-Aldrich, M0894) supplemented with 4.4 mg/mL sodium bicarbonate (Sigma-Aldrich, S6014), 10% FBS, and 1% penicillin-streptomycin.

Generation of TFEB-EGFP- or EGFP-expressing *S/S<sup>MEF</sup>* and *A/A<sup>MEF</sup>* stable cell lines (named *S/S-EGFP*, *S/S-TFEB-EGFP*, *A/A-EGFP*, and *A/A-TFEB-EGFP*) was previously described [51]. Briefly, *S/S<sup>MEF</sup>* or *A/A<sup>MEF</sup>* cells were infected with lentiviral particles containing the pLUB-EGFP-IRES-Bla or pLUB-TFEB-EGFP-IRES-Bla construct. Then, each stable cell line was isolated by blasticidin selection. Cells were maintained in DMEM supplemented with 10% FBS, 1% penicillin-streptomycin, 1% MEM nonessential amino acids, and 5 µg/mL blasticidin S HCl (Invitrogen, R21001).

eIF2α phosphorylation-deficient HeLa cells were generated using CRISPR/Cas9 genome editing technology. A HA-Cas9-expressing HeLa stable cell line (named HeLa-Cas9) was first generated by infecting HeLa cells with lentiviral particles containing pLEF-HA-Cas9-IRES-Bla. HA-Cas9-expressing HeLa stable cell lines were isolated by blasticidin selection (4 µg/mL [Invitrogen, R21001]). Among several HA-Cas9-positive clones identified, one stable cell line that showed high expression and nuclear localization of HA-Cas9 was chosen for subsequent experiments. Next, a HeLa-Cas9 cell line expressing 3xFLAG-eIF2α(S51A) was generated by infecting HeLa-Cas9 cells with lentiviral particles containing pLUB-3xFLAG-eIF2α(S51A)-IRES-Puro. An HA-Cas9- and 3xFLAG-eIF2α(S51A)-overexpressing HeLa stable cell line [named HeLa-Cas9/eIF2α(S51A)OE] was isolated by double selection with both blasticidin (2 µg/mL [Invitrogen, R21001]) and puromycin (5 µg/mL [Santa Cruz Biotechnology, sc-108071]). Selection was confirmed by WB analysis using anti-FLAG (Sigma-Aldrich, F1804) and anti-eIF2α (D-3) (Santa Cruz Biotechnology, sc-133132) antibodies. Microscopic observation using an anti-FLAG antibody (Sigma-Aldrich, F1804) was conducted to check the cytosolic expression of 3xFLAG-eIF2α(S51A) in HeLa-Cas9/eIF2α(S51A)OE cells. Two CRISPR-Cas9 guide RNA target sequences to delete exon

2 of eIF2 $\alpha$  were identified bioinformatically using the CRISPR Design Tool available at <http://www.rgenome.net/>. The targeting sequences were CTCCAAGACCTAAGGATTAA for sgRNA1 and GGATCTTGATAATTGACTCA for sgRNA2. Custom-designed Alt-R<sup>®</sup> CRISPR-Cas9 crRNA (Integrated DNA Technologies, Inc.) and Alt-R<sup>®</sup> CRISPR-Cas9 tracrRNA (Integrated DNA Technologies, Inc., 1072532) were used to generate a functional gRNA duplex. HeLa-Cas9/eIF2 $\alpha$ (S51A) cells were nucleofected, with both sgRNA1 and sgRNA2 duplexes using a SE Cell Line 4D-Nucleofector<sup>™</sup> X Kit S (Lonza, V4XC-1032) on a 4D-Nucleofector<sup>®</sup> X Unit (Lonza, AAF-1003X) with program CN-114 according to the manufacturer's instructions. Nucleofected cells were seeded as single clones (one cell/well) in 96-well plates. After 3–4 weeks, clones were screened for expression of eIF2 $\alpha$  and phosphorylated eIF2 $\alpha$  proteins by WB analysis. Sequencing was performed to confirm that the selected clone [named HeLa-Cas9/eIF2 $\alpha$ (S51A)OE/eIF2 $\alpha$  KO] expressed 3xFLAG-eIF2 $\alpha$ (S51A) but not endogenous eIF2 $\alpha$ .

Wild-type eIF2 $\alpha$ - or EGFP-expressing *A/A*<sup>MEF</sup> stable cell lines were generated by infecting *A/A*<sup>MEF</sup> cells with lentiviral particles containing pLEF-eIF2 $\alpha$ (WT)-IRES-Bla or pLEF-EGFP-IRES-Bla, respectively. Infected *A/A*<sup>MEF</sup> cells were cultured in medium containing blasticidin (5  $\mu$ g/mL [Invitrogen, R21001]) to establish *A/A*<sup>MEF</sup>-eIF2 $\alpha$  or *A/A*<sup>MEF</sup>-EGFP stable cell lines. They were maintained in DMEM (WeiGENE, LM 001-05) supplemented with 10% FBS (WeiGENE, S 001-07), 1% penicillin-streptomycin (WeiGENE, LS 202-02), 1% MEM nonessential amino acids (WeiGENE, LS 005-01), and 5  $\mu$ g/mL blasticidin S HCl (Invitrogen, R21001).

### **Subcellular fractionation**

Cells were grown in 100 mm cell culture dishes until they reached about 90% confluency and were then treated with dimethyl sulfoxide (DMSO, mock) or Tm for the indicated durations. After harvesting cells, the nuclear and cytoplasmic fractions were separated using a previously described procedure [51]. The protein concentration was calculated, and the fractions underwent WB analysis.

### **Co-Immunoprecipitation (Co-IP) assay**

*S/S*- and *A/A-TFEB-EGFP* MEFs were plated in 100 mm culture dishes at a density of  $7 \times 10^5$  cells/dish for longer than 16 h and treated with the specified chemicals for the indicated durations. In HA-ATF6 $\alpha$ (1-373) overexpression experiments, *A/A-TFEB-EGFP* MEFs were plated in 100 mm culture dishes at a density of  $7 \times 10^5$  cells/dish. The next day, cells were transfected with pCGN-vector or pCGN-ATF6 $\alpha$ (1-373) for 24 h and treated with Mock or Tm (100 ng/mL) for 24 h. IP of TFEB-EGFP from *A/A-TFEB-EGFP* MEFs was performed using an anti-GFP antibody (Invitrogen) as described previously [51].

*perk*<sup>+/+</sup> and *perk* KO (*perk*<sup>-/-</sup>) MEFs were plated in 100 mm culture dishes at a density of  $7 \times 10^5$  cells/dish. The next day, cells were transfected with pLUB-TFEB-EGFP-IRES-Bla and pcDNA3.1-HA-14-3-3 for 24 h and treated with Tm (1  $\mu$ g/mL) for 16 h. They were collected in complete growth medium and washed once with phosphate-buffered saline (PBS; 137 mM NaCl [Biosesang, SR1009-250-00], 2.7 mM KCl [USB Corporation, 20598, discontinued], 1.8 mM KH<sub>2</sub>PO<sub>4</sub> [Junsei, 84185-0350], and 10 mM Na<sub>2</sub>HPO<sub>4</sub> [FUJIFILM Wako Pure Chemical Corporation, 197-02865], pH 7.4). The pellets were dissolved in 300  $\mu$ L IP lysis buffer (20 mM Tris-HCl, pH 7.5 [Biosesang, TR2016-050-75], 150 mM NaCl, 1% Triton X-100 [Sigma-Aldrich, T8787], 1 mM EDTA [Thermo Fisher Scientific, 1861275], 1 mM EGTA [BioShop Canada Inc., EDT 001], 2.5 mM sodium pyrophosphate [Sigma-Aldrich, P8010], 1 mM  $\beta$ -glycerophosphate [Sigma-Aldrich, G5422], and 1 mM sodium orthovanadate [Sigma-Aldrich, S6508]) supplemented with Halt Protease Inhibitor Cocktail (Thermo Fisher Scientific, 1861279) at 1 $\times$  final concentration. Cells were lysed by passing the samples through a 26G needle ten times. Cell lysates were kept on ice for 30 min and centrifuged at 13000  $\times$ g for 15 min at 4°C to collect soluble fractions. Then, 1.2 mg protein lysate and 2  $\mu$ g/mL anti-GFP antibody (Invitrogen, A-11122) were diluted in 600  $\mu$ L IP lysis buffer and rotated at 4°C for 6 h. The protein lysate-antibody complexes were transferred to 40  $\mu$ L protein A/G agarose beads (Thermo Fisher Scientific, 20423) (which had been cleaned with 700  $\mu$ L IP lysis buffer containing 5% bovine serum albumin [BSA {Sigma-Aldrich, A7030}] overnight at 4°C) and incubated with rotation for an additional 2 h at 4°C. After incubation, the beads were washed five times with 1 mL IP lysis buffer. Samples were eluted in 40  $\mu$ L of 2 $\times$  sodium dodecyl sulfate (SDS) sample loading buffer (100 mM Tris-HCl [VWR Life Science, 0497], pH 6.8, 200 mM DTT [Promega, V3151], 4% SDS [Promega, H5114], 20% glycerol [USB Corporation, 16374], and 0.2% bromophenol blue [Sigma-Aldrich, B-5525]); boiled at 100°C for 5 min; and separated by SDS-PAGE.

### **WB analysis**

Cells were lysed in Nonidet P40 lysis buffer (1% IGEPAL CA-630 [NP40 {Sigma-Aldrich, I8896}], 50 mM Tris-HCl pH 7.5, 150 mM NaCl, 0.05% SDS, 0.5 mM sodium orthovanadate, 100 mM NaF [Sigma-Aldrich, 201154], 50 mM  $\beta$ -glycerophosphate, and Halt Protease Inhibitor Cocktail). Cell lysates were centrifuged at 13,000  $\times$ g for 15 min at 4°C, and supernatants were collected. For WB analysis of ATF6 $\alpha$  and ATF6 $\beta$ , S/S<sup>Hep</sup> and A/A<sup>Hep</sup> cells were treated with Tm for the indicated durations and then with MG132 (20  $\mu$ M) for 1 h before harvesting samples. Cells were directly lysed in SDS lysis buffer (1% SDS, 50 mM Tris-Cl pH 7.5, 150 mM NaCl, 0.5 mM sodium orthovanadate, 100 mM NaF, and 50 mM  $\beta$ -glycerophosphate) supplemented with Halt Protease Inhibitor Cocktail (Thermo Fisher Scientific, 1861279). The lysates were immediately heated for 15 min at 100°C. The

homogenates were centrifuged at 13,000  $\times g$  for 15 min at 4°C, and the supernatants were collected. Protein concentrations were determined using a Pierce™ BCA Protein Assay Kit (Thermo Fisher Scientific, 23227). Cell lysates were subjected to WB analysis as described previously [51].

### **RNA isolation and quantitative real-time polymerase chain reaction**

Total RNA was isolated from *S/S<sup>Hep</sup>* and *A/A<sup>Hep</sup>* cells treated with Tm for the indicated durations using QIAzol Lysis reagent (QIAGEN, QI-79306). cDNA was synthesized with a High-Capacity cDNA RT Kit (Applied Biosystems, ABS-4368814). Quantitative PCR was performed with Luna® Universal qPCR Master Mix (New England BioLabs, M3003X) and a StepOnePlus Real Time System (Applied Biosystems, CA, USA). The specificity of each primer pair was confirmed by melting curve analysis. The levels of target mRNAs were normalized to that of  *$\beta$ -actin* mRNA. The primer pairs and references used in this study are listed in Table S1.

### **Dual luciferase assay**

The 5XCLEAR luciferase assay was performed to representatively assess the activities of TFEB-regulated genes. *S/S<sup>MEF</sup>* and *A/A<sup>MEF</sup>* cells were cultured overnight in 6-well plates at a density of  $6 \times 10^4$  cells/dish. Both pGL4.14-5XCLEAR-Firefly luciferase (for 5XCLEAR motif-driven fire luciferase) and pRL-CMV (for CMV promoter-driven *Renilla* luciferase) plasmids were transfected using Mirus Bio™ TransIT™-LT1 transfection reagent (Fisher Scientific, MIR2306). CMV promoter-driven *Renilla* luciferase was used to normalize the transfection and expression efficiencies. If necessary, the other indicated constructs (pCGN vectors [pCGN-IRES-DsRed2, pCGN-ATF4-IRES-DsRed2, pCGN-XBP1s-IRES-DsRed2, pCGN-ATF6 $\alpha$ (1-373)-IRES-DsRed2, or pCGN-ATF6 $\beta$ (1-393)-IRES-DsRed2] or pShuttle vectors [pShuttle-CMV, pShuttle-CMV-TFEB-3xFlag, or pShuttle-CMV-TFEB(S211A)-3xFlag]) were also cotransfected for 30 h according to the manufacturer's instructions. After the chemical treatments, cells were washed once with PBS and harvested for luciferase assays using the Dual-Luciferase assay system (Promega, E1980) according to the manufacturer's instructions. Chemiluminescent signals were measured using a Synergy HTX Multi-Mode Microplate Reader (Biotek Instruments, Winooski, VT, USA). Firefly luciferase activity was normalized to *Renilla* luciferase activity for each sample. The presented data were replicated in at least three independent experiments.

### **Live cell imaging using confocal microscopy**

Cells were plated on collagen-coated 35 mm glass bottom confocal dishes (SPL Life Science, 101350) at a density of  $1 \times 10^5$  cells/dish. The next day, cells were treated with DMSO (mock) or Tm (1  $\mu g/mL$ ) in phenol-red free M199 culture medium (GIBCO, 11043023) for the indicated

durations. In HA-ATF6 $\alpha$ (1-373) or TFEB(S211A)-FLAG overexpression experiments, cells were infected with the indicated recombinant adenoviruses (Ad-vector, Ad-HA-ATF6 $\alpha$ (1-373), or Ad-TFEB(S211A)-Flag) for 24 h before Tm treatment. During the last 30 min of the chemical treatment, the cell culture medium was supplemented with LysoTracker Red DND-99 (100 nM) and Hoechst 33258 (10  $\mu$ g/mL) to stain lysosomes and nuclei, respectively. Live cell imaging was performed using an FV1200-OSR microscope (Olympus, Shinjuku, Japan). The intensity of LysoTracker Red staining was measured using the mean fluorescence intensity (MFI) tool of FV10-ASW-4.2 software (Olympus).

### **IF staining**

Cells were plated on collagen-coated glass coverslips in 6-well dishes and cultured overnight. In experiments overexpressing specific proteins, cells were transfected with the indicated plasmids (pCGN-IRES-DsRed2, pCGN-ATF4-IRES-DsRed2, pCGN-XBP1s-IRES-DsRed2, pCGN-ATF6 $\alpha$ (1-373)-IRES-DsRed2, or pCGN-ATF6 $\beta$ (1-393)-IRES-DsRed2) or infected with the indicated recombinant adenoviruses (Ad-vector, Ad-HA-ATF6 $\alpha$ (1-373), Ad-eIF2 $\alpha$ (WT), Ad-eIF2 $\alpha$ (S51A), Ad-TFEB(WT)-Flag, or Ad-TFEB(S211A)-Flag) for 24 h before Tm treatment. Cells were treated with the indicated chemicals for the indicated durations, rinsed twice with PBS, fixed with 4% paraformaldehyde diluted in PBS for 15 min, and permeabilized with 0.1% Triton X-100 (Sigma-Aldrich, T8787) diluted in PBS for 5 min. To visualize LC3A/B, p62, and LAMP1 puncta, cells on coverslips were fixed with 100% methanol (SK Chemical, L260-18) for 10 min at -20°C, washed twice with PBS, blocked with 3% BSA (Sigma-Aldrich, A7030) diluted in PBS for 1 h, and incubated with the indicated primary antibodies (labeled as “IF” in the antibody description section) overnight at 4°C. Cells were incubated with fluorescence-conjugated secondary antibodies for 1 h at room temperature. Nuclei were stained with DAPI (Invitrogen, D1306). Finally, coverslips were mounted using ProLong Gold mounting medium (Invitrogen, P36930). Cells were observed by confocal laser microscopy using a FV1200-OSR microscope (Olympus). Images in colocalization experiments of HA-ATF6 $\alpha$ (1-373) and TFEB-EGFP were obtained using Airyscan super-resolution mode with a Zeiss LSM-780 inverted confocal laser scanning microscope (Carl Zeiss Microscopy, Germany) using a Plan-Apochromat 100 $\times$ /1.46 oil immersion objective lens, and were processed and analyzed with ZEN 2 (Carl Zeiss Microscopy). Colocalization of LC3A/B and p62, p62 and LAMP1, or LC3A/B and LAMP1 was measured using the Pearson’s Correlation Coefficient calculator tool of FV10-ASW-4.2 software (Olympus).

### **Transmission electron microscopy (TEM) analysis**

Cells were seeded in 100 mm culture dishes at a density of  $7 \times 10^4$  cells/dish, cultured for at least 16 h, and then treated with Tm (1  $\mu$ g/mL) for 24 h. In experiments overexpressing HA-

ATF6 $\alpha$ (1-373) or TFEB(S211A)-FLAG, cells were infected with the indicated recombinant adenoviruses (Ad-vector, Ad-HA-ATF6 $\alpha$ (1-373), or Ad-TFEB-(S211A)-Flag) for 24 h before Tm treatment. Cells on dishes were washed twice with 0.1 M phosphate buffer (0.02 M NaH<sub>2</sub>PO<sub>4</sub> [Sigma-Aldrich, S8282] and 0.08 M Na<sub>2</sub>HPO<sub>4</sub> [FUJIFILM Wako Pure Chemical Corporation, 197-02865], pH 7.4), and were fixed by immersion in 2.5% glutaraldehyde (Electron Microscopy Sciences, 16220) diluted in 0.1 M phosphate buffer for 2 h at room temperature. Cells were rinsed twice with 0.1 M phosphate buffer and postfixed with 1% osmium tetroxide (Sigma-Aldrich, 75632) diluted in 0.1 M phosphate buffer for 1 h at 4°C. Next, samples were dehydrated with a series of graded ethyl alcohol solution (Merck Millipore, 1.00983) and then with acetone (Fisher Scientific, A18-4). The samples were next embedded in EPON 812. Ultrathin sections (70–80 nm) were obtained using an ultramicrotome (Leica Ultracut UCT, Wetzlar, Germany), costained with uranyl acetate (Fisher Scientific, NC1375332) and lead citrate (Fisher Scientific, NC1588038), and examined using a transmission electron microscope (JEM-1010; JEOL, Tokyo, Japan) at 60 kV.

#### **Measurement of intracellular Ca<sup>2+</sup> concentrations**

MEFs were plated on 0.1% gelatin-coated microscope cover glasses (Paul Marienfeld GmbH & Co. KG, 0111550) at a density of  $7 \times 10^4$  cells/dish and cultured overnight. Cells were loaded with 1  $\mu$ M Fura-2/AM (Thermo Fisher Scientific, F1221) in DMEM at 37°C for 30 min. Ratiometric Ca<sup>2+</sup> imaging was performed at 340 and 380 nm in 2 mM Ca<sup>2+</sup> Tyrode's solution (129 mM NaCl, 5 mM KCl, 2 mM CaCl<sub>2</sub>, 1 mM MgCl<sub>2</sub>, 30 mM glucose, and 25 mM HEPES) containing Tm (10  $\mu$ g/mL) using an IDX81 fluorescence microscope (Olympus) equipped with an Olympus 40 $\times$  oil objective lens (NA 1.30), a fluorescent arc lamp (Sutter Instrument, LAMBDA LS), an excitation filter wheel (Sutter Instrument, LAMBDA 10-2), a stage controller (Applied Scientific, MS-2000), and a CCD camera (Hamamatsu, C10600) at room temperature. Images were acquired for 5 min with a time interval of 4 s. Fluorescence intensity profiles were processed with MetaMorph (Molecular Devices, San Jose, CA, USA) and analyzed with Igor software (WaveMetrics, Portland, OR, USA).

#### **Proximity Ligation Assay (PLA)**

*A/A-TFEB-EGFP* MEFs were plated on collagen-coated glass coverslips in 6-well dishes at a density of  $1 \times 10^5$  cells/dish, cultured overnight, transfected with pCGN-vector or pCGN-ATF6 $\alpha$ (1-373) for 30 h, and treated with Tm (100 ng/mL) for 16 h. Thereafter, cells were rinsed twice with PBS, fixed with 3.5% paraformaldehyde diluted in PBS for 15 min, and permeabilized with 0.1% Triton X-100 diluted in PBS for 5 min. Finally, cells were blocked with 3% BSA diluted in PBS for 1 h and incubated with primary antibodies (anti-GFP [Invitrogen, A-11122] and anti-HA [Santa Cruz Biotechnology, sc-7392]) overnight at 4°C. The PLA was

performed using a Duolink In Situ Red Starter Kit (Sigma-Aldrich, DUO92101) according to the manufacturer's protocol. Images were obtained using an FV1200-OSR microscope (Olympus). Cells were classified into three groups, namely, those with PLA-positive signals in the nucleus, the nucleus and cytosol, or the cytosol. The ratio of the MFI in the nucleus to that in the cytosol was quantified using CellProfiler software (<https://cellprofiler.org/>, Broad institute, USA). This ratio was  $\geq 1.2$ ,  $\leq 0.7$  and  $< 1.2$ , and  $< 0.7$  in the nucleus, nucleus and cytosol, and cytosol groups, respectively. The PLA signal in the nucleus was measured using the MFI tool of FV10-ASW-4.2 software (Olympus).

### **Statistical analysis**

All data are presented as mean  $\pm$  standard error of the mean (SEM). Data were analyzed using GraphPad Prism 5 (GraphPad Software, San Diego, CA, USA). The statistical significance of differences between groups was evaluated using the unpaired two-tailed Student's t-test.  $p < 0.05$  was considered statistically significant.



**Table 1. List of primers for qPCR**

<b>Genes</b>	<b>Species</b>	<b>Forward primer (5' to 3')</b>	<b>Reverse primer (5' to 3')</b>
<i>ATF6a</i>	Human	GCCTTTATTGCTTCCAGCAG	TGAGACAGCAAACCGTCTG
<i>Atf4</i>	Mouse	ATGGCCGGCTATGGATGAT	CGAAGTCAAACCTTTTCAGATCCATT
<i>Chop</i>	Mouse	CTGCCTTTACCTTGGAGAC	CGTTTCCTGGGGATGAGATA
<i>Gadd34</i>	Mouse	CCCGAGATTCTCTAAAAGC	CCAGACAGCAAGGAAATGG
<i>Asns</i>	Mouse	TACAACCACAAGGCGCTACA	AAGGGCCTGACTCCATAGGT
<i>Cth1</i>	Mouse	TCTTGCTGCCACCATTACGA	GCCTCCATACACTTCATCCAT
<i>Xbp1t</i>	Mouse	CCTGAGCCCGGAGGAGAA	CTGCACCTGCTGCGGAC
<i>Xbp1s</i>	Mouse	GAGTCCGCAGCAGGTG	AGGCTTGGTGTATACATGG
<i>BiP</i>	Mouse	TCATCGGACGCACTTGA	CAACCACCTTGAATGGCAAGA
<i>Lc3b</i>	Mouse	CGTCCTGGACAAGACCAAGT	ACCATCTACAGGAAGCCGTC
<i>P62</i>	Mouse	GCTGCCCTATACCCACATCT	CGCCTTCATCCGAGAAAC
<i>Uvrag</i>	Mouse	CAAGCTGACAGAAAAGGAGCGAG	GGAAGAGTTTGCCTCAAGTCTGG
<i>Atp6v1h</i>	Mouse	GGATGCTGCTGTCCCACTAA	TCTCTTGCTTGTCTCGGAAC
<i>Lamp1</i>	Mouse	ACCTGTGAGTGGCAACTTCA	GGGCACAAGTGGTGGTGAG
<i>Lamp2a</i>	Mouse	GCAGTGCAGATGAAGACAAC	AGTATGATGGCGCTTGAGAC
<i>Lamp2b</i>	Mouse	GGTGTGGTCTTTCAGGCTTGATT	ACCACCCAATCTAAGAGCAGGACT
<i>Lamp2c</i>	Mouse	ATGTGCTGCTGACTCTGACCTCAA	TGGAAGCACGAGACTGGCTTGATT
<i>Cathepsin B</i>	Mouse	ACAGTGCCACACAGCTTCTTC	TCCTTGATCCTTCTTTCTTGCC
<i>Cathepsin D</i>	Mouse	CTGAGTGGCTTCATGGGAAT	CCTGACAGTGGAGAAGGAGC
<i>Cathepsin L</i>	Mouse	ATCAAACCTTTAGTGCAGAGTG	CTGTATTCCCCGTTGTGTAGC
<i>Mcolin-1</i>	Mouse	GCTGGGTTACTCTGATGGGTC	CCACCACGGACATAGGCATAC
<i>Glb1</i>	Mouse	AAATGGCTGGCAGTCCTTCTG	ACCTGCACGGTTATGATCGGT
<i>Hexb</i>	Mouse	CTGGTGTGCTAGTGTGCGC	CAGGGCCATGATGTCTCTTGT
<i>Tpp1</i>	Mouse	CCCCTCATGTGGATTTTGTGG	TGGTTCTGGACGTTGTCTTGG
<i>mTfeb</i>	Mouse	CCTGCCGACCTGACTCAGA	CTCAATTAGGTTGTGATTGTCTTTCTTC
<i>hTfeb</i>	Human	ACCTGTCCGAGACCTATGGG	CGTCCAGACGCATAATGTTGTC
<i>mTfe3</i>	Mouse	CCTGAAGGCATCTGTGGATT	TGTAGGTCCAGAAGGGCATC
<i>β-actin</i>	Mouse	GATCTGGCACCACACCTTCT	GGGGTGTGAAGGTCTCAA

## Results

### Deficiency of eIF2 $\alpha$ phosphorylation dysregulates expression of autophagy and UPR genes during ER stress

I investigated whether eIF2 $\alpha$  phosphorylation contributes to expression of macroautophagy/autophagy genes during ER stress. Wild-type and eIF2 $\alpha$  phosphorylation-deficient immortalized mouse embryonic hepatocytes ( $S/S^{Hep}$  and  $A/A^{Hep}$ , respectively) [58] were treated with the ER stress inducer tunicamycin (Tm) for the indicated durations. Expression levels of proteins and mRNA transcripts of UPR and autophagy genes in  $A/A^{Hep}$  cells were compared with those in  $S/S^{Hep}$  cells. As reported previously [13, 57-59], under ER stress conditions, phosphorylated forms of the UPR sensors PERK and IRE1 $\alpha$  were immediately observed, and their phosphorylation persisted until 24 h in both  $S/S^{Hep}$  and  $A/A^{Hep}$  cells treated with Tm (Figure 1A). By contrast, cleavage of the other UPR sensor ATF6 (ATF6 $\alpha$  and ATF6 $\beta$ ) was diminished and delayed in  $A/A^{Hep}$  cells compared with  $S/S^{Hep}$  cells (Figure 1A) as reported previously [14], indicating that the initiation mechanism of UPR pathways is partly impaired in  $A/A^{Hep}$  cells. Furthermore, as shown in several reports, the expression levels of proteins (ATF4 and CHOP) and mRNAs (*Atf4*, *Chop*, *Gadd34*, *Asns*, and *Cth1*) encoded by PERK pathway genes [7, 57], a protein (XBP1s) and mRNA (*XBP1s*) encoded by a IRE1 $\alpha$  pathway gene [13], and proteins (GRP94 and BiP) and mRNA (*BiP*) encoded by ATF6 downstream genes [14, 60] were significantly reduced in  $A/A^{Hep}$  cells under Tm-induced ER stress conditions (Figure 1A, B). Thus, I showed that eIF2 $\alpha$  phosphorylation is required for cleavage-mediated activation of the UPR sensor ATF6 and expression of multiple genes in all three UPR pathways.

In wild-type ( $S/S^{Hep}$ ) cells, Tm treatment gradually increased the mRNA levels of most examined autophagy genes and the levels of some autophagosome proteins (LC3B-II and p62), whereas the levels of lysosomal proteins (LAMP1 and 2, and cathepsin B and L) were decreased at late time points (12, 16, and 24 h) of Tm treatment (Figure 1C, D). The mRNA and protein levels of most examined autophagy genes, except for *Lc3b* mRNA and LC3B-I/II proteins, were lower in  $A/A^{Hep}$  cells than in  $S/S^{Hep}$  cells at most time points (Figure 1C, D). Although the LC3B-I/II protein levels were higher in  $A/A^{Hep}$  cells than in  $S/S^{Hep}$  cells at all time points, LC3B conversion (LC3B-II/I ratio) was lower in  $A/A^{Hep}$  cells than in  $S/S^{Hep}$  cells at most time points (Figure 1D), suggesting that eIF2 $\alpha$  phosphorylation plays an important role in autophagy pathways. Thus, deficiency of eIF2 $\alpha$  phosphorylation dysregulates expression of not only UPR genes but also autophagy genes during ER stress.

### **Autophagy is defective in *A/A* cells during ER stress**

I further investigated whether deficiency of eIF2 $\alpha$  phosphorylation affects autophagy resulting from Tm-induced ER stress. Formation of autophagosomes and autolysosomes was analyzed in immortalized mouse embryonic hepatocytes treated with Tm (Figure 2). In wild-type (*S/S*<sup>Hep</sup>) cells, Tm treatment strongly increased the numbers of LC3A/B-positive puncta (Figure 2A, C, E left lower panels, and Figure 2B first row second panel), suggesting that ER stress-mediated autophagy induction occurs as previously reported [61-63]. However, there were few prominent LC3A/B-positive puncta in Tm-treated *A/A*<sup>Hep</sup> cells (Figure 2A graph). In addition, most LC3A/B-positive structures were smaller in Tm-treated *A/A*<sup>Hep</sup> cells than in Tm-treated *S/S*<sup>Hep</sup> cells (Figure 2A graph and Figure 2A, C, E lower panels, and Figure 2B first row). Immunofluorescence (IF) signals of LC3A/B were largely concentrated in the perinuclear regions of Tm-treated *A/A*<sup>Hep</sup> cells (Figure 2A graph and Figure 2A, C, E right lower panels, and Figure 2B first row fourth panel). Furthermore, these signals colocalized with IF signals of the ER proteins BiP and GRP94, suggesting that LC3A/B is mislocalized in the ER membrane due to deficiency of eIF2 $\alpha$  phosphorylation during ER stress (Figure 2B). Next, I observed the subcellular colocalizations of LC3A/B (an autophagosome marker) and the cargo receptor p62 (a cargo marker, also known as SQSTM1) to investigate formation of autophagosomes (Figure 2C). In addition, I observed colocalization of LAMP1 (a lysosome marker) with p62 (Figure 2D) and LC3A/B (Figure 2E) to investigate formation of autolysosomes. Colocalization of LC3A/B with p62 was significantly increased in Tm-treated *S/S*<sup>Hep</sup> cells (Figure 2C left lower panels and Figure 2F left graph), indicating that Tm treatment increases autophagosome formation in *S/S*<sup>Hep</sup> cells. Furthermore, an IF assay confirmed the colocalization of LAMP1 with p62 (Figure 2D left lower panels and Figure 2F middle graph) and LC3A/B (Figure 2E left lower panels and Figure 2F right graph), suggesting that Tm treatment increases autophagosome-lysosome fusion in *S/S*<sup>Hep</sup> cells. However, colocalization of LC3A/B with p62 was significantly lower in *A/A*<sup>Hep</sup> cells than in *S/S*<sup>Hep</sup> cells under both normal and ER stress conditions (Figure 2C right panels and Figure 2F left graph), whereas Tm treatment increased the percentage of cells with perinuclear accumulated LC3A/B-positive small structures (Figure 2A, C, E right lower panels, and Figure 1B first row fourth panel). There were few p62 and LAMP1-positive puncta in Tm-treated *A/A*<sup>Hep</sup> cells compared with Tm-treated *S/S*<sup>Hep</sup> cells (Figure 2C-E). In addition, colocalization of LAMP1 with p62 (Figure 2D right lower panels and Figure 2F left graph) and LC3A/B (Figure 2E right lower panels and Figure 2F right graph) was significantly lower in Tm-treated *A/A*<sup>Hep</sup> cells than in Tm-treated *S/S*<sup>Hep</sup> cells, although Tm treatment slightly increased colocalization of LAMP1 with LC3A/B in *A/A*<sup>Hep</sup> cells (Figure 2F right graph). These results indicate that eIF2 $\alpha$  phosphorylation is required for not only autophagosome formation, but also autolysosome formation during ER stress.

Defective lysosomal function contributes to dysregulation of autophagy [19, 64]. I next examined lysosomal dysfunctions in  $A/A^{Hep}$  cells using the pH-sensitive dye LysoTracker Red, which specifically labels acidic vesicles such as functional lysosomes and autolysosomes. Consistent with a defect in autolysosome formation under ER stress conditions (Figure 2D–F), the number of LysoTracker-positive structures (Figure 2G) and fluorescence intensity of LysoTracker (Figure 2H) were decreased much more in  $A/A^{Hep}$  cells than in  $S/S^{Hep}$  cells upon Tm treatment, indicating that eIF2 $\alpha$  phosphorylation is required to maintain functional lysosomes and autolysosomes during ER stress. Upon autophagy induction, lysosomes amass in the perinuclear region, and this increases autophagosome-lysosome fusion rates, whereas dispersion of lysosomes to the cell periphery reduces fusion rates [65-67].  $A/A^{Hep}$  cells exhibited peripherally accumulated lysosomes, whereas substantial numbers of lysosomes were predominantly found in the perinuclear region of  $S/S^{Hep}$  cells after treatment with Tm for 16 and 24 h as expected (Figure 2G). However, an IF assay of the lysosome marker LAMP1 revealed that LAMP1-positive lysosomal vesicles did not accumulate peripherally but were found everywhere in Tm-treated  $A/A^{Hep}$  cells (Figure 2D, E), indicating that only peripheral LAMP1-positive vesicles are acidic and functional in these cells. Therefore, the autophagosome-lysosome fusion rates will be decreased in Tm-treated  $A/A^{Hep}$  cells. These results suggest that eIF2 $\alpha$  phosphorylation is important to maintain the activity and subcellular localization of lysosomes, which can affect formation of autolysosomes under ER stress conditions.

### **Autophagic flux and autophagic degradation of misfolded proteins are impaired in $A/A$ cells**

To fortify the association between eIF2 $\alpha$  phosphorylation and autophagy in Tm-treated cells, I performed transmission electron microscopy (TEM) analysis of  $S/S^{Hep}$  and  $A/A^{Hep}$  cells treated with and without Tm. Autolysosomes accumulated in Tm-treated  $S/S^{Hep}$  cells, but not in Tm-treated  $A/A^{Hep}$  cells, while autophagosomes were hardly detected in  $S/S^{Hep}$  and  $A/A^{Hep}$  cells treated with and without Tm (Figure 3A second row). These results confirmed that eIF2 $\alpha$  phosphorylation deficiency inhibits the formation of autolysosomes under ER stress conditions. In addition, the ER was highly fragmented in Tm-treated  $A/A^{Hep}$  cells, and was also swollen and fragmented in Tm-treated  $S/S^{Hep}$  cells as previously reported [68, 69] (Figure 3A third row and yellow dotted area in the Tm-treated  $A/A^{Hep}$  panel of Figure 3A first row), suggesting that deficiency of eIF2 $\alpha$  phosphorylation also alters the ER structure during ER stress.

Both colocalization analysis of LAMP1/p62 and LAMP1/LC3A/B (Figure 2D, E) and TEM observation of autophagic vesicles (Figure 3A) indicated that autophagic flux is impaired in  $A/A^{Hep}$  cells under ER stress conditions. To explore the impairment of autophagic flux in Tm-treated  $A/A^{Hep}$  cells, I investigated LC3B-II accumulation in Tm-treated cells incubated with

bafilomycin A1 (Baf A1), a specific inhibitor of vacuolar H<sup>+</sup>-ATPases and a blocker of autophagosome-lysosome fusion [70, 71]. During active autophagic flux, LC3B-II protein accumulates upon Baf A1 treatment [72]. In the absence of Tm treatment, Baf A1 increased the level of LC3-II protein as expected (Figure 3B), indicating that autophagic flux is active in both *S/S<sup>Hep</sup>* and *A/A<sup>Hep</sup>* cells under normal conditions. However, Baf A1 failed to induce LC3B-II accumulation in Tm-treated *A/A<sup>Hep</sup>* cells, but still increased the LC3B-II protein level in Tm-treated *S/S<sup>Hep</sup>* cells (Figure 3B), indicating that autophagic flux is impaired in *A/A<sup>Hep</sup>* but not in *S/S<sup>Hep</sup>* cells under ER stress conditions.

A variant of  $\alpha$ 1-antitrypsin with the E342K (Z) mutation (ATZ) is degraded by both autophagy and proteasome-dependent ERAD [73, 74]. Autophagy pathways are defective in eIF2 $\alpha$  phosphorylation-deficient cells; therefore, I investigated whether eIF2 $\alpha$  phosphorylation deficiency affects autophagic degradation of ATZ protein. ATZ-expressing cells were treated with the proteasome inhibitor MG132 alone to inhibit proteasome-mediated degradation, or cotreated with MG132 and cycloheximide (CHX) to inhibit both proteasome-mediated degradation and *de novo* protein synthesis for 3 or 6 h (Figure 3C). Therefore, cotreatment with MG132 and CHX will predominantly allow autophagic degradation of ATZ protein. Western blot (WB) analysis revealed that cotreatment with MG132 and CHX for 6 h significantly increased autophagic degradation of ATZ in *S/S<sup>Hep</sup>* cells, but this degradation was decreased in *A/A<sup>Hep</sup>* cells (Figure 3C). Next, ATZ-expressing cells were treated with Baf A1 alone to inhibit autophagic degradation, or cotreated with Baf A1 and CHX to inhibit both autophagic degradation and *de novo* protein synthesis for 6 h (Figure 3D). Therefore, cotreatment with Baf A1 and CHX will allow proteasome-mediated degradation of ATZ proteins. Proteasome-mediated ATZ degradation was not impaired but improved in *A/A<sup>Hep</sup>* cells compared with *S/S<sup>Hep</sup>* cells upon cotreatment with Baf A1 and CHX (Figure 3D). These results suggest that phosphorylation of eIF2 $\alpha$  is important to maintain autophagic flux (such as autophagosome and autolysosome formation), which can affect degradation of its target substrates.

### **Nuclear translocation of TFEB and TFE3 is impaired in *A/A* cells during ER stress**

Most genes examined in Figure 1C, which displayed lower mRNA levels in *A/A<sup>Hep</sup>* cells than in *S/S<sup>Hep</sup>* cells during ER stress, are downstream targets of TFEB and TFE3, the master transcriptional regulators of autophagy and lysosome biogenesis [20, 26, 27, 75]. TFEB and TFE3 reportedly regulate expression of their target genes by binding to the CLEAR motif sequence [20, 26, 27]. To determine whether eIF2 $\alpha$  phosphorylation deficiency influences CLEAR promoter element activity during ER stress, *S/S* and *A/A* mouse embryonic fibroblasts (MEFs) were transfected with a 5XCLEAR luciferase reporter construct (containing five tandem copies of a CLEAR promoter element). Changes of luciferase activities were

investigated in  $S/S^{MEF}$  and  $A/A^{MEF}$  cells treated with Tm and Earle's Balanced Salt Solution (EBSS) (Figure 4A). ER stress-induced TFEB activity was abolished in  $A/A^{MEF}$  cells, whereas Tm treatment significantly stimulated luciferase activity of the transfected reporter construct in  $S/S^{MEF}$  cells (Figure 4A upper graph). Furthermore, starvation induced by EBSS treatment only modestly increased CLEAR promoter activity in  $A/A^{MEF}$  cells, but substantially induced reporter activity in  $S/S^{MEF}$  cells (Figure 4A lower graph), indicating that eIF2 $\alpha$  phosphorylation is required for expression of autophagy genes induced by TFEB and TFE3 activation. These results (and those presented in Figure 1C, D) demonstrate that eIF2 $\alpha$  phosphorylation plays a novel and important role in transcriptional regulation of autophagy genes during ER stress.

$A/A$  cells had several defects in autophagy pathways, including in autophagic flux and autophagy gene expression in response to Tm treatment; therefore, I postulated that TFEB and TFE3 may be inactive in Tm-treated  $A/A$  cells. To investigate this, I first examined the subcellular distributions of endogenous TFEB and TFE3 in  $S/S^{Hep}$  and  $A/A^{Hep}$  cells treated with Tm. Nuclear translocation of TFEB and TFE3 was observed at 6 h, gradually increased, and reached almost 100% at 24 h in Tm-treated  $S/S^{Hep}$  cells (Figure 4B), whereas very little (<5%) nuclear translocation of TFEB and TFE3 was observed in Tm-treated  $A/A^{Hep}$  cells (Figure 4B). To verify the results, I performed subcellular fractionation analysis of  $S/S^{Hep}$  and  $A/A^{Hep}$  cells treated with and without Tm. As reported previously [37], Tm treatment potently induced accumulation of endogenous TFEB and TFE3 in the nuclear fraction of  $S/S^{Hep}$  cells (Figure 4C, D). However, levels of TFEB and TFE3 were significantly lower in the nuclear fraction of Tm-treated  $A/A^{Hep}$  cells than in that of Tm-treated  $S/S^{Hep}$  cells (Figure 4C, D). These data indicate that eIF2 $\alpha$  phosphorylation is necessary for nuclear accumulation of TFEB and TFE3 in response to ER stress.

Furthermore, I conducted subcellular localization experiments using multiple cell lines to confirm that defective nuclear translocation of TFEB and TFE3 is not limited to particular eIF2 $\alpha$  phosphorylation-deficient cell types. First, similar to  $A/A^{Hep}$  cells,  $A/A^{MEF}$  cells displayed defective nuclear translocation of TFEB and TFE3 in response to Tm treatment (Figure 5A–C). In addition, as previously reported [37], nuclear translocation of TFEB and TFE3 was severely impaired in *perk*-knockout (KO) (*perk*<sup>-/-</sup>) MEFs in response to Tm treatment, whereas these proteins substantially translocated from the cytosol to the nucleus in wild-type MEFs treated with Tm for 16 h (Figure 5A–C). Second, defective nuclear translocation of TFEB and TFE3 in response to Tm treatment was completely restored by overexpression of human wild-type eIF2 $\alpha$  in  $A/A^{MEF}$  cells (Figure 5D–F). Third, to conveniently analyze changes in the cellular localization of TFEB under diverse experimental conditions, I established  $S/S^{MEF}$  and  $A/A^{MEF}$  cell lines expressing human TFEB fused with enhanced green fluorescent protein (EGFP) at the C-terminus and control  $S/S^{MEF}$  and  $A/A^{MEF}$  cell lines expressing EGFP only (Figure 5G)

[51]. Stable highly expressing clones (*S/S-TFEB-EGFP* clone 5 and *A/A-TFEB-EGFP* clone 5) were chosen by fluorescence microscopy and WB analyses (Figure 5G, H). Under normal conditions, TFEB-EGFP expressed in *S/S-TFEB-EGFP* and *A/A-TFEB-EGFP* MEFs mainly localized to the cytoplasm (Figure 5H, I). Similar to *A/A<sup>Hep</sup>* and *A/A<sup>MEF</sup>* cells, after Tm treatment for 16 h, nuclear localized TFEB-EGFP was observed in only a very small percentage (<5%) of *A/A-TFEB-EGFP* MEFs, whereas almost 80% of *S/S-TFEB-EGFP* MEFs displayed nuclear localized TFEB-EGFP (Figure 5H, I). However, the nuclear translocation defect of TFEB-EGFP in response to Tm treatment was efficiently corrected by recombinant adenovirus-mediated overexpression of wild-type eIF2 $\alpha$ , but not of mutant eIF2 $\alpha$ (S51A), in *A/A-TFEB-EGFP* MEFs (Figure 5J–L). Finally, I examined nuclear translocation of TFEB and TFE3 in an eIF2 $\alpha$  phosphorylation-deficient human cell line. To establish a HeLa cell line that lacks phosphorylation of eIF2 $\alpha$  residue S51, a HeLa cell line expressing both the HA-tagged Cas9 (CRISPR-associated protein 9) restriction enzyme and the FLAG-tagged human eIF2 $\alpha$  (S51A) mutant (HeLa-Cas9/eIF2 $\alpha$ (S51A)OE) was first generated. Then, the HeLa-Cas9/eIF2 $\alpha$ (S51A)OE/eIF2 $\alpha$  KO cell line, in which the endogenous wild-type *eIF2 $\alpha$*  gene was knocked out, was established from HeLa-Cas9/eIF2 $\alpha$ (S51A) cells using CRISPR/Cas9 technology. Similar observations were made in HeLa-Cas9/eIF2 $\alpha$ (S51A)OE/eIF2 $\alpha$  KO cells, which were engineered to express FLAG-tagged eIF2 $\alpha$ (S51A) and lacked endogenous wild-type eIF2 $\alpha$  (Figure 4E–H). HeLa-Cas9/eIF2 $\alpha$ (S51A)OE/eIF2 $\alpha$  KO cells displayed significant nuclear translocation impairment (Figure 4E, F) and diminished nuclear accumulation (Figure 4G, H) of TFEB and TFE3 during ER stress. These data indicate that impairment of TFEB/TFE3 nuclear translocation induced by eIF2 $\alpha$  phosphorylation deficiency is not a species- or cell type-specific event during ER stress.

In addition to Tm treatment, other conditions induce autophagy. These include treatment with other ER stress inducers such as thapsigargin (Tg) and dithiothreitol (DTT) [62, 76], as well as diverse cellular stress conditions such as mTOR inhibition (Torin2), nutrient starvation (EBSS), and inflammation (lipopolysaccharide [LPS]) [31]. I examined nuclear translocation of endogenous TFEB and TFE3 in *S/S<sup>Hep</sup>* and *A/A<sup>Hep</sup>* cells in response to these autophagic stimuli (Figure 6A–C). As expected, all stimuli induced nuclear localization of TFEB and TFE3 in *S/S<sup>Hep</sup>* cells with different sensitivities (Figure 6A, B). They immediately induced eIF2 $\alpha$  phosphorylation in *S/S<sup>Hep</sup>* cells but not in *A/A<sup>Hep</sup>* cells (Figure 6C). By contrast, their nuclear translocation was almost completely abolished in *A/A<sup>Hep</sup>* cells in response to all five stimuli tested (Figure 6A–C). To confirm these results, I analyzed the nuclear localization of TFEB in *S/S-TFEB-EGFP* and *A/A-TFEB-EGFP* MEFs treated with the same stimuli. In agreement with the hepatocyte data, all stimuli induced nuclear translocation of TFEB-EGFP in *S/S-TFEB-EGFP* MEFs but not in *A/A-TFEB-EGFP* MEFs (Figure 6D, E). These data

suggest that eIF2 $\alpha$  phosphorylation plays a novel and crucial role in regulating nuclear translocation of TFEB and TFE3 in response to diverse cellular stresses including ER stress.

Collectively, these observations raise the question of whether eIF2 $\alpha$  phosphorylation influences nuclear translocation of multiple proteins under ER stress conditions. Koromilas's group found that ER stress accelerates cytoplasmic degradation of p53 through a mechanism dependent on the E3 ubiquitin-ligase MDM2 [77, 78]. Cytoplasmic degradation of p53 by MDM2 requires phosphorylation of p53, which is required for its nuclear export, by GSK3 $\beta$  [78], suggesting that GSK3 $\beta$  translocates into the nucleus under ER stress conditions. In addition, eIF2 $\alpha$  kinases (such as PERK and PKR) control the nuclear localization and activation of GSK3 $\beta$  under stresses [77]. Although their reports indicate that nuclear export of p53 mediated by eIF2 $\alpha$  kinases occurs independently of eIF2 $\alpha$  phosphorylation, they did not provide direct evidence showing whether eIF2 $\alpha$  phosphorylation is necessary for nuclear localization of GSK3 $\beta$  under ER stress. Therefore, I examined nuclear localization of GSK3 $\beta$  in *S/S-TFEB-EGFP* and *A/A-TFEB-EGFP* MEFs under ER stress conditions. As already shown in Figures 5H–K and 6D, E, nuclear translocation of TFEB-EGFP was markedly inhibited in *A/A-TFEB-EGFP* MEFs under ER stress conditions, whereas nuclear translocation of GSK3 $\beta$  was not inhibited in TFEB-EGFP-expressing *S/S* or *A/A* MEFs (Figure 6F, G). These results indicate that impairment of nuclear translocation by eIF2 $\alpha$  phosphorylation deficiency is a specific defect that only affects TFEB, TFE3, and a few related proteins under ER stress conditions.

### **eIF2 $\alpha$ phosphorylation deficiency does not impair 14-3-3-mediated regulation of TFEB and TFE3 nuclear translocation**

Tm treatment induces nuclear translocation of TFEB and TFE3 via a process that is dependent on calcium-activated calcineurin [37], which can weaken 14-3-3-mediated retention of these TFs in the cytosol [33, 35]. Furthermore, PERK is thought to be necessary for calcineurin activation in response to Tm treatment because it can modulate calcium levels in the ER and cytoplasm [79-81]. In my experimental systems, inactivation of calcineurin by the calcineurin inhibitor FK506 completely abolished translocation of TFEB-EGFP to the nucleus in Tm-treated *S/S-TFEB-EGFP* MEFs (Figure 7A), confirming that calcineurin-mediated dephosphorylation of TFEB is important for ER stress-induced nuclear translocation of TFEB. Consistently, FK506 treatment inhibited the Tm-induced rapid migration of TFEB-EGFP and endogenous TFEB protein in *S/S-TFEB-EGFP* MEFs (Figure 7B left panels). Dephosphorylated TFEB and TFE3 migrate faster in gels than phosphorylated TFEB and TFE3 [35, 82, 83]. Phosphorylation of TFEB-EGFP at S211 was elevated in FK506- and Tm-cotreated *S/S-TFEB-EGFP* MEFs (Figure 7B right panels). Furthermore, the level of 14-3-3 coimmunoprecipitated with TFEB-EGFP was significantly higher in FK506- and Tm-cotreated



*S/S-TFEB-EGFP* MEFs than in Tm-treated *S/S-TFEB-EGFP* MEFs. These results indicate that activation of the PERK-Ca<sup>2+</sup>-calcineurin pathway determines nuclear translocation of TFEB and TFE3 in response to Tm treatment (Figure 5A and Figure 7A, B). However, PERK activation was not dysregulated in *A/A* cells (Figure 1A). Therefore, I next investigated whether cytosolic Ca<sup>2+</sup> mobilization is impaired in Tm-treated *A/A* cells. Although Tm treatment changed the cytoplasmic Ca<sup>2+</sup> levels in all MEFs, *perk* KO (*perk*<sup>-/-</sup>) MEFs displayed lower cytosolic Ca<sup>2+</sup> levels than *perk*<sup>+/+</sup> MEFs before and after Tm treatment (Appendix 2A), whereas *A/A*<sup>MEF</sup> cells exhibited higher cytosolic Ca<sup>2+</sup> levels than *S/S*<sup>MEF</sup> cells after Tm treatment (Appendix 2B). These results indicate that there is no PERK- and Ca<sup>2+</sup>-dependent calcineurin-related impairment of TFEB and TFE3 nuclear translocation in *A/A* cells.

To corroborate the above conclusion, I compared the migration of TFEB and TFE3 in lysates of Torin2- or Tm-treated *S/S*<sup>Hep</sup> and *A/A*<sup>Hep</sup> cells on sodium dodecyl sulfate-polyacrylamide gel electrophoresis (SDS-PAGE) gels. As expected, after Torin2 and Tm treatment, the rapidly migrating TFEB and TFE3 forms were observed in both *S/S*<sup>Hep</sup> and *A/A*<sup>Hep</sup> cells with no significant difference, although they appeared slightly slower in *A/A*<sup>Hep</sup> cells than in *S/S*<sup>Hep</sup> cells in response to Tm treatment (Figure 7C, D). By contrast, molecular weight shifts of TFEB and TFE3 proteins were not significant in *perk*<sup>-/-</sup> MEFs compared with *perk*<sup>+/+</sup> MEFs (Figure 8A), possibly due to defective cytosolic Ca<sup>2+</sup> mobilization under ER stress conditions (Figure 7C). Furthermore, I directly assessed the phosphorylation statuses of S211 and S142 in TFEB-EGFP, which are important for regulation of nuclear translocation [33, 35] and export [29] of TFEB, respectively. mTORC1 is responsible for phosphorylation of TFEB residues S211 and S142 [30, 31, 33]. Torin2 treatment strongly inhibited mTORC1, resulting in almost complete dephosphorylation of its target proteins (p70S6K and 4E-BP1) in both *S/S*<sup>Hep</sup> and *A/A*<sup>Hep</sup> cells (Figure 8B left panels). Consistently, Torin2 treatment strongly inhibited phosphorylation of TFEB-EGFP residues S211 and S142 in both *S/S-TFEB-EGFP* and *A/A-TFEB-EGFP* MEFs (Figure 7E). In addition, I investigated whether Tm treatment inhibits mTORC1, which might contribute to the decreased phosphorylation of TFEB and its target proteins (p70S6K and 4E-BP1). Consistent with Martina's report [37], Tm treatment decreased mTORC1 phosphorylation in both *S/S*<sup>Hep</sup> and *A/A*<sup>Hep</sup> cells (Figure 8B). In addition, phosphorylation of p70S6K was significantly reduced, although phosphorylation of 4E-BP was unchanged (Figure 8B). Consistent with the results presented in Figure 5E, F, the dephosphorylation levels of TFEB-EGFP residues S211 and S142 did not differ in *S/S-TFEB-EGFP* and *A/A-TFEB-EGFP* MEFs (Figure 7E).

Finally, I checked whether changes of the phosphorylation status of TFEB-EGFP residues S211 and S142 affect dissociation of the TFEB-EGFP/14-3-3 complex, which may result in transport of TFEB-EGFP to the nucleus. As expected, dephosphorylation of TFEB-EGFP residue S211 in *perk*<sup>-/-</sup> MEFs compared with *perk*<sup>+/+</sup> MEFs was insufficient to completely

dissociate the TFEB-EGFP/14-3-3 protein complex after Tm treatment (Figure 8C), suggesting that activation of the PERK-Ca<sup>2+</sup>-calcineurin pathway determines TFEB/14-3-3 dissociation and subsequent nuclear translocation of TFEB in response to Tm treatment. However, TFEB-EGFP protein immunoprecipitated from lysates of cells treated not only with Torin2 (Figure 7F) but also with Tm (Figure 7G) showed greatly reduced phosphorylation of both S211 and S142, resulting in a strong reduction of the TFEB-EGFP/14-3-3 complex in both wild-type and eIF2 $\alpha$  phosphorylation-deficient cells. Nevertheless, translocation of TFEB to the nucleus was significantly prevented in eIF2 $\alpha$  phosphorylation-deficient cells, but not in wild-type cells under ER stress conditions as well as under mTORC1-inhibited conditions (Figures 4, 5, and 6).

My results (Figures 7 and 8) and Martina's report [37] strongly suggest that PERK- and Ca<sup>2+</sup>-dependent calcineurin activation is required but insufficient for nuclear translocation of TFEB and TFE3 under ER stress conditions. In other words, there is an unknown mechanism(s) that regulates the subcellular localization of TFEB/TFE3 and is controlled by eIF2 $\alpha$  phosphorylation under ER stress conditions.

#### **TFEB translocates from the cytosol to the nucleus but cannot be retained in the nucleus in A/A cells under ER stress conditions**

Recent studies demonstrate that TFEB continuously shuttles between the cytosol and nucleus via nuclear export dependent on the major exportin CRM1 under normal conditions [29, 30, 42]. Phosphorylation of S211 of TFEB mediates its cytosolic retention via 14-3-3 binding [30, 33], whereas phosphorylation of S142 and S138 is required for recognition and binding of the TFEB NES by CRM1, which is crucial for efficient nuclear export [29, 30]. However, as shown in Figure 7E, G, Tm treatment significantly reduced phosphorylation of S211 and S142, but TFEB was sequestered in the cytosol of A/A cells. Therefore, I investigated whether TFEB undergoes continuous nucleocytoplasmic shuttling in A/A cells even after Tm treatment. The effect of treatment with the CRM1 inhibitor leptomycin B (LMB) was investigated in S/S-TFEB-EGFP and A/A-TFEB-EGFP MEFs (Figure 9A-E). Treatment with LMB only and Tm plus LMB induced nuclear translocation of TFEB-EGFP at 6 h and almost 100% nuclear translocation of TFEB-EGFP at 16 h in both S/S-TFEB-EGFP and A/A-TFEB-EGFP MEFs, whereas nuclear translocation of TFEB-EGFP was impaired in A/A-TFEB-EGFP MEFs but not in S/S-TFEB-EGFP MEFs after Tm treatment for 16 h, indicating that nucleocytoplasmic shuttling of TFEB continues in eIF2 $\alpha$  phosphorylation-deficient cells but not in wild-type cells under ER stress conditions (Figure 9A-E). To observe dynamic changes of the subcellular localization of TFEB due to inhibition of its nuclear export, cells were sequentially treated with Tm and LMB (Figure 9F, G). Sequential treatment with Tm and LMB increased nuclear translocation of TFEB-EGFP, whereas treatment with only Tm did not induce its nuclear translocation at all in A/A-TFEB-

EGFP MEFs (Figure 9F, G). These results indicate that TFEB translocates from the cytosol to the nucleus but is continuously re-exported to the cytosol by a CRM1-dependent nuclear export pathway in *A/A* cells under ER stress conditions.

### **Overexpression of the activated ATF6 $\alpha$ form promotes nuclear translocation of TFEB in *A/A* cells**

Multiple reports (and the data presented in Figure 1A) demonstrate that eIF2 $\alpha$  phosphorylation is required for expression or activation of several UPR TFs, including ATF4 [84-87], XBP1s [13], and ATF6 $\alpha$  and  $\beta$  [14], under ER stress conditions. Therefore, I examined whether overexpression of active forms of the UPR TFs (ATF4, XBP1s, ATF6 $\alpha$ (1-373), or ATF6 $\beta$ (1-392)) affects nuclear translocation of TFEB-EGFP in *A/A-TFEB-EGFP* MEFs before and/or after Tm treatment. Nuclear localization of TFEB-EGFP was increased in most TF-expressing *A/A-TFEB-EGFP* MEFs regardless of ER stress (Figure 10A). To determine the magnitude of TFEB-EGFP nuclear localization induced by each TF, I calculated the nuclear vs. cytosolic distribution ratio of TFEB-EGFP (Figure 10A graphs). Among TFs, the ratio was largest in cells expressing HA-ATF6 $\alpha$ (1-373) regardless of Tm treatment and was further increased by Tm treatment. I next assessed changes of the transcriptional activity of TFEB upon ectopic overexpression of HA-ATF6 $\alpha$ (1-373) and other HA-tagged TFs in *A/A<sup>MEF</sup>* cells before and after Tm treatment. To this end, I used a 5XCLEAR luciferase reporter construct. Consistent with the results presented in Figure 10A, luciferase activity was highest upon overexpression of HA-ATF6 $\alpha$ (1-373) among TFs and was further enhanced by Tm treatment (Figures 10B and 11). Surprisingly, the increase in reporter activities induced by HA-ATF6 $\alpha$ (1-373) was almost equivalent to that induced by an TFEB active mutant (TFEB(S211A)-FLAG) (Figure 10B). IF analysis confirmed that overexpression of HA-ATF6 $\alpha$ (1-373) by a recombinant adenovirus (*Ad-ATF6 $\alpha$ (1-373)*) significantly promoted nuclear translocation of endogenous TFEB in most *A/A<sup>Hep</sup>* cells (up to 90%) after Tm treatment (Figure 10C), verifying that the active ATF6 $\alpha$  fragment can prevent the impaired nuclear translocation of TFEB induced by eIF2 $\alpha$  phosphorylation deficiency. Quantification of TFEB and TFE3 levels in the cytosolic and nuclear fractions by WB analyses confirmed that HA-ATF6 $\alpha$ (1-373) potently induced nuclear translocation of endogenous TFEB and TFE3 in *A/A<sup>Hep</sup>* cells regardless of ER stress, although Tm treatment further increased the nuclear TFEB level slightly (Figure 10D). Consistent with the increased nuclear translocation of TFEB in HA-ATF6 $\alpha$ (1-373)-overexpressing *A/A<sup>Hep</sup>* cells, overexpression of HA-ATF6 $\alpha$ (1-373) greatly induced dephosphorylation of TFEB-EGFP on S211 and S142 (Figures 10E and 12A), and resulted in dissociation of the TFEB-EGFP/14-3-3 complex without Tm treatment (Figure 10E). Coimmunoprecipitation (Co-IP) assays revealed that ectopically expressed HA-ATF6 $\alpha$ (1-373) coprecipitated with TFEB-EGFP in *A/A-TFEB-EGFP* MEFs before Tm treatment (Figure 10E), suggesting that HA-ATF6 $\alpha$ (1-373)

induces nuclear translocation of TFEB (as well as TFEB dephosphorylation and 14-3-3 dissociation) through a physical interaction with TFEB. To confirm this, I performed a proximity ligation assay (PLA) and immunostaining assays. Most PLA signals were found in the nucleus regardless of Tm treatment, demonstrating that the interaction between TFEB and the activated ATF6 $\alpha$  form retains TFEB in the nucleus (Figures 10F, G and 12B). In addition, a significant portion of PLA signals were in the cytosol regardless of Tm treatment, and cytosolic PLA signals decreased after Tm treatment in HA-ATF6 $\alpha$ (1-373)-expressing *A/A-TFEB-EGFP* MEFs (Figures 10F, G and 12B), indicating that complexes of TFEB and the activated ATF6 $\alpha$  form are generated in the cytosol and translocate to the nucleus, where they are retained. Immunostaining assays of *A/A<sup>MEF</sup>* cells coexpressing TFEB-EGFP and HA-ATF6 $\alpha$ (1-373) also showed colocalization of TFEB with the activated ATF6 $\alpha$  form in the nucleus, confirming that TFEB and the activated ATF6 $\alpha$  form interact in the nucleus (Figures 10H and 12C).

### **Overexpression of the activated ATF6 $\alpha$ form enhances expression of autophagy genes and ameliorates autophagic defects in *A/A* cells during ER stress**

Ectopically expressed HA-ATF6 $\alpha$ (1-373) potentially induced nuclear translocation of TFEB and TFE3, and increased the activity of the TFEB binding motif (CLEAR)-driven luciferase reporter in *A/A* cells. Therefore, I assessed whether the activated ATF6 $\alpha$  form upregulates expression of TFEB/TFE3-dependent autophagy genes in *A/A<sup>Hep</sup>* cells. To this end, *A/A<sup>Hep</sup>* cells were infected with *Ad-vector* or *Ad-HA-ATF6 $\alpha$ (1-373)* and then treated with Tm for the indicated durations. Quantitative PCR and WB analyses confirmed that HA-ATF6 $\alpha$ (1-373) was overexpressed and harbored transcriptional activities (Figure 13A, B), as judged by increased mRNA and protein expression of the UPR target genes *BiP* [88-91], *Chop* [91-94], and *Xbp1t/s* [91, 93]. Among the examined genes, *Atf4* mRNA and ATF4 protein were also upregulated in HA-ATF6 $\alpha$ (1-373)-expressing cells without Tm treatment (Figure 13A, B), which has not been previously reported. Expression analysis of autophagy genes demonstrated that the mRNA and protein levels of *Lc3b*, *p62*, and *Ctsb* genes were significantly higher in *Ad-HA-ATF6 $\alpha$ (1-373)*-infected cells than in *Ad-vector*-infected cells without Tm treatment, and their mRNA levels were further increased by Tm treatment (Figure 13A, B). Although LC3B conversion (LC3B-II/I ratio) was lower in *A/A<sup>Hep</sup>* cells than in *S/S<sup>Hep</sup>* cells at most time points (Figure 1D), overexpression of HA-ATF6 $\alpha$ (1-373) in *A/A<sup>Hep</sup>* cells increased LC3B conversion (LC3B-II/I ratio) at the late stages (12 and 24 h), implying that the activated ATF6 $\alpha$  form enhances autophagosome formation in *A/A* cells during ER stress. Although HA-ATF6 $\alpha$ (1-373) expression itself did not increase mRNA (*Atp6v1h*, *Ctsd*, *Ctsl*, *Lamp1*, *Lamp2a/b/c*, *Mcolin1*, *Ttp*, and *Glb1*) (Figure 13A) or protein (CtsL, LAMP1, and LAMP2) (Figure 13B) expression of many other autophagy genes, Tm treatment strongly enhanced the levels of these transcripts (Figure 13A) and proteins (Figure 13B) in HA-ATF6 $\alpha$ (1-373)-expressing *A/A<sup>Hep</sup>* cells. These

results suggest that enhancement of autophagy gene expression by the activated ATF6 $\alpha$  form requires other components (such as other TFs and ATF6 $\alpha$  PTMs) that are induced by ER stress. These data indicate that overexpression of the activated ATF6 $\alpha$  form can ameliorate the dysregulated expression of TFEB/TFE3-dependent autophagy genes and some UPR genes in *A/A* cells during ER stress.

Nuclear translocation of TFEB/TFE3 is important for regulation of lysosome biogenesis and function [22, 26, 27]. Therefore, I checked whether ectopically expressed HA-ATF6 $\alpha$ (1-373)-mediated nuclear translocation of TFEB prevents perturbation of lysosome biogenesis and function in *A/A*<sup>Hep</sup> cells under ER stress conditions. Similar to the results presented in Figure 2G, null expressing *A/A*<sup>Hep</sup> cells exhibited markedly decreased LysoTracker Red staining and peripheral accumulation of lysosomes, whereas HA-ATF6 $\alpha$ (1-373)-expressing *A/A*<sup>Hep</sup> cells displayed significant increases in the intensity of LysoTracker Red staining and perinuclear accumulation of lysosomes after Tm treatment (Figure 13C). This indicates that TFEB/TFE3 activation mediated by the activated ATF6 $\alpha$  form prevents lysosomal dysfunction in *A/A* cells under ER stress conditions.

I next investigated if the ability of the activated ATF6 $\alpha$  form to induce TFEB/TFE3 activation ameliorates autophagic defects in *A/A* cells during ER stress. Overexpression of HA-ATF6 $\alpha$ (1-373) significantly reduced accumulation of LC3A/B-positive structures in perinuclear regions, and conversely increased the number of puncta positive for LC3A/B (autophagosomes) and LAMP1 (autolysosomes or lysosomes) in Tm-treated *A/A*<sup>Hep</sup> cells (Figure 13D, E). Furthermore, HA-ATF6 $\alpha$ (1-373) overexpression markedly enhanced the colocalization of LC3A/B and LAMP1 in Tm-treated *A/A*<sup>Hep</sup> cells (Figure 13D, F). Similarly, HA-ATF6 $\alpha$ (1-373) overexpression enhanced the colocalization of p62 and LAMP1 in Tm-treated *A/A*<sup>Hep</sup> cells (Figure 14A, B). Finally, TEM analyses demonstrated that overexpression of HA-ATF6 $\alpha$ (1-373) increased the number of autolysosomes in Tm-treated *A/A*<sup>Hep</sup> cells (Figure 13G). In addition, as reported previously [54], overexpression of HA-ATF6 $\alpha$ (1-373) induced ER expansion in *A/A*<sup>Hep</sup> cells not treated with Tm and reduced ER fragmentation in Tm-treated *A/A*<sup>Hep</sup> cells (Figure 13G). This data suggest that overexpression of the activated ATF6 $\alpha$  form increases expression of TFEB/TFE3-dependent autophagy genes and ameliorates autophagic defects in *A/A* cells during ER stress.

### **Overexpression of the constitutively active TFEB mutant enhances expression of autophagy genes and ameliorates autophagic defects in *A/A* cells during ER stress**

The results presented in Figures 10 and 13 indicate that the effects of the activated ATF6 $\alpha$  form on autophagy are mediated by TFEB/TFE3 activation in *A/A* cells during ER stress. Therefore, I investigated whether TFEB overexpression increases expression of autophagy genes and thereby prevents autophagic defects in Tm-treated *A/A* cells. First, I overexpressed

wild-type TFEB (TFEB(WT)-FLAG) or a constitutively active TFEB mutant (TFEB(S211A)-FLAG) in *A/A<sup>Hep</sup>* cells and then treated these cells with Tm for the indicated durations. Similar to endogenous TFEB in *S/S<sup>Hep</sup>* and *A/A<sup>Hep</sup>* cells, the subcellular localization of overexpressed TFEB(WT)-FLAG differed depending on the genetic background of the cells and stress conditions, although TFEB(WT)-FLAG exhibited a nuclear localization in almost 25% of *A/A<sup>Hep</sup>* cells treated with Tm for 24 h (Figure 15A), possibly due to altered regulation by overexpression. On the other hand, the TFEB mutant (TFEB(S211A)-FLAG) primarily accumulated in the nucleus regardless of the genetic background of the cells and stress conditions (Figure 15B), possibly due to the absence of 14-3-3-mediated cytoplasmic sequestration [33, 35]. Second, I compared the transcriptional activities of TFEB(WT)-FLAG and TFEB(S211A)-FLAG in *A/A<sup>MEF</sup>* cells using the 5XCLEAR luciferase reporter construct before and after Tm treatment (Figure 16A, B). TFEB(S211A)-FLAG exhibited stronger transcriptional activity than TFEB(WT)-FLAG after Tm treatment, whereas their transcriptional activities were similar before Tm treatment (Figure 16A, B). Thus, overexpression of the constitutively active TFEB mutant and even wild-type TFEB may enhance expression of autophagy genes in *A/A* cells during ER stress.

Next, I assessed the expression levels of individual TFEB/TFE3 target genes in TFEB(WT)-FLAG- and TFEB(S211A)-FLAG-expressing *A/A<sup>Hep</sup>* cells after Tm treatment. First, because Martina et al. reported that overexpression of TFEB(S211A) enhances the ATF4-mediated ER stress response in wild-type MEFs [37], I investigated whether overexpression of TFEB(WT)-FLAG or TFEB(S211A)-FLAG increases the transcript levels of ER stress responsive genes (*Atf4*, *Chop*, *Xbp1t/s*, and *BiP*) in Tm-treated *A/A<sup>Hep</sup>* cells. The levels of *Atf4* and *Chop* mRNAs were slightly increased in TFEB(S211A)-FLAG-expressing Tm-treated *A/A<sup>Hep</sup>* cells (Figure 16C). However, TFEB(S211A)-FLAG-mediated transcriptional upregulation of *Atf4* and the downstream target *Chop* did not lead to increases of their protein levels, possibly due to the absence of eIF2 $\alpha$  phosphorylation in *A/A<sup>Hep</sup>* cells during ER stress [7, 57, 85] (Figure 16D). Second, overexpression of TFEB(WT)-FLAG and TFEB(S211A)-FLAG increased expression of multiple autophagy genes (Figure 16C), but the transcriptional activity of TFEB(S211A)-FLAG was much stronger than that of TFEB(WT)-FLAG, although their mRNA (Figure 16C) and protein (Figure 16E) levels were similar. LC3B conversion (LC3B-II/I ratio) as well as LC3B-I and II protein levels were higher in TFEB(WT)-FLAG- and TFEB(S211A)-FLAG-expressing *A/A<sup>Hep</sup>* cells than in null expressing *A/A<sup>Hep</sup>* cells at all time points (Figure 16E). In addition, the p62 protein level gradually decreased, whereas its mRNA level increased, in TFEB(S211A)-FLAG-expressing *A/A<sup>Hep</sup>* cells treated with Tm (Figure 16C, E). Expression levels of lysosomal proteins (LAMP1, LAMP2, CTSB, and CTSL) were increased in proportion to their mRNA levels in both TFEB(WT)-FLAG- and TFEB(S211A)-FLAG-expressing *A/A<sup>Hep</sup>* cells (Figure 16B, C). Thus, I confirmed that TFEB activation in eIF2 $\alpha$

phosphorylation-deficient cells can prevent dysregulated expression of autophagy genes during ER stress.

Next, based on the gene expression analysis, I reasoned that TFEB(S211A)-FLAG overexpression would improve autophagic processes such as autophagosome formation and autophagosome-lysosome fusion in *A/A<sup>Hep</sup>* cells under ER stress conditions. To test this idea, I investigated whether TFEB(S211A)-FLAG overexpression increases the number of *A/A<sup>Hep</sup>* cells containing LC3A/B-positive puncta after Tm treatment. TFEB(S211A)-FLAG overexpression markedly increased the number of *A/A<sup>Hep</sup>* cells containing LC3A/B-positive puncta (~70%, Figure 16F graph) after Tm treatment, suggesting that overexpression of the active TFEB mutant alleviates dysregulated autophagosome formation in *A/A<sup>Hep</sup>* cells during ER stress. Furthermore, TFEB(S211A)-FLAG overexpression significantly reduced perinuclear accumulation of LC3A/B-positive structures in Tm-treated *A/A<sup>Hep</sup>* cells (Figure 16F). TFEB overexpression increased expression of several lysosomal genes such as *Ctsb*, *Ctsd*, *Ctsl*, *Lamp1*, *Lamp2a*, *Lamp2b*, and *Tpp1* (Figure 16C, E). Therefore, I next determined the effects of TFEB(S211A)-FLAG overexpression on lysosome biogenesis and function under ER stress conditions. TFEB(S211A)-FLAG overexpression attenuated the decrease of LysoTracker Red staining intensity and perinuclear accumulation of lysosomes in *A/A<sup>Hep</sup>* cells under ER stress conditions (Figure 16G). These results confirmed that TFEB activation can prevent lysosomal dysfunction in *A/A* cells under ER stress conditions. I next investigated if overexpression of the active TFEB mutant ameliorates the impairment of autolysosome formation in *A/A* cells during ER stress. TFEB(S211A)-FLAG overexpression significantly enhanced the colocalization of LC3A/B and LAMP1 in Tm-treated *A/A<sup>Hep</sup>* cells (Figure 16F), indicating that autolysosome formation was increased. Collectively, these results demonstrate that TFEB activation can resolve most autophagic defects in eIF2 $\alpha$  phosphorylation-deficient cells during ER stress.

### **The constitutively active TFEB mutant restores autophagic flux and promotes autophagic degradation of misfolded proteins in *A/A* cells**

To substantiate the effects of TFEB on autophagy induced by ER stress in *A/A* cells, I performed TEM analyses of vector- and TFEB(S211A)-FLAG-expressing *A/A<sup>Hep</sup>* cells treated with and without Tm. TFEB(S211A)-FLAG-expressing *A/A<sup>Hep</sup>* cells exhibited an increased number of autolysosomes, whereas vector-expressing *A/A<sup>Hep</sup>* cells had few autolysosomes after Tm treatment, indicating that overexpression of the constitutively active TFEB mutant increases autolysosome formation in *A/A* cells during ER stress (Figure 17A). However, in contrast with the activated ATF6 $\alpha$  form, TFEB(S211A)-FLAG did not reduce the severity of ER fragmentation and dilation (yellow dotted areas in Tm-treated *A/A<sup>Hep</sup>* panels of Figure 17A, B), indicating that the altered ER structures observed in Tm-treated *A/A* cells are not critical

obstacles of autophagy pathways. I next performed the autophagic flux assay using Baf A1 to biochemically confirm that TFEB(S211A)-FLAG expression changes autophagic activity in Tm-treated *A/A<sup>Hep</sup>* cells. In the absence of Tm treatment, the increase (lanes 1–2 vs. lanes 3–4) of LC3-II levels induced by Baf A1 did not significantly differ between vector- and TFEB(S211A)-FLAG-expressing *A/A<sup>Hep</sup>* cells (Figure 17C). By contrast, Tm treatment alone strongly decreased (lane 5 vs. lane 7) LC3-II levels in TFEB(S211A)-FLAG-expressing *A/A<sup>Hep</sup>* cells compared with vector-expressing *A/A<sup>Hep</sup>* cells, and consequently, the increase (lanes 5–6 vs. lanes 7–8) of LC3-II levels induced by Baf A1 was significantly higher in the former cells than in the latter cells. These results confirm that the constitutively active TFEB mutant restores autophagic flux in *A/A<sup>Hep</sup>* cells under ER stress conditions.

Finally, I examined the effects of overexpression of the constitutively active TFEB mutant on autophagic degradation of ATZ protein. ATZ-expressing *A/A<sup>Hep</sup>* cells were cotreated with MG132 and CHX to retain only autophagic activity (Figure 17D). Therefore, upon cotreatment with MG132 and CHX, ATZ protein will be predominantly degraded by autophagy pathways. WB analysis revealed that cotreatment with MG132 and CHX for 6 h decreased the ATZ levels in both vector- and TFEB(S211A)-FLAG-expressing *A/A<sup>Hep</sup>* cells (lanes 3 and 6). However, ATZ degradation was much more efficient in TFEB(S211A)-FLAG-expressing *A/A<sup>Hep</sup>* cells than in vector-expressing *A/A<sup>Hep</sup>* cells (Figure 17D, lane 3 vs. lane 6). These results indicate that the constitutively active TFEB mutant enhances autophagic degradation of misfolded proteins in *A/A* cells.



## Discussion

In this study, I showed that eIF2 $\alpha$  phosphorylation plays an essential role in nuclear translocation of TFEB and TFE3 during ER stress. Under ER stress conditions, eIF2 $\alpha$  phosphorylation-deficient *A/A* cells display dysregulated expression of autophagy genes and impairment of multiple autophagic processes (such as autophagosome and autolysosome formation, and autophagic flux), which are regulated by the nuclear translocation and functional activity of TFEB and TFE3. Particularly, I revealed that overexpression of the activated ATF6 $\alpha$  form (HA-ATF6 $\alpha$ (1-373)), which was significantly reduced and delayed in *A/A* cells during ER stress, ameliorated these autophagic defects of *A/A* cells by promoting the nuclear translocation and functional activity of TFEB and TFE3. In turn, overexpression of a constitutively active TFEB mutant (TFEB(S211A)-FLAG) alleviated the autophagic defects of *A/A* cells during ER stress. Collectively, these results reveal how eIF2 $\alpha$  phosphorylation connects the UPR pathways to autophagy.

As reported previously [37], I found that nuclear translocation of TFEB in Tm-treated wild-type cells requires Ca<sup>2+</sup>-dependent calcineurin activation, TFEB dephosphorylation, and 14-3-3 dissociation (Figures 7A, B, D, E, G, and 8A, C). Furthermore, I showed that PERK was necessary for nuclear translocation of TFEB and TFE3 (Figure 7A) [37] because it contributed to cytosolic Ca<sup>2+</sup> flux during ER stress (Appendix 2A). Tm-mediated cytosolic Ca<sup>2+</sup> flux was not reduced but increased in PERK-sufficient *A/A* cells (Figure 1A) compared with *S/S* cells (Appendix 2B). Likewise, *A/A* cells displayed TFEB dephosphorylation and 14-3-3 dissociation similar to *S/S* cells during ER stress (Figure 7D, E, G). In addition, Tm treatment induced mTORC1 inhibition, which may contribute to reduced phosphorylation of TFEB in *A/A* cells (Figure 8B). Nevertheless, nuclear translocation of TFEB and TFE3 was strongly suppressed in *A/A* cells under ER stress conditions (Figures 4, 5, and 6). However, experiments using the CRM1 inhibitor LMB revealed that activated TFEB translocated to the nucleus but was continuously re-exported to the cytosol via a CRM1-dependent nuclear export pathway in *A/A* cells under ER stress conditions (Figure 9). Therefore, I postulate that the TFEB nuclear import pathway is not defective, but the TFEB nuclear export pathway is dysregulated in *A/A* cells during ER stress. Diverse PTMs including phosphorylation regulate nuclear translocation of TFEB and TFE3 [28-32]. Most PTM studies focused on a change in the localizations of TFEB and TFE3 from the cytosol to the nucleus to explain their nuclear translocation [31, 35-38]. However, recent reports including a study by Napolitano et al. [29, 30, 41] imply that nuclear translocation of TFEB and TFE3 can be accomplished when their nuclear export pathway is inhibited because these TFs undergo nucleocytoplasmic shuttling.

Based on previous reports and my results described above, I propose three possible explanations for dysregulation of the TFEB nuclear export pathway in *A/A* cells during ER

stress. First, dysregulation of the TFEB nuclear export pathway may arise due to malfunction of the CRM1-mediated nuclear export pathway. eIF2 $\alpha$  phosphorylation deficiency may dysregulate the CRM1-mediated nuclear export pathway, which is responsible for nuclear export of diverse CRM1 cargo proteins [95] including TFEB and TFE3, under ER stress conditions. However, this is not a plausible explanation because previous reports indicate that the CRM1-mediated nuclear export pathway works properly for nuclear localization or export of specific target proteins in *A/A* cells under ER stress conditions. For example, nuclear factor erythroid-2-related factor 2 (NRF2) is a TF essential for antioxidant response element-mediated gene expression and a direct PERK substrate [96]. Under normal conditions, NRF2 also continuously shuttles between the cytosol and nucleus via CRM1-dependent nuclear export [95, 97]. However, Tm treatment induces nuclear translocation of NRF2 independently of eIF2 $\alpha$  phosphorylation [96]. In addition, it was reported that nuclear export of p53 mediated by eIF2 $\alpha$  kinases such as PERK and PKR occurs independently of eIF2 $\alpha$  phosphorylation under ER stress conditions [77]. Thus, dysregulation of the TFEB nuclear export pathway may arise due to impairment of a pathway that specifically exports TFEB and a few related proteins from the nucleus, rather than due to malfunction of the CRM1-mediated nuclear export pathway, which can affect diverse CRM1 cargo proteins.

Second, dysregulation of the TFEB nuclear export pathway may arise due to the absence or presence of a specific modification (such as phosphorylation or other PTMs) on a specific residue(s) of TFEB that can determine its nuclear export. Phosphorylation of S142 and S138 is proposed to be required for recognition and binding of the TFEB NES by CRM1 [29, 30, 42], which is crucial for efficient nuclear export, whereas phosphorylation of S211 is required for cytosolic retention of TFEB via 14-3-3 binding [35-38]. Phosphorylation of S138 is dependent on prior phosphorylation of S142 [29, 30]. Furthermore, reports indicate that S142 and/or S138 phosphorylation may be nuclear events mediated by several kinases such as mTORC1 (at S142 and S138), extracellular signal-regulated kinase (at S142), and GSK3 $\beta$  (at S138) [29, 30]. Yin et al. reported that CDK4/6 interact with and phosphorylate TFEB on S142 in the nucleus [41]. Thus, the status of S142 phosphorylation is an important determinant of TFEB nuclear export. However, dephosphorylation levels of total TFEB proteins on S142 were similar in *S/S* and *A/A* cells treated with Tm (Figure 7E). Therefore, it is possible that impairment of TFEB nuclear translocation may not arise due to dysregulation of TFEB dephosphorylation on S142 in *A/A* cells during ER stress. However, although WB analysis of total TFEB proteins indicates that S142 of TFEB is dephosphorylated by Ca<sup>2+</sup>-dependent calcineurin, I cannot rule out the possibility that S142 of nuclear TFEB is immediately and temporarily rephosphorylated by nuclear kinases (such as mTORC1 or CDK4/6), and that phosphorylated TFEB is rapidly exported to the cytosol in *A/A* cells during ER stress. Thus, even under ER stress conditions, the continuous cycle of nuclear import and export of TFEB

according to its dephosphorylation and rephosphorylation may give the impression that it never enters the nuclei of *A/A* cells. Therefore, it is worth examining whether specific nuclear kinases (such as mTORC1 and CDK4/6) are activated and localized to the nucleus for rephosphorylation of TFEB on S142 in *A/A* cells during ER stress. These issues require further investigation.

Lastly, dysregulation of the TFEB nuclear export pathway may arise due to the lack of a TFEB-interacting nuclear protein that retains TFEB in the nucleus. In this report, I suggested that the activated ATF6 $\alpha$  form (HA-ATF6 $\alpha$ (1-373)) is a missing TFEB-interacting nuclear protein in *A/A* cells during ER stress. Co-IP assays (Figure 10E), the PLA (Figures 10F, G and 12B), and colocalization experiments (Figures 10H and 12C) indicate there is a physical interaction between TFEB and the activated ATF6 $\alpha$  form, and that most of these complexes are in the nucleus, although the interaction might also occur in the cytosol. This nuclear interaction retains TFEB in the nucleus. In addition, this specific interaction can induce TFEB dephosphorylation, 14-3-3 dissociation, and nuclear translocation of TFEB, regardless of ER stress. However, further studies are required to answer many questions about the detailed molecular mechanisms underlying activated ATF6 $\alpha$  form-mediated dephosphorylation and nuclear translocation of TFEB. Furthermore, although I used the activated ATF6 $\alpha$  form to promote the nuclear translocation and functional activity of TFEB and TFE3 in *A/A* cells because its activities were highest, other TFs (ATF4 and XBP1s) also significantly affected nuclear translocation of TFEB in *A/A* cells (Figure 10A, B). In addition, expression and activation of ATF4, XBP1, and ATF6 are influenced by each other. ATF4 facilitates synthesis of ATF6 $\alpha$  and its trafficking from the ER to the Golgi for its proteolytic activation [14]. The activated ATF6 $\alpha$  form activates transcription of the *Xbp1* genes [93] and heterodimerizes with XBP1s to induce UPR genes [88]. In addition, overexpression of the activated ATF6 $\alpha$  form increased the mRNA and protein levels of *Atf4* and *Xbp1t/s* (Figure 13A, B). Furthermore, ATF4 is reportedly required to induce transcription of a set of autophagy genes in response to ER stress [50] and hepatic overexpression of XBP1s enhances *Tfeb* transcription and autophagy [98]. Thus, I cannot rule out the possibility that ATF4 and XBP1s play roles in activated ATF6 $\alpha$  form-overexpressing *A/A* cells under ER stress conditions. Further work is needed to investigate whether ATF4 and/or XBP1s are required for the improvement of autophagy by the activated ATF6 $\alpha$  form in *A/A* cells during ER stress.

Under ER stress conditions, *A/A* cells displayed abnormal phenotypes of LC3A/B-positive structures (such as few autophagic puncta and perinuclear accumulated small LC3A/B-positive structures) (Figure 2A, B). Although expression of autophagy genes was not changed as much by the activated ATF6 $\alpha$  form as by the constitutively active TFEB mutant (TFEB(S211A)-FLAG) (Figure 13A, B vs. Figure 16C, E), the activated ATF6 $\alpha$  form prevented the abnormal phenotypes more strongly than the constitutively active TFEB mutant (Figure

13D–F vs. Figure 16F, H) in *A/A* cells during ER stress, indicating that the activated ATF6 $\alpha$  form has additional roles in autophagy besides induction of nuclear translocation of TFEB and TFE3 in *A/A* cells. The ER is thought to be the central organelle for *de novo* lipid synthesis. *De novo* phosphatidylcholine synthesis is required for autophagosome membrane formation and maintenance during autophagy [99, 100]. In addition, overexpression of the activated ATF6 $\alpha$  form modulates enzymatic activities of the CDP-choline pathway and thereby enhances phosphatidylcholine biosynthesis and ER expansion [54] (Figure 13G). Therefore, overexpression of the activated ATF6 $\alpha$  form may increase *de novo* lipid synthesis required for autophagosome formation in ER membranes, which may not occur or be insufficient in *A/A* cells during ER stress. However, accumulation of the fragmented ER in Tm-treated *A/A*<sup>Hep</sup> cells was prevented by the activated ATF6 $\alpha$  form (Figure 13G) but not by the constitutively active TFEB mutant (Figure 17A, B), indicating that the altered ER structures in Tm-treated *A/A* cells are not critical obstacles of autophagy pathways. Furthermore, extensive accumulation of the fragmented ER may indicate that lipid biosynthesis is increased in Tm-treated *A/A* cells. However, lipid biosynthesis may not provide specific or sufficient lipid species required for autophagosome formation during ER stress due to deficiency of the activated ATF6 $\alpha$  form, indicating that *A/A* cells might require lipid biosynthesis mediated by the activated ATF6 $\alpha$  form during ER stress. Further investigation is needed to define the molecular details of autophagy improvement by activated ATF6 $\alpha$  form-mediated phosphatidylcholine synthesis in *A/A* cells during ER stress.

In most cases, the activated ATF6 $\alpha$  form is introduced as a TF that is required for expression of diverse UPR genes responsible for increasing the folding capacity of the ER and restoring ER homeostasis [88, 89, 101]. However, multiple reports indicate that ATF6 $\alpha$  exhibits stress-specific transcriptional gene induction that may arise by changing its interacting TFs, such as PGC1 $\alpha$  [101], CRT2 [102], and C/EBP- $\beta$  [103]. Therefore, many proteins encoded by the activated ATF6 $\alpha$  form reside outside the ER and have no ER-related roles, including catalase, which functions in stimulated ischemia/reperfusion [104, 105]; Rheb (Ras homolog enriched in brain), which functions in cardiac hypertrophy [104]; and DAPK1 (death-associated protein kinase 1), which functions in the INF- $\gamma$ -induced pathway [103]. In particular, DAPK1 can regulate the nucleation step of autophagy via formation of the Beclin1-Vps34 complex [106]. Additionally, I propose that the activated form of ATF6 $\alpha$  has another important role, namely, interacting with the autophagy master TFs TFEB and TFE3, and thereby inducing their nuclear retention under ER stress conditions. Therefore, the activated form of ATF6 $\alpha$  can contribute to expression of genes required for autophagy during ER stress. Thus, the results demonstrate that ATF6 $\alpha$  is a multifunctional TF that can reprogram cellular proteostasis by activating both UPR and autophagy pathways under ER stress conditions.

Under ER stress conditions, cells induce autophagy in addition to the UPR, to restore ER homeostasis by degrading unfolded and aggregated proteins [43-46]. Therefore, UPR pathways can directly and indirectly control autophagy through ER membrane localized proteins (such as IRE1 $\alpha$  and inositol 1,4,5-trisphosphate receptor) and several UPR TFs (such as XBP1s, ATF4, CHOP, and ATF6) [45, 46]. Among these proteins, expression and activation of many TFs (such as XBP1s, ATF4, CHOP, and ATF6) are regulated by eIF2 $\alpha$  phosphorylation under ER stress conditions. Regulation of eIF2 $\alpha$  phosphorylation may have a great impact on cellular homeostasis. These findings suggest that fine-tuning of eIF2 $\alpha$  phosphorylation can be a potential tool to treat rapidly growing tumors, which use both UPR and autophagy pathways to maintain cellular homeostasis.

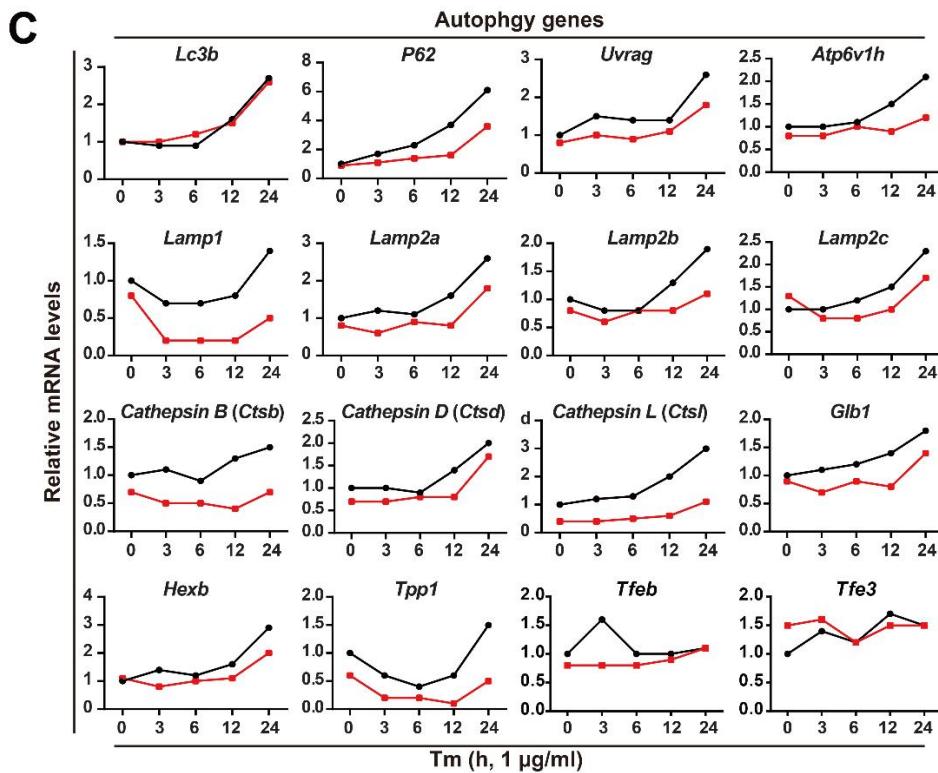
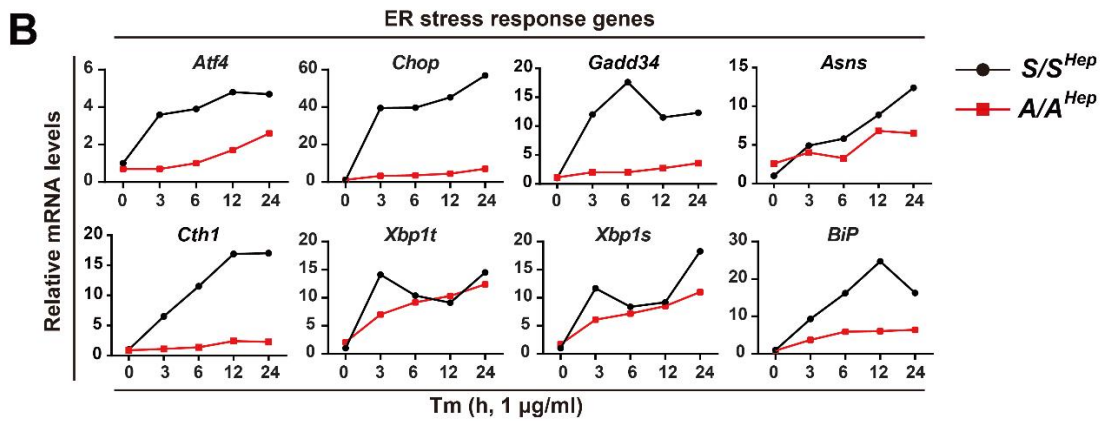
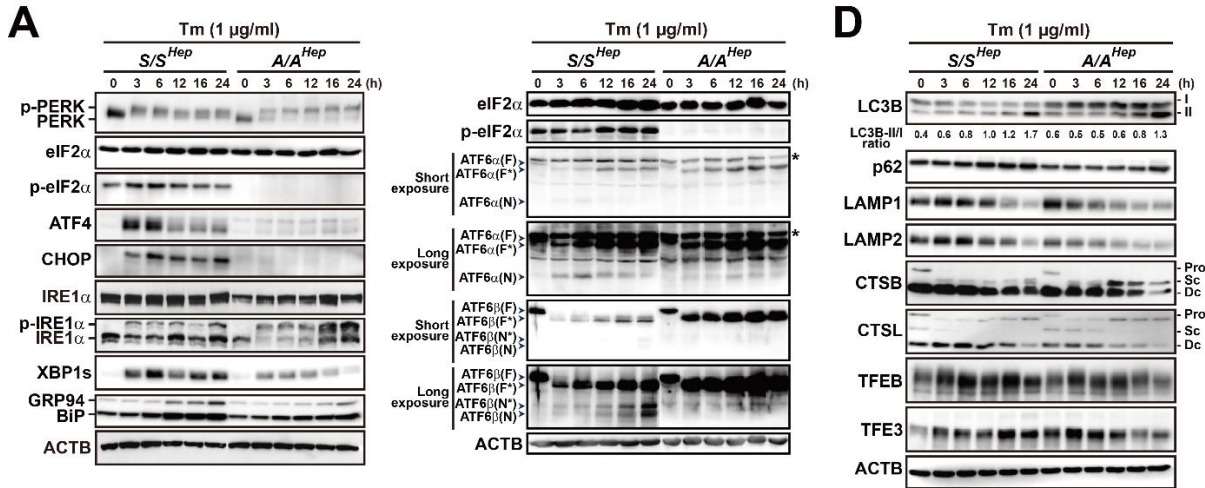


**Figure 1. Protein and mRNA expression of autophagy and UPR genes is dysregulated in A/A cells during ER stress.**

(A) WB analysis of UPR proteins in lysates of *S/S<sup>Hep</sup>* and *A/A<sup>Hep</sup>* cells treated with Tm (1 µg/mL) for the indicated durations. ATF6α(F): full-length glycosylated ATF6α; ATF6α(F\*): full-length unglycosylated ATF6α; ATF6α(N): cleaved N-terminal fragment of ATF6α; ATF6β(F): full-length glycosylated ATF6β; ATF6β(F\*): full-length unglycosylated ATF6β; ATF6β(N\*) and ATF6β(N): cleaved N-terminal fragments of ATF6β. (B and C) Quantitative RT-PCR analysis of mRNA expression of ER stress response (B) and autophagy (C) genes in *S/S<sup>Hep</sup>* and *A/A<sup>Hep</sup>* cells treated with Tm (1 µg/mL) for the indicated durations. (D) WB analysis of autophagy proteins in lysates of *S/S<sup>Hep</sup>* and *A/A<sup>Hep</sup>* cells treated with Tm (1 µg/mL) for the indicated durations. CTSB: cathepsin B; CTSL: cathepsin L.

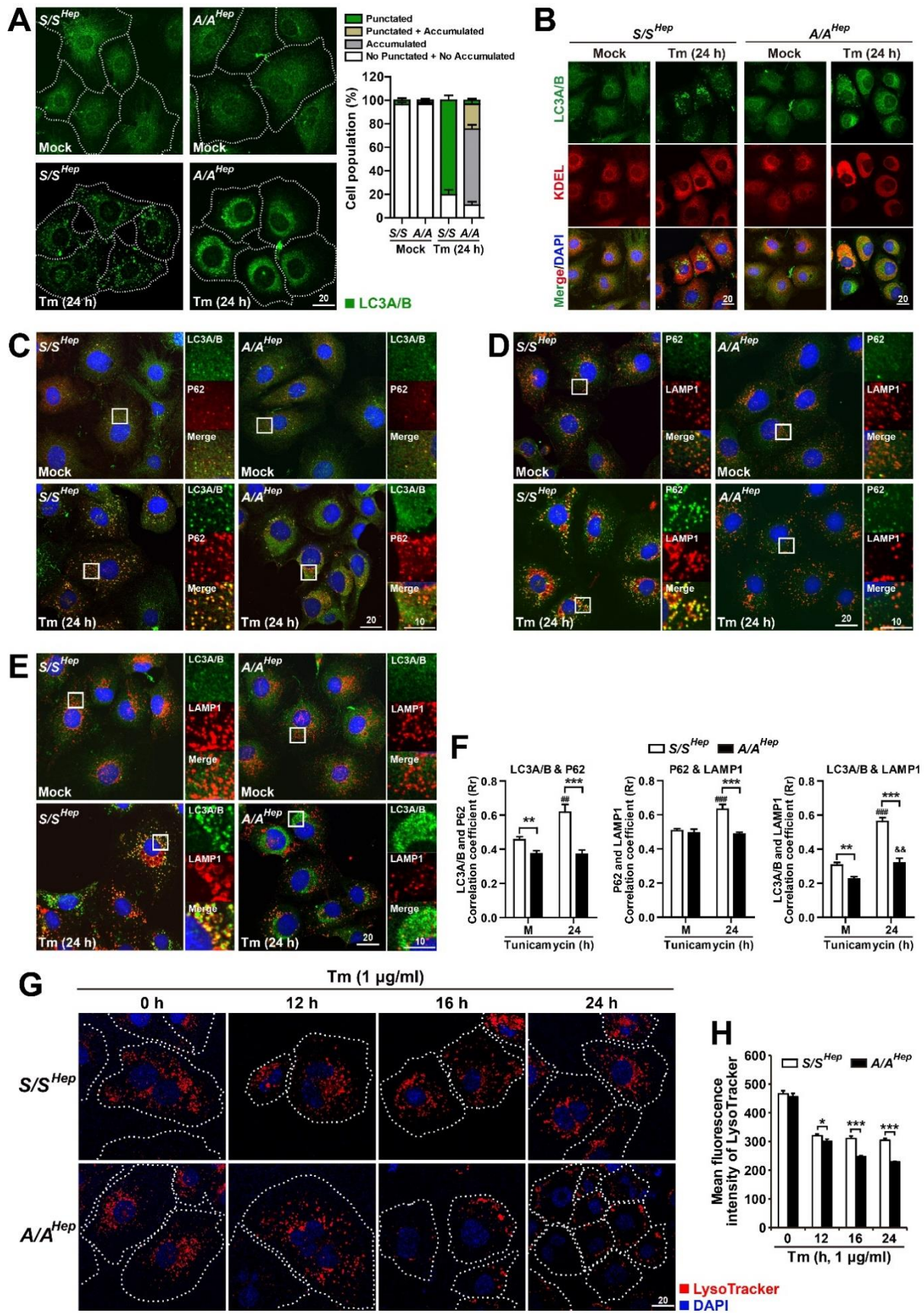
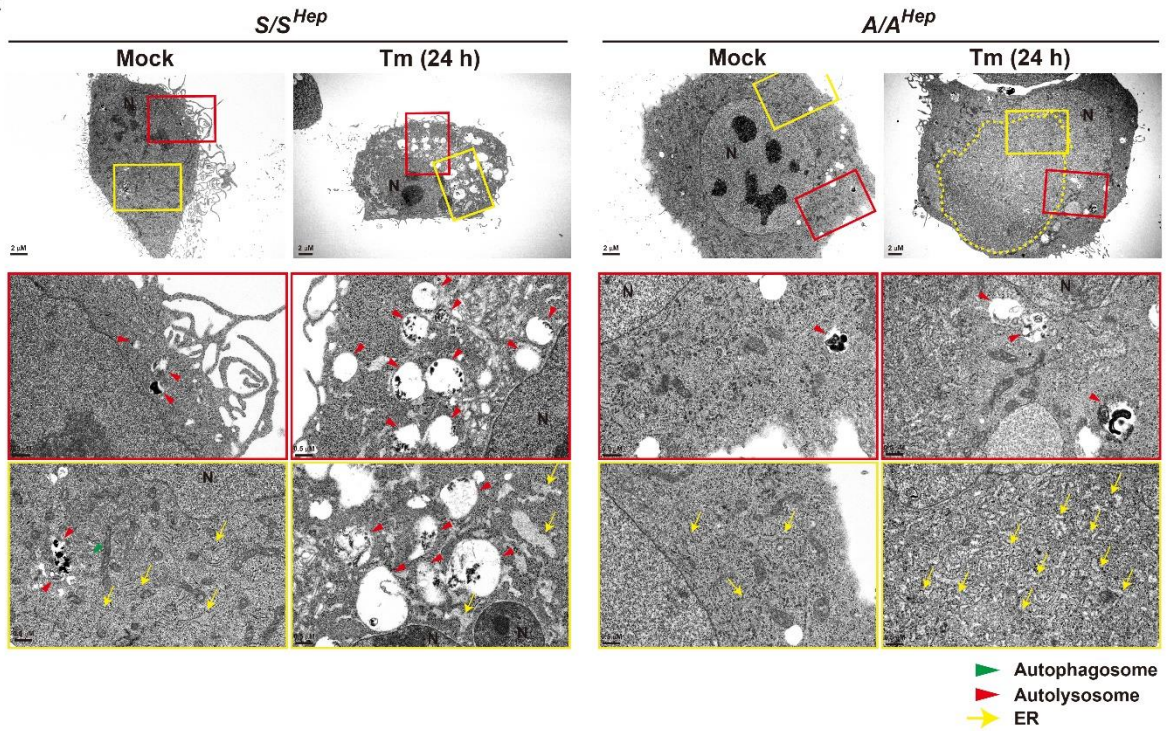




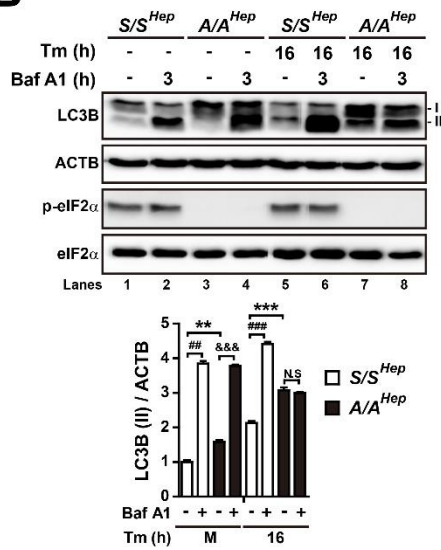
**Figure 2. Autophagy is impaired in A/A cells during ER stress.**

(A) Representative IF images of LC3A/B in *S/S<sup>Hep</sup>* and *A/A<sup>Hep</sup>* cells treated without (Mock) or with Tm (1 µg/mL) for 24 h. The dotted white line defines the cell boundary. Scale bar, 20 µm. The graph depicts the fraction (%) of cells with different LC3A/B staining patterns (the “punctated” group represents cells with LC3A/B-positive puncta only, the “punctated + accumulated” group represents cells with both LC3A/B-positive puncta and condensed LC3A/B staining in the perinuclear region, the “accumulated” group represents cells with condensed LC3A/B staining only in the perinuclear region, and “no punctated + no accumulated” represents cells with neither LC3A/B-positive puncta nor condensed LC3A/B staining in the perinuclear region). Data are presented as mean ± SEM of at least 50 cells from ten random fields per group. (B) Representative IF images of an autophagosome marker (LC3A/B, green) and an ER marker (KDEL, red) in *S/S<sup>Hep</sup>* and *A/A<sup>Hep</sup>* cells treated without (Mock) or with Tm (1 µg/mL) for 24 h. Nuclei were stained with DAPI (blue). Scale bar, 20 µm. (C–E) Representative IF images of autophagy markers (LC3A/B or p62) and a lysosome marker (LAMP1) in *S/S<sup>Hep</sup>* and *A/A<sup>Hep</sup>* cells treated without (Mock) or with Tm (1 µg/mL) for 24 h. Cells were fixed and costained with anti-LC3A/B (green) and anti-p62 (red) antibodies in (C), anti-p62 (green) and anti-LAMP1 (red) antibodies in (D), and anti-LC3A/B (green) and anti-LAMP1 (red) antibodies in (E). Nuclei were stained with DAPI (blue). The right panels are magnified images of the boxes in the left panels. Scale bars, left panels (20 µm) and right panels (10 µm). (F) Quantification of the colocalization of LC3A/B with p62 in (C) and LAMP1 with p62 or LC3A/B in (D and E). Data are presented as mean ± SEM of at least 50 cells from ten random fields per group. \*\*p < 0.01 and \*\*\*p < 0.001, *S/S<sup>Hep</sup>* vs. *A/A<sup>Hep</sup>*, ##p < 0.01 and ###p < 0.001, Mock (M) vs. 24 h in *S/S<sup>Hep</sup>*, &&p < 0.01, Mock (M) vs. 24 h in *A/A<sup>Hep</sup>* (Student’s t-test). (G) Representative LysoTracker staining images of *S/S<sup>Hep</sup>* and *A/A<sup>Hep</sup>* cells. Cells were treated with Tm (1 µg/mL) for the indicated durations and stained with LysoTracker (100 nM, red) and Hoechst 33258 (10 µg/mL, blue) for the last 30 min of the treatment. The dotted white line defines the cell boundary. Scale bar, 20 µm. (H) Quantification of the MFI of LysoTracker in (G). Data are presented as mean ± SEM of at least 50 cells from ten random fields per group. \*p < 0.05 and \*\*\*p < 0.001, *S/S<sup>Hep</sup>* vs. *A/A<sup>Hep</sup>* (Student’s t-test).

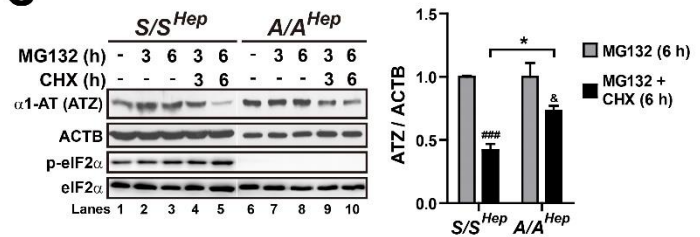
**A**



**B**



**C**



**D**

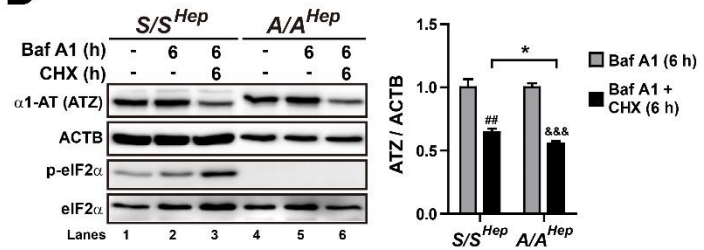


**Figure 3. Autophagic flux is impaired in A/A cells during ER stress.**

(A) Representative TEM images of  $S/S^{Hep}$  and  $A/A^{Hep}$  cells treated without (Mock) or with Tm (1  $\mu\text{g}/\text{mL}$ ) for 24 h. The panels of the second (red) and third (yellow) rows are magnified images of the red and yellow boxes in the panels of the first row, respectively. Green arrowheads indicate autophagosomes, red arrowheads indicate autolysosomes, and yellow arrows indicate the ER. The dotted yellow line defines a region of dilated and fragmented ER structures. Scale bars, first row (2  $\mu\text{m}$ ) and second and third rows (0.5  $\mu\text{m}$ ). (B) WB analysis of LC3B in protein lysates of  $S/S^{Hep}$  and  $A/A^{Hep}$  cells. Cells were treated without or with Tm (1  $\mu\text{g}/\text{mL}$ ) for 16 h in the absence or presence of the lysosomal inhibitor Baf A1 (200 nM) for 3 h before harvest. The graph depicts the LC3B-II level normalized to the ACTB level. Data are presented as mean  $\pm$  SEM of three independent experiments. \*\* $p < 0.01$  and \*\*\* $p < 0.001$ ,  $S/S^{Hep}$  vs.  $A/A^{Hep}$ ; ## $p < 0.01$  and ### $p < 0.001$ , Baf A1(-) vs. Baf A1(+) in  $S/S^{Hep}$ ; && $p < 0.01$  and &&& $p < 0.001$ , Baf A1(-) vs. Baf A1(+) in  $A/A^{Hep}$ ; N.S, no significant difference (Student's t-test). (C and D) WB analysis of alpha-1-antitrypsin mutant Z ( $\alpha 1$ -AT (ATZ)) in protein lysates of  $S/S^{Hep}$  and  $A/A^{Hep}$  cells. Cells were transfected with the pcDNA3.1- $\alpha 1$ -AT(ATZ) plasmid for 24 h. Transfected cells were treated with Mock, the proteasome inhibitor MG132 only (20  $\mu\text{M}$ ) (C), the lysosomal inhibitor Baf A1 only (100 nM) (D), MG132 plus the translation inhibitor CHX (100  $\mu\text{g}/\text{mL}$ ) (C), or Baf A1 plus CHX (D) for the indicated durations. The graphs depict the ATZ level normalized to the ACTB level after treatment for 6 h. Data are presented as mean  $\pm$  SEM of three independent experiments. \* $p < 0.05$ ,  $S/S^{Hep}$  vs.  $A/A^{Hep}$  in MG132 + CHX (6 h); ## $p < 0.01$  and ### $p < 0.001$ , MG132 (6 h) vs. MG132 + CHX (6 h) or Baf A1 (6 h) vs. Baf A1 + CHX (6 h) in  $S/S^{Hep}$ ; & $p < 0.05$  and &&& $p < 0.001$ , MG132 (6 h) vs. MG132 + CHX (6 h) or Baf A1 (6 h) vs. Baf A1 + CHX (6 h) in  $A/A^{Hep}$  (Student's t-test).

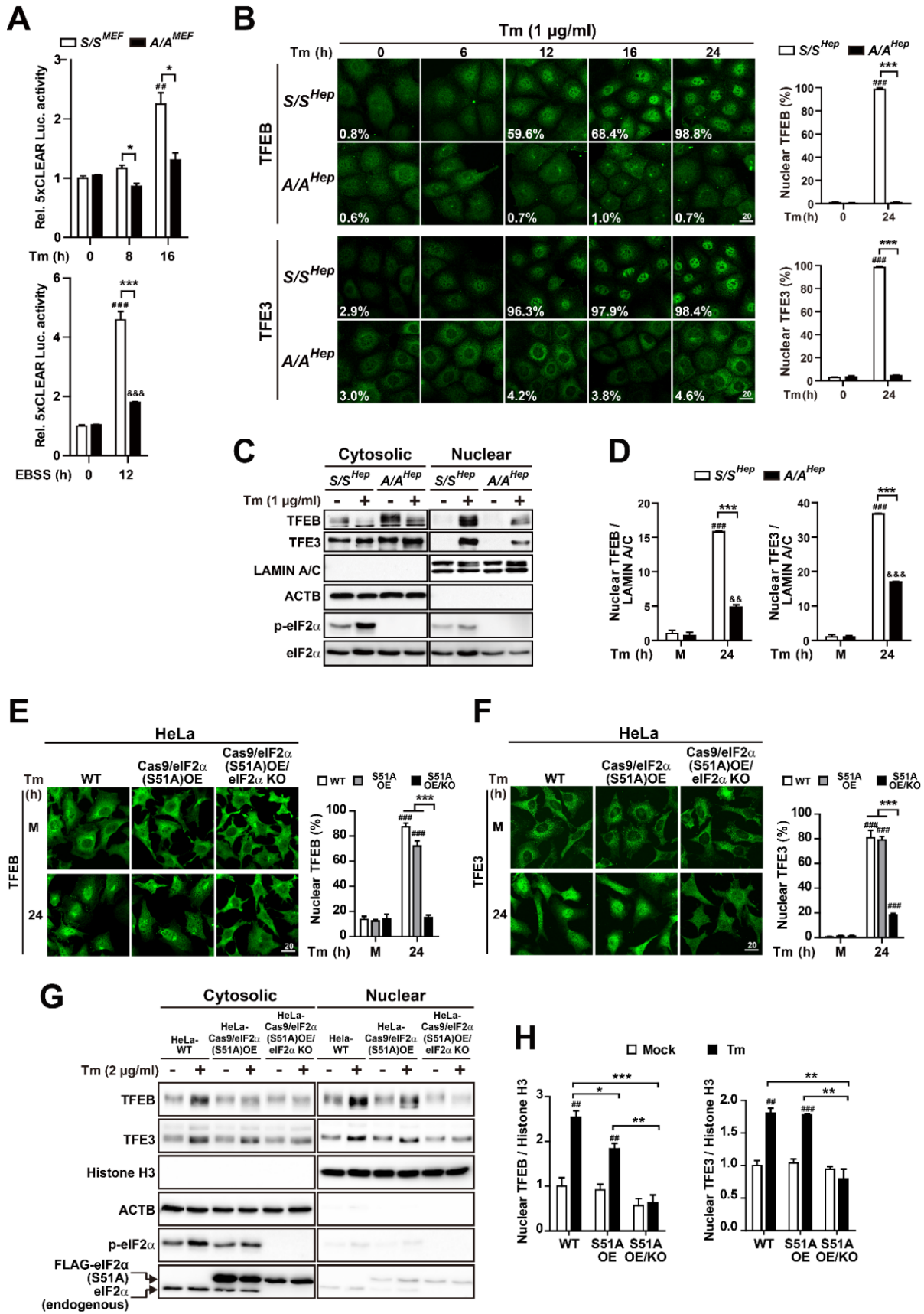


**Figure 4. Nuclear translocation of TFEB and TFE3 is impaired in A/A cells during ER stress.**

(A) Luciferase activity assay of the 5xCLEAR luciferase reporter. *S/S<sup>MEF</sup>* and *A/A<sup>MEF</sup>* cells were cotransfected with plasmids expressing 5xCLEAR-driven firefly luciferase and CMV-driven *Renilla* luciferase for 30 h. Cells were treated with Tm (100 ng/mL) for the indicated durations or starved with EBSS for 12 h, and then luciferase activities were measured. Data are presented as mean  $\pm$  SEM of three independent experiments. \* $p < 0.05$  and \*\*\* $p < 0.001$ , *S/S<sup>MEF</sup>* vs. *A/A<sup>MEF</sup>*; ## $p < 0.01$  and ### $p < 0.001$ , 0 h vs. other time points in *S/S<sup>MEF</sup>*; && $p < 0.001$ , 0 h vs. 12 h in *A/A<sup>MEF</sup>* (Student's t-test). (B) Representative IF images of TFEB (upper) and TFE3 (lower) in *S/S<sup>Hep</sup>* and *A/A<sup>Hep</sup>* cells treated with Tm (1  $\mu$ g/mL) for the indicated durations. Scale bar, 20  $\mu$ m. The percentage of cells with nuclear localized TFEB or TFE3 is indicated in each image and shown in the graphs (left panel). Data are presented as mean  $\pm$  SEM of about 140–500 cells from six random fields per group. \*\*\* $p < 0.001$ , *S/S<sup>Hep</sup>* vs. *A/A<sup>Hep</sup>*; ### $p < 0.001$ , 0 h vs. 24 h (Student's t-test). (C) WB analysis of the subcellular distributions of TFEB and TFE3 in *S/S<sup>Hep</sup>* and *A/A<sup>Hep</sup>* cells treated without or with Tm (1  $\mu$ g/mL) for 24 h. Lamin A/C and ACTB were used as loading controls of the nuclear and cytoplasmic fractions, respectively. (D) Densitometric quantification of nuclear TFEB and TFE3 in (C). Values were normalized against Lamin A/C levels. Data are presented as mean  $\pm$  SEM of three independent experiments. \*\*\* $p < 0.001$ , *S/S<sup>Hep</sup>* vs. *A/A<sup>Hep</sup>* at 24 h; ### $p < 0.001$ , Mock (M) vs. 24 h in *S/S<sup>Hep</sup>*; && $p < 0.01$  and &&& $p < 0.001$ , Mock (M) vs. 24 h in *A/A<sup>Hep</sup>* (Student's t-test). (E and F) Representative IF images of TFEB (E) and TFE3 (F) in wild-type HeLa cells (HeLa-WT), HA-Cas9- and FLAG-eIF2 $\alpha$ (S51A)-expressing HeLa cells (HeLa-Cas9/eIF2 $\alpha$ (S51A)OE), and HA-Cas9- and FLAG-eIF2 $\alpha$ (S51A)-expressing and eIF2 $\alpha$ -KO HeLa cells (HeLa-Cas9/eIF2 $\alpha$ (S51A)OE/eIF2 $\alpha$  KO). Cells were treated without or with Tm (2  $\mu$ g/mL) for 24 h. Scale bar, 20  $\mu$ m. The graphs depict the percentage of cells with nuclear TFEB or TFE3. Data are presented as mean  $\pm$  SEM of at least 150 cells from six random fields per group. \*\*\* $p < 0.001$ , HeLa-WT or HeLa-Cas9/eIF2 $\alpha$ (S51A)OE vs. HeLa-Cas9/eIF2 $\alpha$ (S51A)OE/eIF2 $\alpha$  KO; ### $p < 0.001$ , Mock vs. 24 h (Student's t-test). (G) WB analysis of the subcellular distributions of TFEB and TFE3 in HeLa-WT, HeLa-Cas9/eIF2 $\alpha$ (S51A), and HeLa-Cas9/eIF2 $\alpha$ (S51A)/eIF2 $\alpha$  KO cells treated without or with Tm (2  $\mu$ g/mL) for 24 h. Histone H3 and ACTB were used as loading controls of the nuclear and cytoplasmic fractions, respectively. (H) Densitometric quantification of nuclear TFEB and TFE3 in (G). Values were normalized against Histone H3 levels. Data are presented as mean  $\pm$  SEM of three independent experiments. \* $p < 0.05$ , \*\* $p < 0.01$ , and \*\*\* $p < 0.001$ , HeLa-WT or HeLa-Cas9/eIF2 $\alpha$ (S51A)OE vs. HeLa-Cas9/eIF2 $\alpha$ (S51A)OE/eIF2 $\alpha$  KO; ## $p < 0.01$  and ### $p < 0.001$ , Mock vs. Tm (Student's t-test).

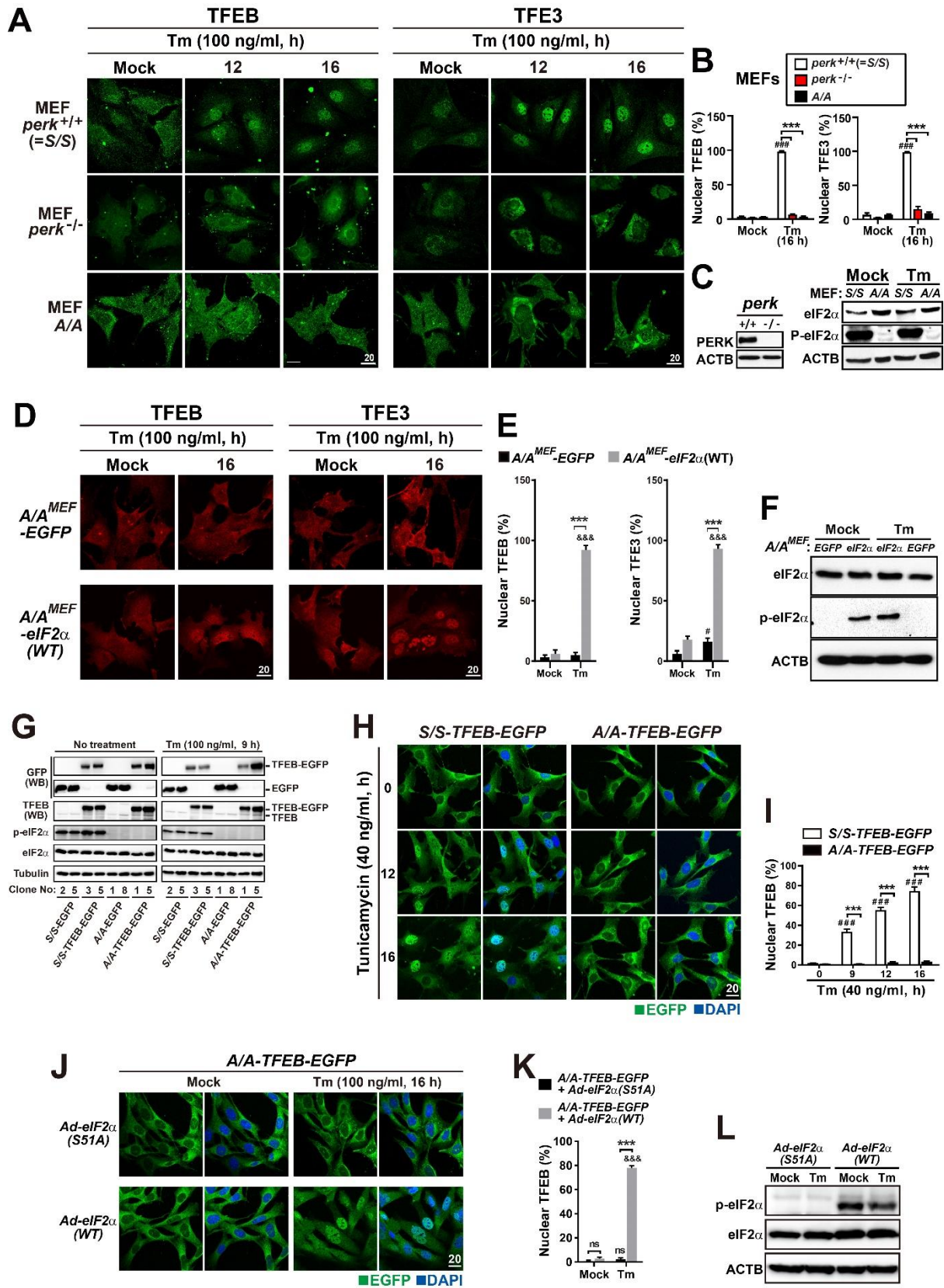


**Figure 5. Overexpression of wild-type eIF2 $\alpha$  rescues the impairment of TFEB and TFE3 nuclear translocation in several A/A cell lines during ER stress.**

(A) Representative IF images of TFEB (left) and TFE3 (right) in MEFs (*perk*<sup>+/+</sup> (=S/S), *perk*<sup>-/-</sup>, and A/A) treated with Tm (100 ng/mL) for the indicated durations. Scale bar, 20  $\mu$ m. (B) The percentage of cells with nuclear TFEB and TFE3 in (A) at 16 h. Data are presented as mean  $\pm$  SEM of at least 70 cells from six random fields per group. \*\*\**p* < 0.001, *perk*<sup>+/+</sup> (=S/S) vs. other cells; ###*p* < 0.001, Mock vs. Tm in *perk*<sup>+/+</sup> (=S/S) (Student's t-test). (C) WB analysis of protein lysates of MEFs used in (A and B) treated with Mock or Tm (100 ng/mL) for 16 h. (D) Representative IF images of TFEB and TFE3 in EGFP- or wild-type eIF2 $\alpha$ -expressing A/A<sup>MEF</sup> (A/A<sup>MEF</sup>-EGFP or A/A<sup>MEF</sup>-eIF2 $\alpha$ (WT)) cells treated with Tm (100 ng/mL) for the indicated durations. Scale bar, 20  $\mu$ m. (E) The percentage of cells with nuclear TFEB and TFE3 in (D) at 16 h. Data are presented as mean  $\pm$  SEM of at least 90 cells from six random fields per group. \*\*\**p* < 0.001, A/A<sup>MEF</sup>-EGFP vs. A/A<sup>MEF</sup>-eIF2 $\alpha$ (WT); #*p* < 0.05, Mock vs. Tm in A/A<sup>MEF</sup>-EGFP; &&&*p* < 0.001, Mock vs. Tm in A/A<sup>MEF</sup>-eIF2 $\alpha$ (WT) (Student's t-test). (F) WB analysis of protein lysates of A/A<sup>MEF</sup>-EGFP and A/A<sup>MEF</sup>-eIF2 $\alpha$ (WT) cells treated with Mock or Tm (100 ng/mL) for 16 h. (G) WB analysis of GFP and TFEB-EGFP in protein lysates of S/S and A/A MEF cell lines stably expressing EGFP or TFEB-EGFP treated with Mock or Tm (100 ng/mL) for 9 h. (H) Representative fluorescence images of TFEB-EGFP in S/S-TFEB-EGFP and A/A-TFEB-EGFP MEFs. Cells were treated with Tm (40 ng/mL) for the indicated durations. The cellular localization of TFEB-EGFP was indicated by the green fluorescence signal of EGFP in cells. Nuclei were stained with DAPI (blue). Scale bar, 20  $\mu$ m. (I) The percentage of cells with nuclear TFEB-EGFP in (H). Data are presented as mean  $\pm$  SEM of at least 150 cells from six random fields per group. \*\*\**p* < 0.001, S/S-TFEB-EGFP vs. A/A-TFEB-EGFP; ###*p* < 0.001, 0 h vs. other time points in S/S-TFEB-EGFP (Student's t-test). (J) Representative fluorescence images of TFEB-EGFP in A/A-TFEB-EGFP MEFs. Cells infected with eIF2 $\alpha$ (S51A)- or eIF2 $\alpha$ (WT)-expressing adenoviruses for 30 h were treated with Mock or Tm (100 ng/mL) for 16 h. The cellular localization of TFEB-EGFP was indicated by the green fluorescence signal of EGFP in cells. Nuclei were stained with DAPI (blue). Scale bar, 20  $\mu$ m. (K) The percentage of cells with nuclear TFEB-EGFP in (J). Data are presented as mean  $\pm$  SEM of at least 130 cells from six random fields per group. \*\*\**p* < 0.001; Ad-eIF2 $\alpha$ (S51A) vs. Ad-eIF2 $\alpha$ (WT), &&&*p* < 0.001; Mock vs. Tm in Ad-eIF2 $\alpha$ (WT) (Student's t-test). (L) WB analysis of phosphorylated and total eIF2 $\alpha$  in protein lysates of the cells used in (J).

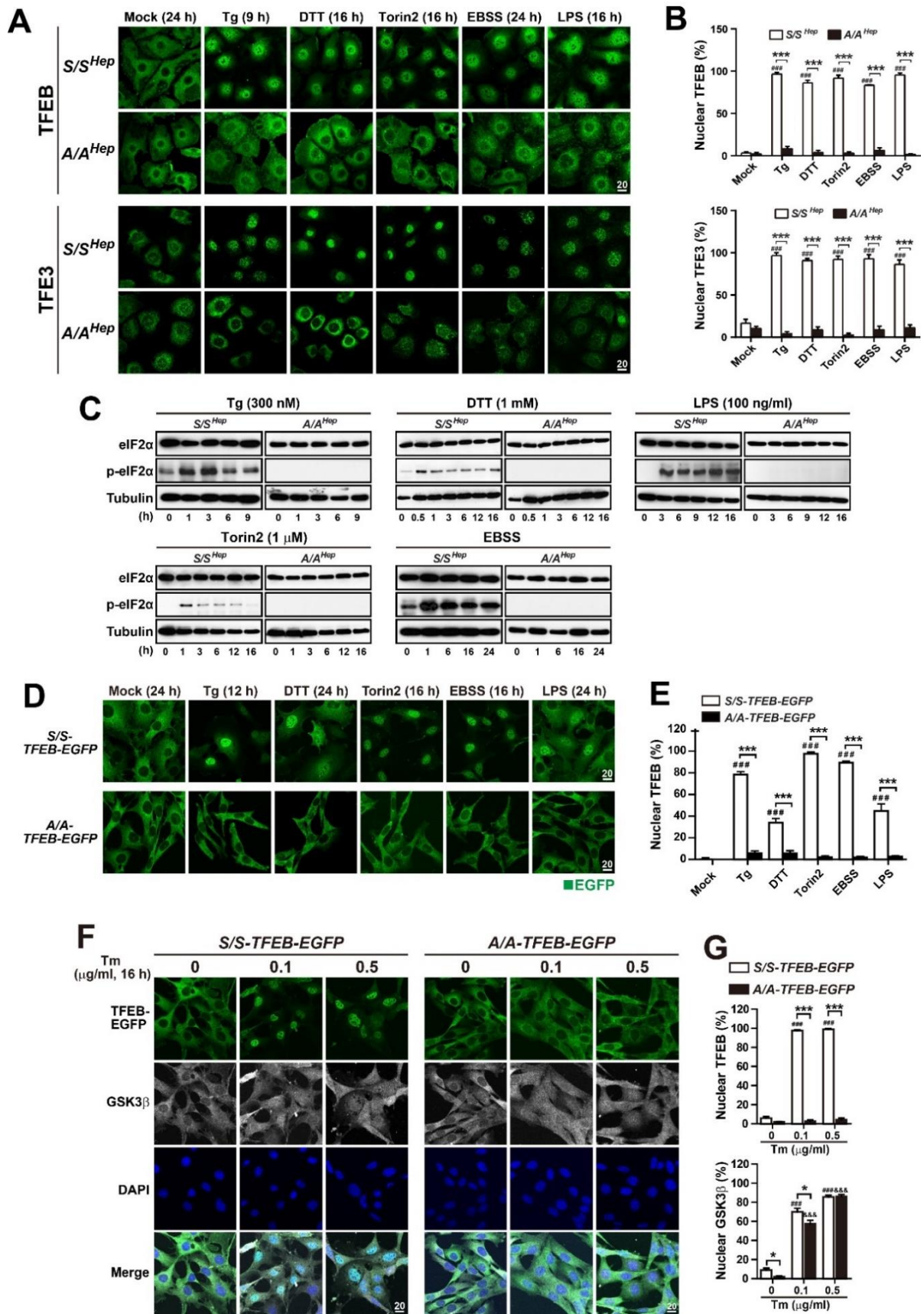




**Figure 6. Nuclear translocation of TFEB and TFE3, but not GSK3 $\beta$ , is specifically impaired in A/A cells under diverse autophagy-inducing conditions.**

(A) Representative IF images of TFEB (upper) and TFE3 (lower) in *S/S<sup>Hep</sup>* and *A/A<sup>Hep</sup>* cells treated with Mock, Tg (300 nM, 9 h), DTT (1 mM, 16 h), Torin2 (1  $\mu$ M, 16 h), EBSS (24 h), or LPS (100 ng/mL, 16 h). Scale bar, 20  $\mu$ m. (B) The percentage of cells with nuclear TFEB and TFE3 in (A). Data are presented as mean  $\pm$  SEM of at least 90 cells from six random fields per group. \*\*\* $p$  < 0.001, *S/S<sup>Hep</sup>* vs. *A/A<sup>Hep</sup>*; ### $p$  < 0.001, Mock vs. other treatments (Student's t-test). (C) WB analysis of phosphorylated and total eIF2 $\alpha$  in protein lysates of *S/S<sup>Hep</sup>* and *A/A<sup>Hep</sup>* cells treated with the chemicals as described in (A) for the indicated durations. (D) Representative fluorescence images of TFEB-EGFP in *S/S-TFEB-EGFP* and *A/A-TFEB-EGFP* MEFs. Cells were treated with Mock, Tg (500 nM, 12 h), DTT (2 mM, 24 h), Torin2 (250 nM, 16 h), EBSS (16 h), or LPS (300 ng/mL, 24 h). The cellular localization of TFEB-EGFP was indicated by the green fluorescence signal of EGFP in the cells. Nuclei were stained with DAPI (blue). Scale bar, 20  $\mu$ m. (E) The percentage of cells with nuclear TFEB-EGFP in (D). Data are presented as mean  $\pm$  SEM of at least 100 cells from six random fields per group. \*\*\* $p$  < 0.001, *S/S-TFEB-EGFP* vs. *A/A-TFEB-EGFP*; ### $p$  < 0.001, Mock vs. other treatments (Student's t-test). (F) Representative IF images (gray) of GSK3 $\beta$  in *S/S-* and *A/A-TFEB-EGFP* MEFs. Cells were treated with different concentrations (0, 0.1, or 0.5  $\mu$ g/mL) of Tm for 16 h. The cellular localization of TFEB-EGFP was indicated by the green fluorescence signal of EGFP in the cells. Nuclei were stained with DAPI (blue). Scale bar 20  $\mu$ m. (G) The percentage of cells with nuclear TFEB-EGFP or GSK3 $\beta$  in (F). Data are presented as mean  $\pm$  SEM of at least 170 cells from six random fields per group. \* $p$  < 0.05 and \*\*\* $p$  < 0.001, *S/S-TFEB-EGFP* vs. *A/A-TFEB-EGFP*; ### $p$  < 0.001, Mock vs. different concentrations in *S/S-TFEB-EGFP*; &&& $p$  < 0.001, Mock vs. different concentrations in *A/A-TFEB-EGFP* (Student's t-test).

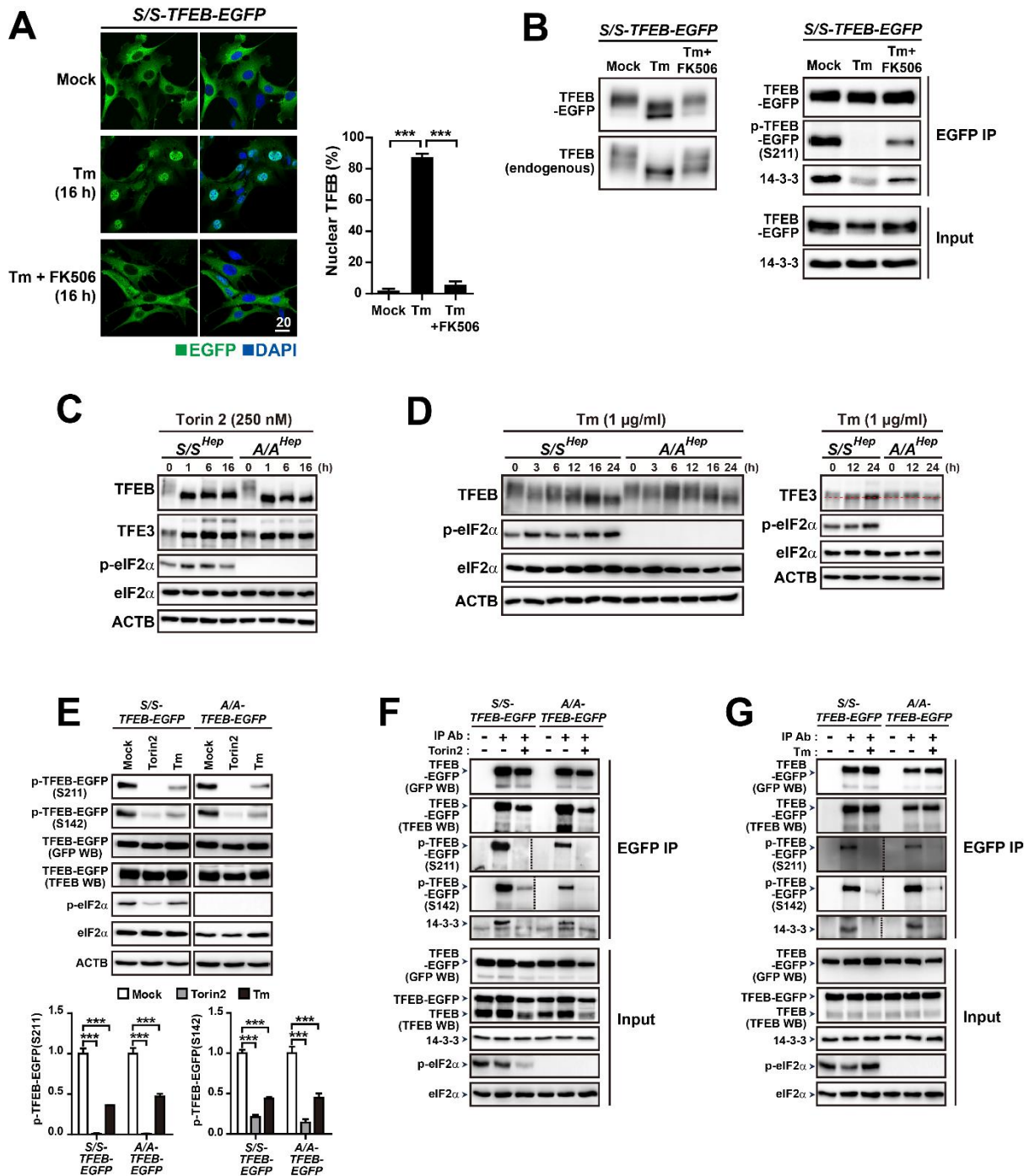


**Figure 7. eIF2 $\alpha$  phosphorylation deficiency does not impede regulation of TFEB and TFE3 nuclear translocation by 14-3-3.**

(A) Representative fluorescence images of TFEB-EGFP in *S/S-TFEB-EGFP* MEFs. *S/S-TFEB-EGFP* MEFs were treated without or with Tm only (50 ng/mL) or Tm (50 ng/mL) plus the calcineurin inhibitor FK506 (5  $\mu$ M) for 16 h. The cellular localization of TFEB-EGFP was indicated by the green fluorescence signal of EGFP in cells. Nuclei were stained with DAPI (blue). Scale bar 20  $\mu$ m. The graph depicts the percentage of cells with nuclear TFEB-EGFP. Data are presented as mean  $\pm$  SEM of at least 130 cells from six random fields per group. \*\*\*p < 0.001, Mock vs. Tm or Tm vs. Tm + FK506 (Student's t-test). (B) WB analysis of TFEB-EGFP and endogenous TFEB in protein lysates of cells treated with the same chemicals used in (A). In the left panel, proteins were separated by 6% SDS-PAGE and then subjected to WB analysis with antibodies against GFP or TFEB to detect TFEB-EGFP or endogenous TFEB, respectively. In the right panel, cells were lysed and subjected to IP with an anti-GFP antibody. Immunoprecipitates were analyzed by immunoblotting with antibodies against GFP (to detect TFEB-EGFP), phospho-(Ser)-14-3-3 binding motif (which binds to phosphorylated TFEB-EGFP at S211), or 14-3-3. (C and D) WB analysis of TFEB and TFE3 in protein lysates of *S/S<sup>Hep</sup>* and *A/A<sup>Hep</sup>* cells treated with the mTOR inhibitor Torin2 (250 nM) (C) or Tm (1  $\mu$ g/mL) (D) for the indicated durations. Proteins were separated by 6% SDS-PAGE to detect differences in the migration of TFEB and TFE3 proteins. (E) WB analysis of the phosphorylation status of TFEB-EGFP in protein lysates of *S/S-* and *A/A-TFEB-EGFP* MEFs treated with Torin2 (250 nM, 3 h) or Tm (100 ng/mL, 16 h). The phosphorylation status of TFEB-EGFP was analyzed using specific antibodies against phosphorylated S211 and phosphorylated S142. The graphs depict the levels of TFEB-EGFP phosphorylated at S211 or S142 normalized to that of total TFEB-EGFP. Data are presented as mean  $\pm$  SEM of three independent experiments. \*\*\*p < 0.001, Mock vs. Torin2 or Tm (Student's t-test). (F and G) WB analysis of immunoprecipitated TFEB-EGFP and 14-3-3 in *S/S-* and *A/A-TFEB-EGFP* MEFs treated with Torin2 (50 nM, 3 h) (F) or Tm (50 ng/mL, 16 h) (G). Cells were lysed and subjected to IP with an anti-GFP antibody. Immunoprecipitates were analyzed by immunoblotting with antibodies against GFP (to detect TFEB-EGFP), phospho-(Ser)-14-3-3 binding motif (which binds to phosphorylated TFEB-EGFP at S211), phospho-TFEB-(S142), or 14-3-3.

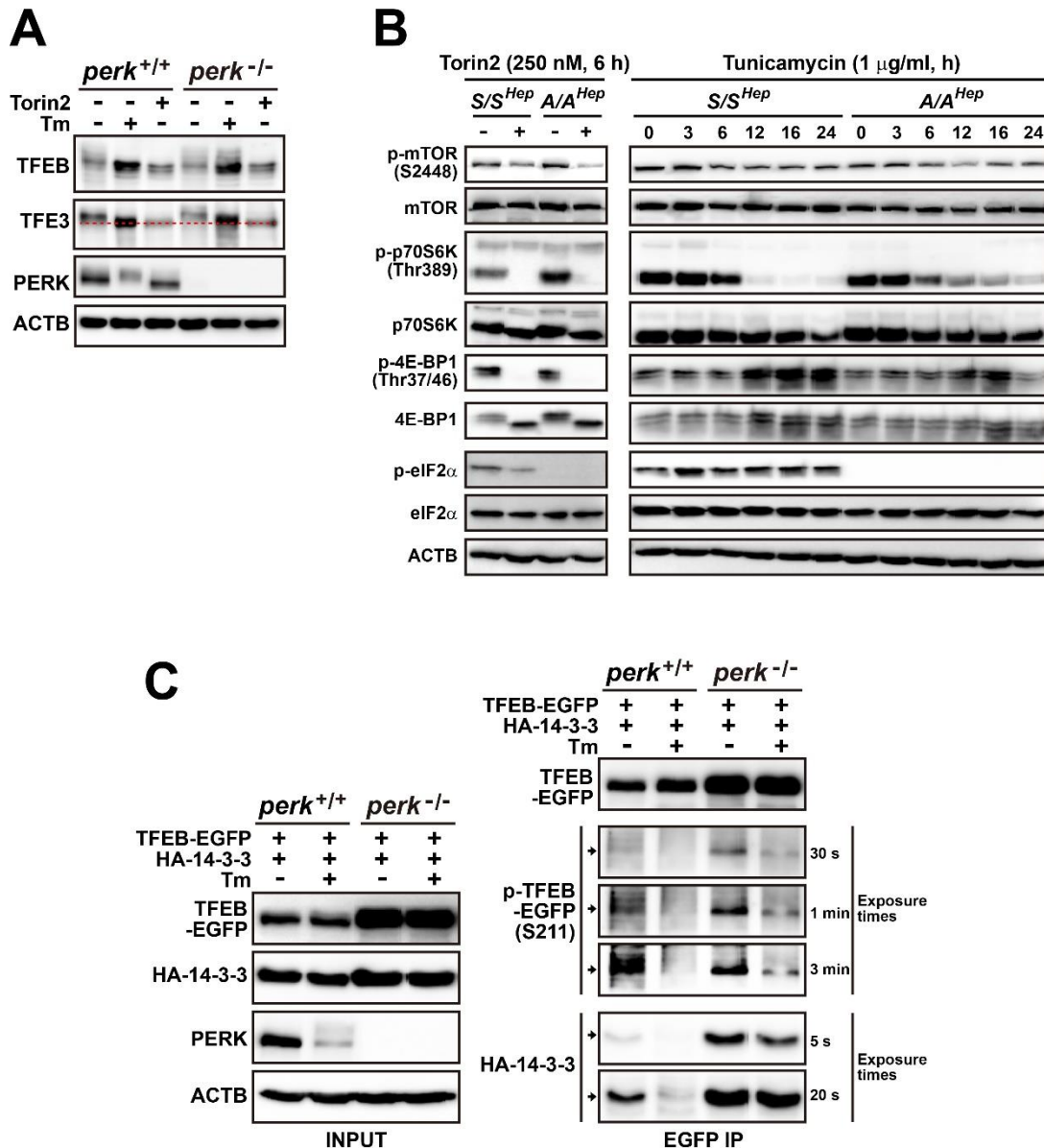


**Figure 8. PERK is required for TFEB and TFE3 dephosphorylation, and mTORC1 is inactivated during ER stress.**

(A) WB analysis of TFEB, TFE3, and PERK in wild-type (*perk*<sup>+/+</sup>) and *Perk*-KO (*perk*<sup>-/-</sup>) MEFs treated with Torin2 (250 nM) or Tm (100 ng/mL) for 16 h. (B) WB analysis of mTOR and its target proteins (p70S6K and 4E-BP1) in lysates of *S/S*<sup>Hep</sup> and *A/A*<sup>Hep</sup> cells treated without or with Torin2 (250 nM) and Tm (1 μg/mL) for the indicated durations. (C) WB analysis of immunoprecipitated TFEB-EGFP and HA-14-3-3 in wild-type (*perk*<sup>+/+</sup>) and *Perk*-KO (*perk*<sup>-/-</sup>) MEFs. Cells were cotransfected with plasmids expressing TFEB-EGFP and HA-14-3-3 for 24 h, treated with Tm (1 μg/mL) for 16 h, and lysed. Cell lysates were subjected to IP with an anti-GFP antibody. Immunoprecipitates were analyzed by immunoblotting with antibodies against GFP (to detect TFEB-EGFP), phospho-(Ser)-14-3-3 binding motif (which binds to phosphorylated TFEB-EGFP at S211), or HA (to detect HA-14-3-3).

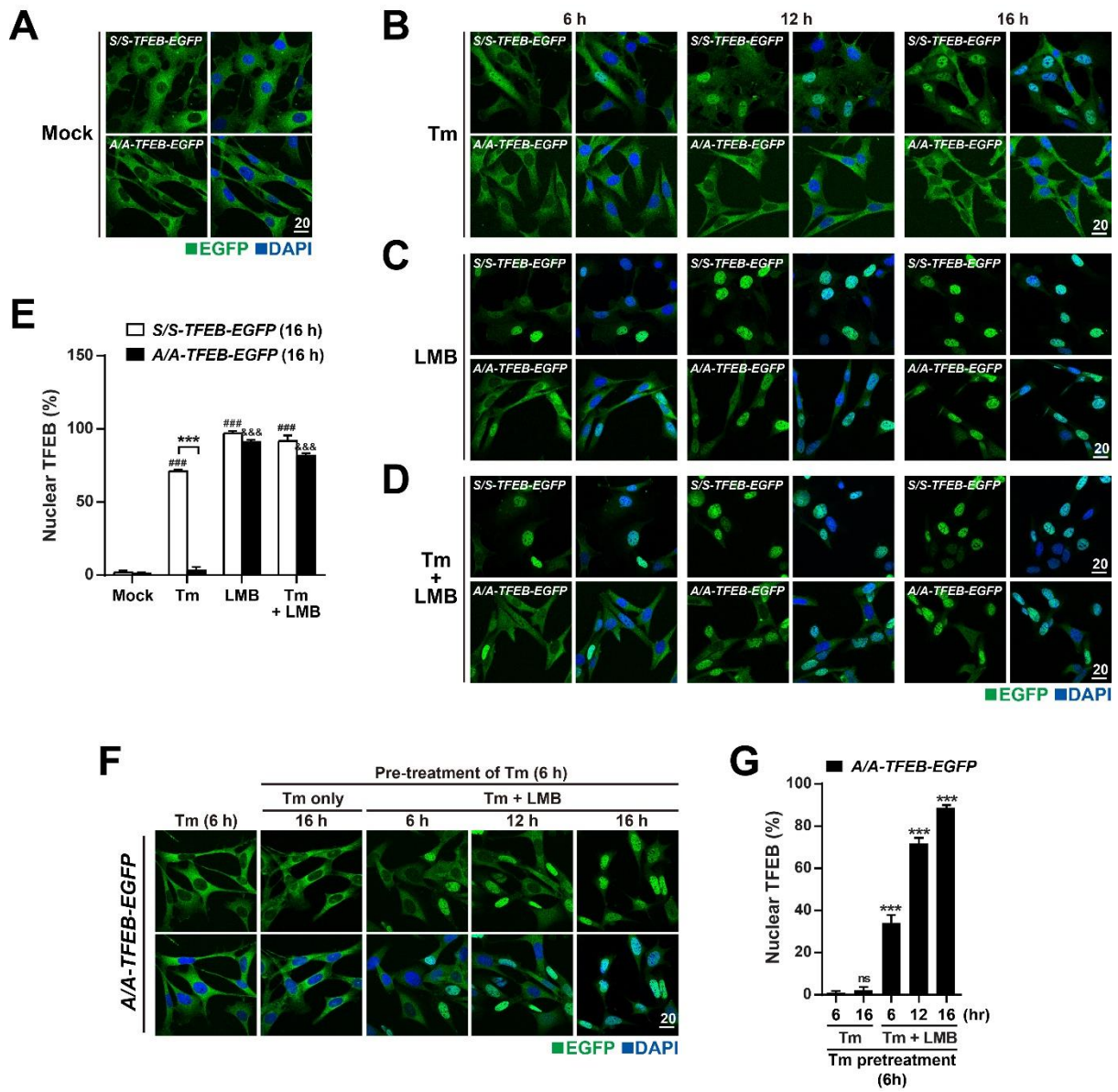


**Figure 9. TFEB translocates to the nucleus in *A/A* cells but is subsequently exported to the cytoplasm under ER stress conditions.**

(**A–D**) Representative fluorescence images of TFEB-EGFP in *S/S*- and *A/A*-TFEB-EGFP MEFs. MEFs were treated with Mock (**A**), Tm (40 ng/mL) only (**B**), the nuclear export inhibitor LMB (20 nM) only (**C**), or Tm (40 ng/mL) plus LMB (20 nM) (**D**) for the indicated durations. The cellular localization of TFEB-EGFP was indicated by the green fluorescence signal of EGFP in cells. Nuclei were stained with DAPI (blue). Scale bar, 20  $\mu$ m. (**E**) The percentage of cells with nuclear TFEB-EGFP in (**A–D**) at 16 h. Data are presented as mean  $\pm$  SEM of at least 140 cells from six random fields per group. \*\*\* $p < 0.001$ , *S/S*-TFEB-EGFP vs. *A/A*-TFEB-EGFP; ### $p < 0.001$ , Mock vs. chemicals in *S/S*-TFEB-EGFP; &&& $p < 0.001$ , Mock vs. chemicals in *A/A*-TFEB-EGFP (Student's t-test). (**F**) Representative fluorescence images of TFEB-EGFP in *A/A*-TFEB-EGFP MEFs. MEFs were pretreated with Tm (40 ng/mL) for 6 h and further incubated with Tm in the absence or presence of LMB (20 nM) for the indicated durations. The cellular localization of TFEB-EGFP was indicated by the green fluorescence signal of EGFP in cells. Nuclei were stained with DAPI (blue). Scale bar, 20  $\mu$ m. (**G**) The percentage of cells with nuclear TFEB-EGFP in (**F**). Data are presented as mean  $\pm$  SEM of at least 130 cells from six random fields per group. \*\*\* $p < 0.001$ , Tm (6 h) vs. other conditions (Student's t-test).

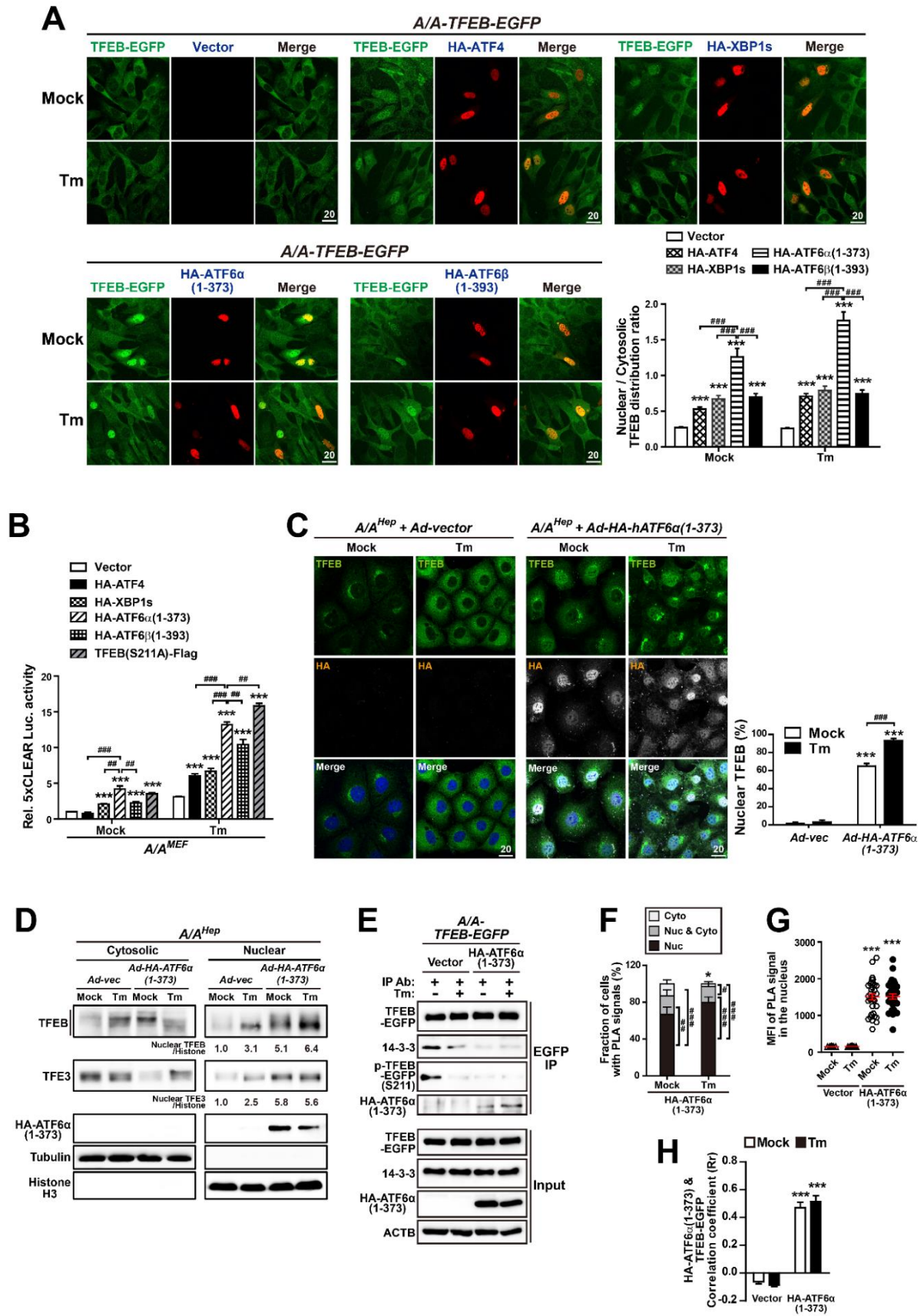
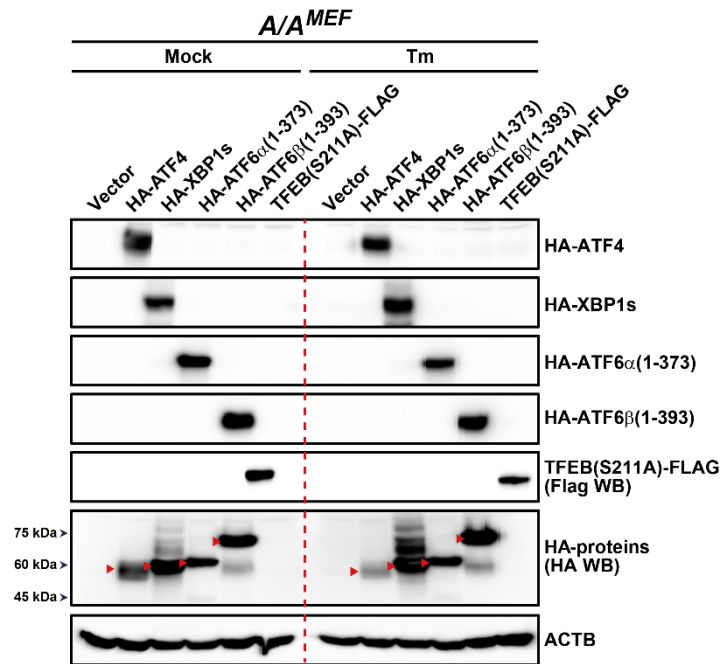


**Figure 10. Overexpression of the activated ATF6 $\alpha$  form induces nuclear translocation of TFEB in A/A cells.**

(A) Representative fluorescence images of TFEB-EGFP in UPR TF-overexpressing A/A-*TFEB-EGFP* MEFs. HA-tagged active forms of UPR TFs (ATF4, XBP1s, ATF6 $\alpha$ (1-373), or ATF6 $\beta$ (1-393)) were overexpressed in A/A-*TFEB-EGFP* cells. Cells were then treated with Mock or Tm (100 ng/mL) for 16 h. The cellular localization of TFEB-EGFP was indicated by the green fluorescence signal of EGFP in cells. HA-tagged UPR TFs were visualized by red fluorescence. Nuclei were stained with DAPI (blue). Scale bar, 20  $\mu$ m. The graph depicts the ratio of nuclear and cytosolic TFEB-EGFP. Data are presented as mean  $\pm$  SEM of at least 50 cells from six random fields per group. \*\*\*p < 0.001, vector vs. TFs; ###p < 0.001, ATF6 $\alpha$ (1-373) vs. other TFs (Student's t-test). (B) Luciferase activity assay of the 5xCLEAR luciferase reporter. A/A<sup>MEF</sup> cells were cotransfected with plasmids expressing 5xCLEAR-driven firefly luciferase, CMV-driven *Renilla* luciferase, and HA-tagged UPR TFs (Vector, ATF4, XBP1s, ATF6 $\alpha$ (1-373), or ATF6 $\beta$ (1-393)) for 36 h. Cells were then treated with Mock or Tm (100 ng/mL) for 16 h, and luciferase activities were measured. Data are presented as mean  $\pm$  SEM of three independent experiments. \*\*\*p < 0.001, vector vs. TFs; ###p < 0.001, ATF6 $\alpha$ (1-373) vs. other TFs (Student's t-test). (C) Representative IF images of endogenous TFEB (green) and HA-ATF6 $\alpha$ (1-373) (gray) in A/A<sup>Hep</sup> cells. Cells were infected with vector- or HA-ATF6 $\alpha$ (1-373)-expressing adenoviruses for 24 h and then treated with Mock or Tm (1  $\mu$ g/mL) for 24 h. Nuclei were stained with DAPI (blue). Scale bar, 20  $\mu$ m. The graph depicts the percentage of HA-positive cells with nuclear TFEB. Data are presented as mean  $\pm$  SEM of at least 50 cells from six random fields per group. \*\*\*p < 0.001, vector vs. HA-ATF6 $\alpha$ (1-373); ###p < 0.001, Mock vs. Tm (Student's t-test). (D) WB analysis of the subcellular distributions of endogenous TFEB and TFE3 in vector- or HA-ATF6 $\alpha$ (1-373)-overexpressing A/A<sup>Hep</sup> cells. Cells infected with vector- or HA-ATF6 $\alpha$ (1-373)-expressing adenoviruses for 24 h were treated with Mock or Tm (1  $\mu$ g/mL) for 24 h. Nuclear TFEB and TFE3 levels normalized by Histone H3 levels are shown below the panels. Data are presented as mean  $\pm$  SEM of three independent experiments. Histone H3 and ACTB were used as loading controls of the nuclear and cytoplasmic fractions, respectively. (E) WB analysis of immunoprecipitated TFEB-EGFP and 14-3-3 in vector- or HA-ATF6 $\alpha$ (1-373)-overexpressing A/A-*TFEB-EGFP* MEFs treated with Mock or Tm (100 ng/mL, 24 h). Cells were lysed and subjected to IP with an anti-GFP antibody. Immunoprecipitates were analyzed by immunoblotting with antibodies against GFP (to detect TFEB-EGFP), phospho-(Ser)-14-3-3 binding motif (which binds to phosphorylated TFEB-EGFP at S211), 14-3-3, or HA-ATF6 $\alpha$ (1-373). (F and G) Quantified results of the PLA between TFEB-EGFP and HA-ATF6 $\alpha$ (1-373) in Figure 14B. A/A-*TFEB-EGFP* MEFs transfected with plasmids expressing vector or HA-ATF6 $\alpha$ (1-373) for 30 h were treated with Mock or Tm (100 ng/mL) for 16 h. The graph (F) depicts the fraction (%) of cells with PLA signals in the nucleus, nucleus

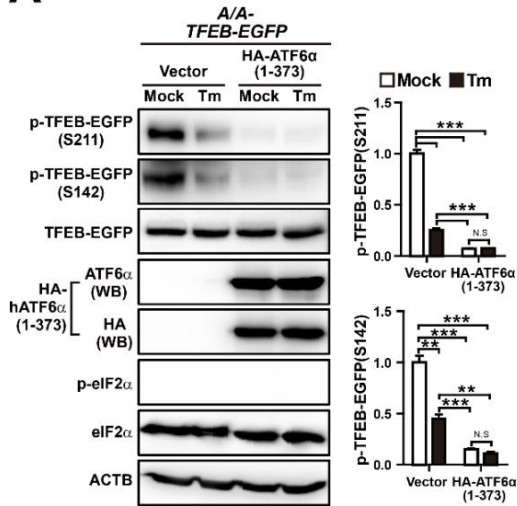
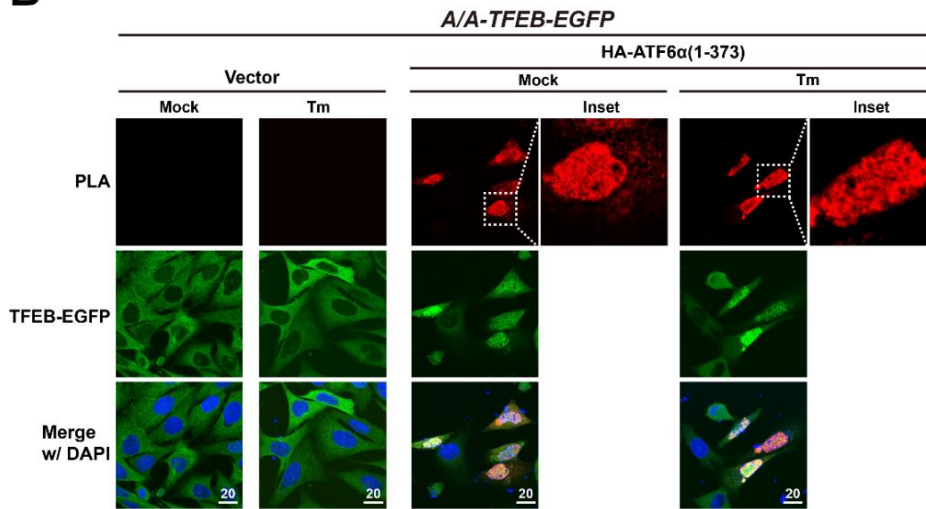
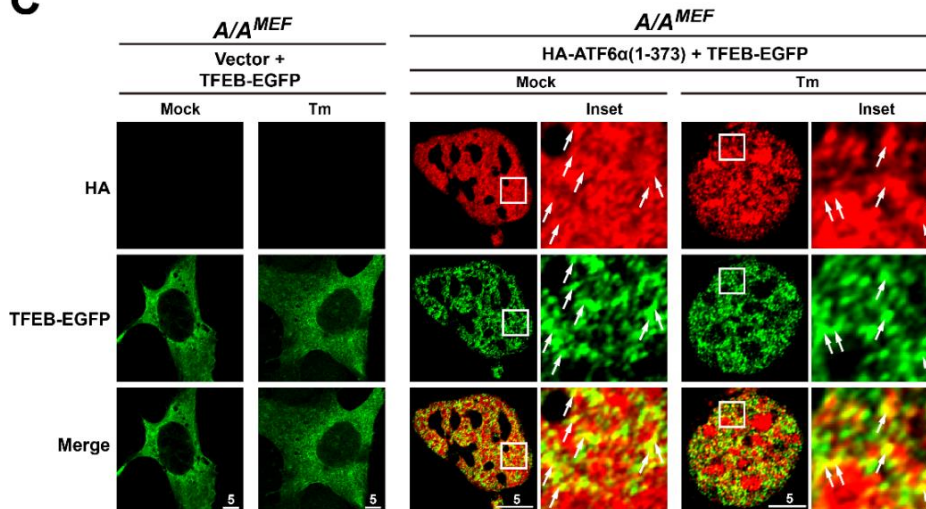


and cytosol, or cytosol. Data are presented as mean  $\pm$  SEM of at least 70 cells per group. #p < 0.05, ##p < 0.001, and ###p < 0.0001, nucleus vs. nucleus and cytosol, nucleus vs. cytosol, or nucleus and cytosol vs. cytosol; \*p < 0.05, Mock vs. Tm for cytosolic PLA-positive cells (Student's t-test). The graph (**G**) depicts quantification of the relative PLA MFI in the nucleus. Data are presented as mean  $\pm$  SEM of at least 32 cells per group. \*\*\*p < 0.001, vector vs. HA-ATF6 $\alpha$ (1-373) (Student's t-test). Representative PLA images of *A/A-TFEB-EGFP* MEFs are presented in Figure 14B. (**H**) Quantification of colocalization of TFEB-EGFP with HA-ATF6 $\alpha$ (1-373) in Figure 14C. *A/A<sup>MEF</sup>* cells were cotransfected with plasmids expressing TFEB-EGFP and vector or TFEB-EGFP and HA-ATF6 $\alpha$ (1-373). They were treated with Mock or Tm (100 ng/mL) for 16 h, fixed, and stained with an anti-HA antibody (red) to detect HA-ATF6 $\alpha$ (1-373). Representative colocalization IF images of HA-ATF6 $\alpha$ (1-373) and TFEB-EGFP in *A/A<sup>MEF</sup>* cells are presented in Figure 14C. Data are presented as mean  $\pm$  SEM of at least 25 cells per group. \*\*\*p < 0.001, vector vs. HA-ATF6 $\alpha$ (1-373) (Student's t-test).



**Figure 11. Overexpression of the active forms of the UPR TFs in *A/A* cells during ER stress.**

Similar to Figure 8B, *A/A<sup>MEF</sup>* cells were cotransfected with plasmids expressing 5XCLEAR-driven firefly luciferase, CMV-driven *Renilla* luciferase, and HA-tagged UPR TFs (Vector, ATF4, XBP1s, ATF6 $\alpha$ (1-373), or ATF6 $\beta$ (1-393)) for 36 h, and then treated with Mock or Tm (100 ng/mL) for 16 h. Cell lysates were subjected to WB analysis of the indicated proteins.

**A****B****C**

**Figure 12. Overexpression of the activated ATF6 $\alpha$  form induces TFEB dephosphorylation, and the activated ATF6 $\alpha$  form interacts with TFEB in the nucleus.**

(A) WB analysis of phosphorylated TFEB-EGFP in protein lysates of HA-ATF6 $\alpha$ (1-373)-overexpressing *A/A-TFEB-EGFP* MEFs. Cells were transfected with plasmids expressing Vector or HA-ATF6 $\alpha$ (1-373) and treated with Mock or Tm (50 ng/mL, 16 h). The phosphorylation status of TFEB-EGFP was analyzed using specific antibodies against phosphorylated S211 and phosphorylated S142. The graphs depict the levels of TFEB-EGFP phosphorylated at S211 or S142 normalized to total TFEB-EGFP levels. Data are presented as mean  $\pm$  SEM of three independent experiments. \*\* $p < 0.01$  and \*\*\* $p < 0.001$ , vector vs. HA-ATF6 $\alpha$ (1-373) (Student's t-test). (B) Representative PLA images of vector- or HA-ATF6 $\alpha$ (1-373)-expressing *A/A-TFEB-EGFP* MEFs. Cells were transfected with plasmids expressing vector or HA-ATF6 $\alpha$ (1-373) and treated with Mock or Tm (100 ng/mL) for 16 h. The PLA was performed as described in the Materials and Methods. The cellular localization of TFEB-EGFP was indicated by the green fluorescence signal of EGFP in the cells. In *A/A-TFEB-EGFP* MEFs expressing HA-ATF6 $\alpha$ (1-373), the right panels (insets) are magnified images of the boxes in the left panels. Scale bar, 20  $\mu$ m. The quantified results of the PLA are presented as graphs in Figure 9F, G. (C) Representative colocalization IF images of HA-ATF6 $\alpha$ (1-373) (red) and TFEB-EGFP (green) in *A/A<sup>MEF</sup>* cells. Cells were cotransfected with plasmids expressing TFEB-EGFP and vector, or TFEB-EGFP and HA-ATF6 $\alpha$ (1-373). They were treated with Mock or Tm (100 ng/mL) for 16 h, fixed, and stained with an anti-HA antibody (red) to detect HA-ATF6 $\alpha$ (1-373). The cellular localization of TFEB-EGFP was indicated by the green fluorescence signal of EGFP in the cells. In *A/A<sup>MEF</sup>* cells coexpressing HA-ATF6 $\alpha$ (1-373) and TFEB-EGFP, the right panels (insets) are magnified images of the boxes in the left panels. Arrowheads indicate colocalized proteins. Scale bar, 5  $\mu$ m. The quantified results of the colocalization of HA-ATF6 $\alpha$ (1-373) with TFEB-EGFP are presented as a graph in Figure 9H.

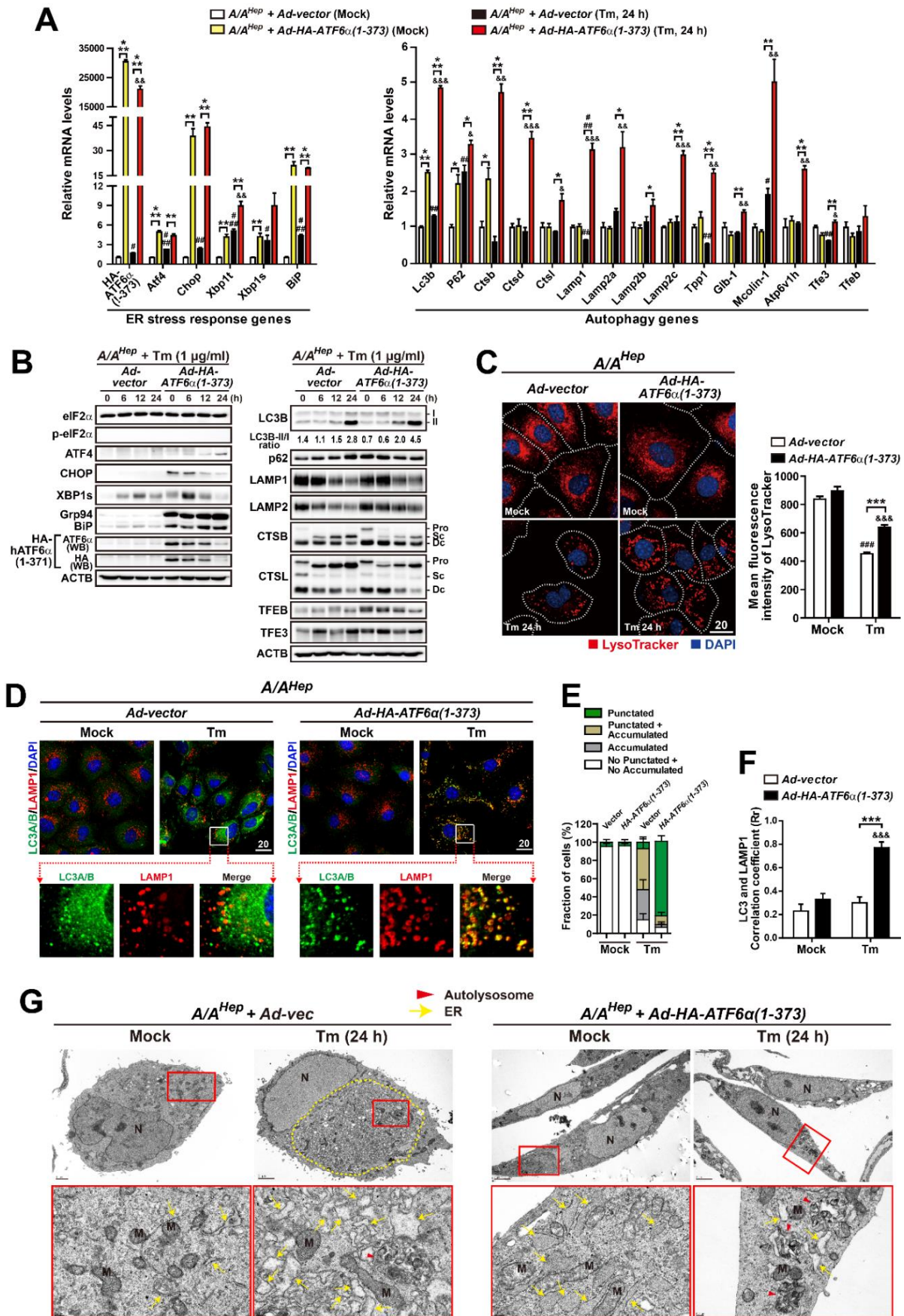


**Figure 13. Overexpression of the activated ATF6 $\alpha$  form increases expression of autophagy genes and improves autophagic defects in A/A cells during ER stress.**

*A/A*<sup>Hep</sup> cells infected with vector- or HA-ATF6 $\alpha$ (1-373)-expressing adenoviruses for 24 h were treated with Mock or Tm (1  $\mu$ g/mL) for the indicated durations. **(A)** Quantitative RT-PCR analysis of mRNA expression of ER stress response and autophagy genes. Data are presented as mean  $\pm$  SEM of three independent experiments. \* $p$  < 0.05, \*\* $p$  < 0.01, and \*\*\* $p$  < 0.001, *Ad-vector* vs. *Ad-HA-ATF6 $\alpha$ (1-373)*; # $p$  < 0.05, ## $p$  < 0.01, and ### $p$  < 0.001, Mock vs. Tm in *Ad-vector*; &#p < 0.05, &&p < 0.01, and &&&p < 0.001, Mock vs. Tm in *Ad-HA-ATF6 $\alpha$ (1-373)* (Student's t-test). **(B)** WB analysis of ER stress and autophagy proteins in cell lysates. The LC3B-II/I ratios are shown below the right first panel. CTSB: cathepsin B; CTSL: cathepsin L; Pro: procathepsin; Sc: mature single-chain cathepsin; Dc: heavy chain of mature double-chain cathepsin. **(C)** Representative images of LysoTracker staining in vector- or HA-ATF6 $\alpha$ (1-373)-overexpressing *A/A*<sup>Hep</sup> cells. Cells were stained with LysoTracker (100 nM, red) and Hoechst 33258 (10  $\mu$ g/mL, blue) for the last 30 min of the treatment. The dotted white line defines the cell boundary. Scale bar, 20  $\mu$ m. The graph depicts quantification of the MFI of LysoTracker. Data are presented as mean  $\pm$  SEM of at least 50 cells from ten random fields per group. \*\*\* $p$  < 0.001, *Ad-vector* vs. *Ad-HA-ATF6 $\alpha$ (1-373)*; #### $p$  < 0.001, Mock vs. Tm in *Ad-vector*; &&&p < 0.001, Mock vs. Tm in *Ad-HA-ATF6 $\alpha$ (1-373)* (Student's t-test). **(D)** Representative IF images of LC3A/B (green) and LAMP1 (red) in vector- or HA-ATF6 $\alpha$ (1-373)-overexpressing *A/A*<sup>Hep</sup> cells. Nuclei were stained with DAPI (blue). The bottom panels are magnified images of the boxes in the upper panels. Scale bar, 20  $\mu$ m. **(E)** The graph depicts the fraction (%) of cells with different LC3A/B staining patterns as described in Figure 2A. Data are presented as mean  $\pm$  SEM of at least 50 cells from ten random fields per group. **(F)** The graph depicts quantification of the colocalization of LC3A/B with LAMP1 in **(D)**. Data are presented as mean  $\pm$  SEM of at least 50 cells from ten random fields per group. \*\*\* $p$  < 0.001, *Ad-vector* vs. *Ad-HA-ATF6 $\alpha$ (1-373)*; &&&p < 0.001, Mock vs. Tm in *Ad-HA-ATF6 $\alpha$ (1-373)* (Student's t-test). **(G)** Representative TEM images of vector- or HA-ATF6 $\alpha$ (1-373)-overexpressing *A/A*<sup>Hep</sup> cells. The bottom panels are magnified images of the red boxes in the upper panels. Red arrowheads indicate autolysosomes, and yellow arrows indicate the ER. The dotted yellow line defines a region of dilated and fragmented ER structures. Scale bars, upper panels (1 or 2  $\mu$ m) and bottom panels (0.2  $\mu$ m).

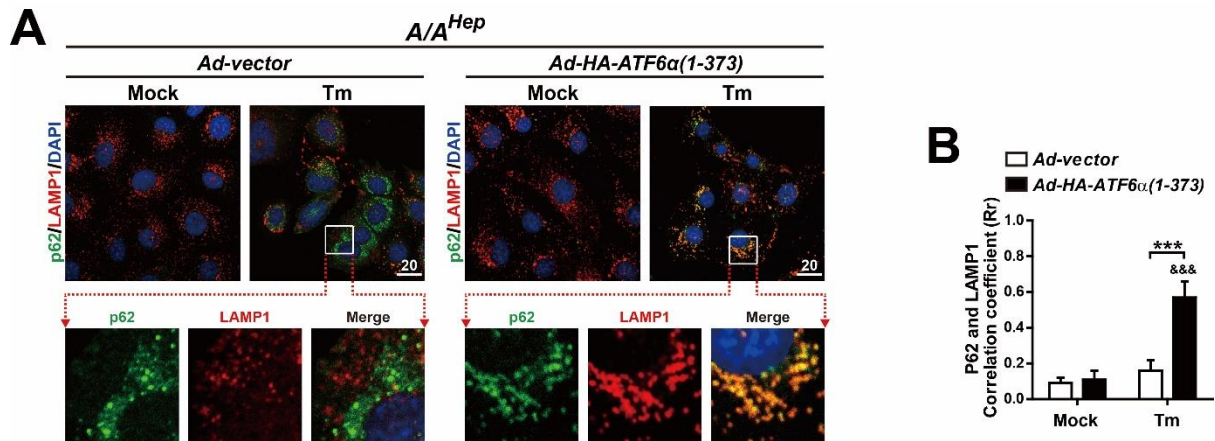


**Figure 14. Overexpression of the activated ATF6α form increases autophagosome-lysosome fusion in *A/A* cells during ER stress.**

(A) Representative IF images of p62 (green) and LAMP1 (red) in vector- or HA-ATF6α(1-373)-overexpressing *A/A<sup>Hep</sup>* cells. Nuclei were stained with DAPI (blue). The bottom panels are magnified images of the boxes in the upper panels. Scale bar, 20 μm. (B) Quantification of the colocalization of p62 with LAMP1. Data are presented as mean ± SEM of at least 50 cells from ten random fields per group. \*\*\*p < 0.001, *Ad-vector* vs. *Ad-HA-ATF6α(1-373)*; &&&p < 0.001, Mock vs. Tm in *Ad-HA-ATF6α(1-373)* (Student's t-test).

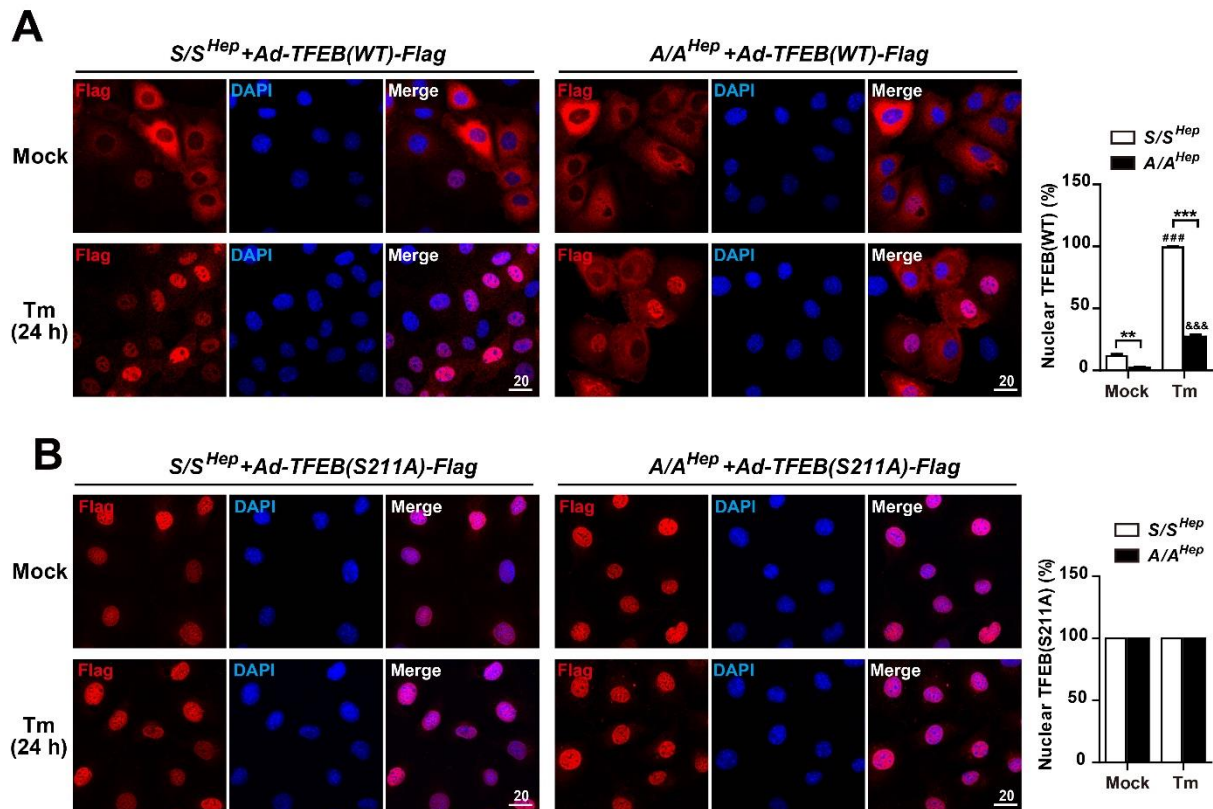


**Figure 15. The constitutively active TFEB mutant localizes to the nucleus in *A/A* cells regardless of ER stress.**

(**A and B**) Representative IF images of TFEB(WT)-FLAG (red) or TFEB(S211A)-FLAG (red) in *S/S<sup>Hep</sup>* and *A/A<sup>Hep</sup>* cells. Cells infected with TFEB(WT)-FLAG- (**A**) or TFEB(S211A)-FLAG (**B**)-expressing adenoviruses for 24 h were treated with Mock or Tm (1  $\mu$ g/mL) for 24 h, fixed, and stained with an anti-FLAG antibody (red). Nuclei were stained with DAPI (blue). Scale bar, 20  $\mu$ m. The graphs depict the percentage of cells with nuclear TFEB(WT)-FLAG or TFEB(S211A)-FLAG. Data are presented as mean  $\pm$  SEM of at least 130 cells from six random fields per group. \*\* $p < 0.01$  and \*\*\* $p < 0.001$ , *S/S<sup>Hep</sup>* vs. *A/A<sup>Hep</sup>*; ### $p < 0.001$ , Mock vs. Tm in *S/S<sup>Hep</sup>*; &&& $p < 0.001$ , Mock vs. Tm in *A/A<sup>Hep</sup>* (Student's t-test).



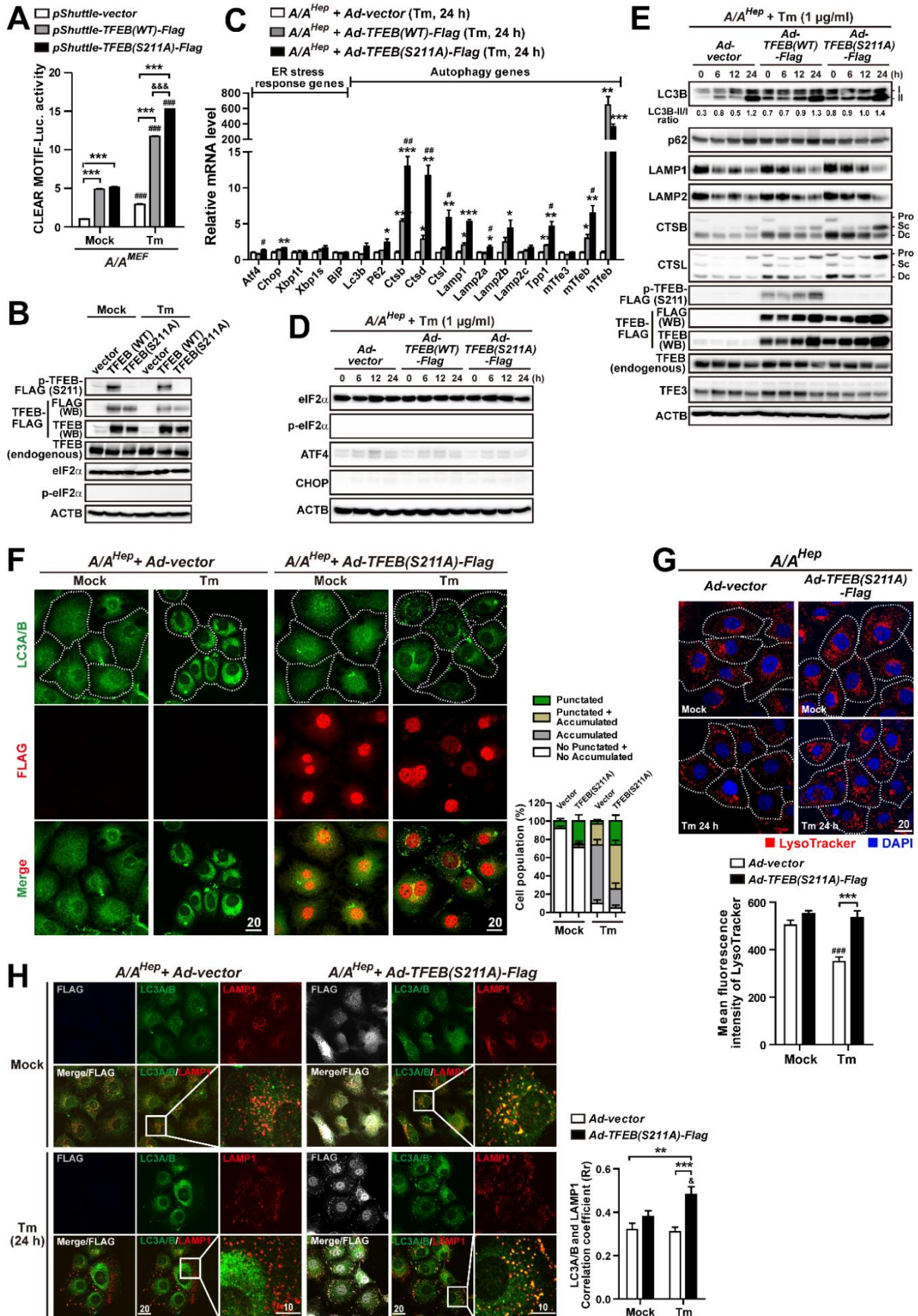
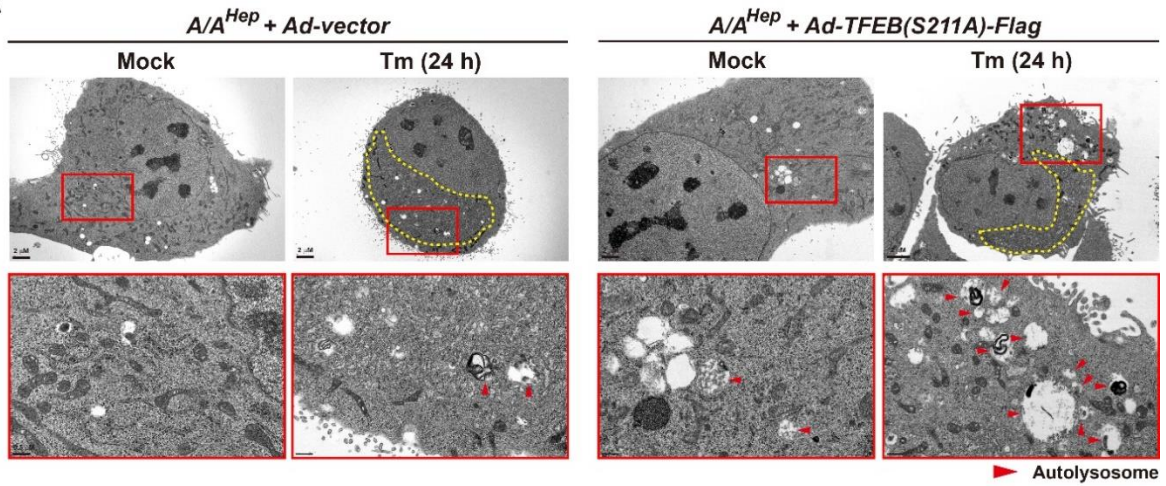


**Figure 16. Overexpression of the constitutively active TFEB mutant enhances expression of autophagy genes and improves autophagic defects in *A/A* cells during ER stress.**

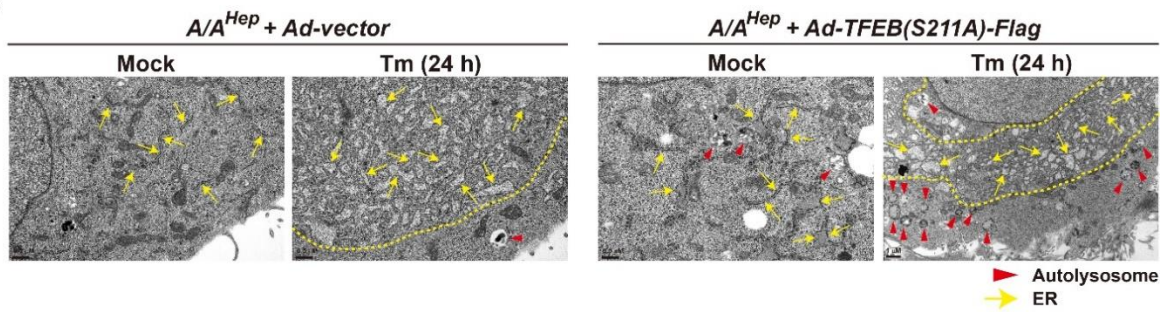
(A) Luciferase activity assay of the 5xCLEAR luciferase reporter. *A/A*<sup>MEF</sup> cells were cotransfected with plasmids expressing 5xCLEAR-driven firefly luciferase, CMV-driven *Renilla* luciferase, and FLAG-tagged TFEB (TFEB(WT)-FLAG or TFEB(S211A)-FLAG) for 30 h. Cells were then treated with Mock or Tm (100 ng/mL) for 16 h, and luciferase activities were measured. Data are presented as mean ± SEM of three independent experiments. \*\*\*p < 0.001, Vector vs. TFEB(WT)-FLAG or TFEB(S211A)-FLAG; ###p < 0.001, Mock vs. Tm; &&&p < 0.001, TFEB(WT)-FLAG vs. TFEB(S211A)-FLAG (Student's t-test). (B) WB analysis of overexpressed TFEB(WT)-FLAG and TFEB(S211A)-FLAG proteins in *A/A*<sup>MEF</sup> cells in (A). (C) Quantitative RT-PCR analysis of mRNA expression of ER stress response and autophagy genes in vector-, TFEB(WT)-FLAG-, or TFEB(S211A)-FLAG-overexpressing *A/A*<sup>Hep</sup> cells. *A/A*<sup>Hep</sup> cells infected with vector-, TFEB(WT)-FLAG-, or TFEB(S211A)-FLAG-expressing adenoviruses for 24 h were treated without or with Tm (1 µg/mL) for 24 h. Data are presented as mean ± SEM of three independent experiments. \*p < 0.05, \*\*p < 0.01, and \*\*\*p < 0.001, *Ad-vector* vs. *Ad-TFEB(WT)-Flag* or *Ad-TFEB(S211A)-Flag*; #p < 0.05 and ###p < 0.01, *Ad-TFEB(WT)-Flag* vs. *Ad-TFEB(S211A)-Flag* (Student's t-test). Ctsb: cathepsin b; Ctsd: cathepsin d; Ctsl: cathepsin l. (D and E) WB analysis of eIF2α, p-eIF2α, its downstream target proteins (D), and autophagy and lysosomal proteins (E) in vector-, TFEB(WT)-FLAG-, or TFEB(S211A)-FLAG-overexpressing *A/A*<sup>Hep</sup> cells. Cells infected with vector-, TFEB(WT)-FLAG-, or TFEB(S211A)-FLAG-expressing adenoviruses for 24 h were treated with Mock or Tm (1 µg/mL) for the indicated durations. The LC3B-II/I ratios are shown below the first panel. CTSB: cathepsin B; CTSL: cathepsin L; Pro: procathepsin; Sc: mature single-chain cathepsin; Dc: heavy chain of mature double-chain cathepsin. (F) Representative IF images of LC3A/B (green) and TFEB(S211A)-FLAG (red) in vector- or TFEB(S211A)-FLAG-overexpressing *A/A*<sup>Hep</sup> cells. Cells were treated with Mock or Tm (1 µg/mL) for 24 h. The dotted white line defines the cell boundary. Scale bar, 20 µm. The graph depicts the fraction (%) of cells with different LC3A/B staining patterns as described in Figure 2A. Data are presented as mean ± SEM of at least 50 cells from ten random fields per group. (G) Representative LysoTracker staining images of vector- or TFEB(S211A)-FLAG-overexpressing *A/A*<sup>Hep</sup> cells. Cells were stained with LysoTracker (100 nM, red) and Hoechst 33258 (10 µg/mL, blue) for the last 30 min of the treatment. The dotted white line defines the cell boundary. Scale bar, 20 µm. The graph depicts quantification of the MFI of LysoTracker. Data are presented as mean ± SEM of at least 50 cells from ten random fields per group. \*\*\*p < 0.001, *Ad-vector* vs. *Ad-HA-ATF6α(1-373)*; ###p < 0.001, Mock vs. Tm in *Ad-vector* (Student's t-test). (H) Representative

IF images of LC3A/B (green) and LAMP1 (red) in vector- or TFEB(S211A)-FLAG-overexpressing *A/A<sup>Hep</sup>* cells. Cells were treated with Mock or Tm (1  $\mu$ g/mL) for 24 h. Nuclei were stained with DAPI (blue). The third panels in the bottom row are magnified images of the boxes in the second panels. Scale bars, 20  $\mu$ m except for the magnified images (10  $\mu$ m). The graph depicts quantification of the colocalization of LC3A/B with LAMP1. Data are presented as mean  $\pm$  SEM of at least 50 cells from ten random fields per group. \*\*p < 0.01 and \*\*\*p < 0.001, *Ad-vector* vs. *Ad-TFEB(S211A)-Flag*; &p < 0.05, Mock vs. Tm in *Ad-TFEB(S211A)-Flag* (Student's t-test).

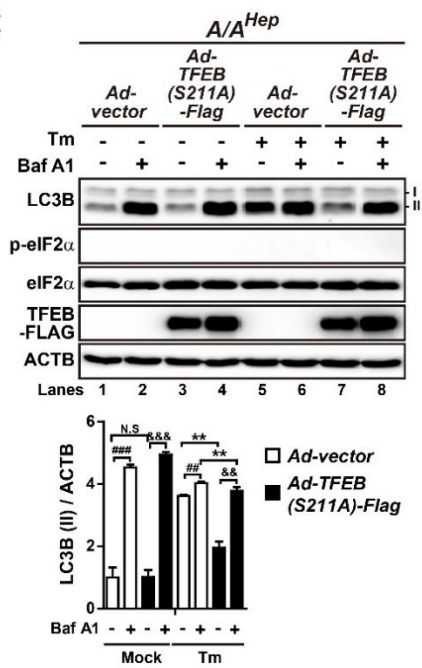
**A**



**B**



**C**



**D**

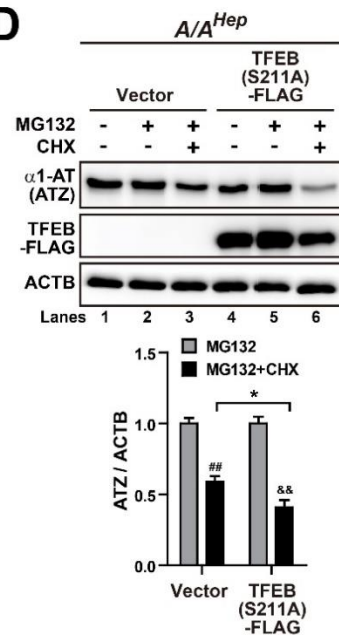


**Figure 17. Overexpression of the constitutively active TFEB mutant rescues the autophagic flux defect in *A/A* cells during ER stress.**

(**A and B**) Representative TEM images of vector- or TFEB(S211A)-FLAG-overexpressing *A/A<sup>Hep</sup>* cells. Cells infected with vector- or TFEB(S211A)-FLAG-expressing adenoviruses for 24 h were treated with Mock or Tm (1 µg/mL) for 24 h. The bottom panels in (**A**) are magnified images of the red boxes in the upper panels. Red arrowheads indicate autolysosomes and yellow arrows indicate the ER. The dotted yellow line defines a region of dilated and fragmented ER structures. Scale bars, upper panels of (**A**) (2 µm) and bottom panels of (**A**) and (**B**) (0.5 µm). (**C**) WB analysis of LC3B in protein lysates of vector- or TFEB(S211A)-FLAG-overexpressing *A/A<sup>Hep</sup>* cells. Cells infected with vector- or TFEB(S211A)-FLAG-expressing adenoviruses for 24 h were treated with Mock or Tm (1 µg/mL) for 16 h in the absence or presence of the lysosomal inhibitor Baf A1 (200 nM) for 3 h before harvest. The graph depicts the LC3B-II level normalized to the ACTB level. Data are presented as mean ± SEM of three independent experiments, \*\*p < 0.01, *Ad-vector* vs. *Ad-TFEB(S211A)-Flag*; ###p < 0.01 and ###p < 0.001, Baf A1(-) vs. Baf A1(+) in *Ad-vector*; &&p < 0.01 and &&&p < 0.001, Baf A1(-) vs. Baf A1(+) in *Ad-TFEB(S211A)-Flag*; N.S., no significant difference (Student's t-test). (**D**) WB analysis of ATZ in protein lysates of vector- or TFEB(S211A)-FLAG-overexpressing *A/A<sup>Hep</sup>* cells. Cells were cotransfected with plasmids expressing ATZ and vector or TFEB(S211A)-FLAG for 24 h and then treated with Mock, MG132 only (20 µM), or MG132 plus CHX (100 µg/mL) for 6 h. The graphs depict the ATZ level normalized to the ACTB level after treatment for 6 h. Data are presented as mean ± SEM of three independent experiments. \*p < 0.05, Vector vs. TFEB(S211A)-FLAG in MG132 + CHX; ###p < 0.01, MG132 vs. MG132 + CHX in Vector; &&p < 0.01, MG132 vs. MG132 + CHX in TFEB(S211A)-FLAG (Student's t-test).

## Reference

1. Sonenberg, N. and A.G. Hinnebusch, Regulation of translation initiation in eukaryotes: mechanisms and biological targets. *Cell*, **2009**. 136(4): p. 731-45.
2. Donnelly, N., et al., The eIF2alpha kinases: their structures and functions. *Cell Mol Life Sci*, **2013**. 70(19): p. 3493-511.
3. Wek, R.C., H.Y. Jiang, and T.G. Anthony, Coping with stress: eIF2 kinases and translational control. *Biochem Soc Trans*, **2006**. 34(Pt 1): p. 7-11.
4. Taniuchi, S., et al., Integrated stress response of vertebrates is regulated by four eIF2alpha kinases. *Sci Rep*, **2016**. 6: p. 32886.
5. Young, S.K. and R.C. Wek, Upstream Open Reading Frames Differentially Regulate Gene-specific Translation in the Integrated Stress Response. *J Biol Chem*, **2016**. 291(33): p. 16927-35.
6. Back, S.H., Roles of the Translation Initiation Factor eIF2alpha Phosphorylation in Cell Structure and Function. *Cell Struct Funct*, **2020**. 45(1): p. 65-76.
7. Pakos-Zebrucka, K., et al., The integrated stress response. *EMBO Rep*, **2016**. 17(10): p. 1374-1395.
8. Ron, D., Translational control in the endoplasmic reticulum stress response. *J Clin Invest*, **2002**. 110(10): p. 1383-8.
9. Walter, P. and D. Ron, The unfolded protein response: from stress pathway to homeostatic regulation. *Science*, **2011**. 334(6059): p. 1081-6.
10. Wang, M. and R.J. Kaufman, Protein misfolding in the endoplasmic reticulum as a conduit to human disease. *Nature*, **2016**. 529(7586): p. 326-35.
11. Yoshida, H., ER stress and diseases. *FEBS J*, **2007**. 274(3): p. 630-58.
12. Back, S.H. and R.J. Kaufman, Endoplasmic reticulum stress and type 2 diabetes. *Annu Rev Biochem*, **2012**. 81: p. 767-93.
13. Majumder, M., et al., A novel feedback loop regulates the response to endoplasmic reticulum stress via the cooperation of cytoplasmic splicing and mRNA translation. *Mol Cell Biol*, **2012**. 32(5): p. 992-1003.
14. Teske, B.F., et al., The eIF2 kinase PERK and the integrated stress response facilitate activation of ATF6 during endoplasmic reticulum stress. *Mol Biol Cell*, **2011**. 22(22): p. 4390-405.
15. Mizushima, N., Autophagy: process and function. *Genes Dev*, 2007. **21**(22): p. 2861-73.
16. Yang, Z. and D.J. Klionsky, Mammalian autophagy: core molecular machinery and signaling regulation. *Curr Opin Cell Biol*, **2010**. 22(2): p. 124-31.
17. Dikic, I. and Z. Elazar, Mechanism and medical implications of mammalian autophagy. *Nat Rev Mol Cell Biol*, **2018**. 19(6): p. 349-364.

18. Li, L., et al., Lipids and membrane-associated proteins in autophagy. *Protein Cell*, **2021**. **12**(7): p. 520-544.
19. Nakamura, S. and T. Yoshimori, New insights into autophagosome-lysosome fusion. *J Cell Sci*, **2017**. **130**(7): p. 1209-1216.
20. Palmieri, M., et al., Characterization of the CLEAR network reveals an integrated control of cellular clearance pathways. *Hum Mol Genet*, **2011**. **20**(19): p. 3852-66.
21. Galluzzi, L., et al., Molecular definitions of autophagy and related processes. *EMBO J*, **2017**. **36**(13): p. 1811-1836.
22. Raben, N. and R. Puertollano, TFEB and TFE3: Linking Lysosomes to Cellular Adaptation to Stress. *Annu Rev Cell Dev Biol*, **2016**. **32**: p. 255-278.
23. Di Malta, C., L. Cinque, and C. Settembre, Transcriptional Regulation of Autophagy: Mechanisms and Diseases. *Front Cell Dev Biol*, **2019**. **7**: p. 114.
24. Napolitano, G. and A. Ballabio, TFEB at a glance. *J Cell Sci*, **2016**. **129**(13): p. 2475-81.
25. Steingrimsson, E., N.G. Copeland, and N.A. Jenkins, Melanocytes and the microphthalmia transcription factor network. *Annu Rev Genet*, **2004**. **38**: p. 365-411.
26. Sardiello, M., et al., A gene network regulating lysosomal biogenesis and function. *Science*, **2009**. **325**(5939): p. 473-7.
27. Settembre, C., et al., TFEB links autophagy to lysosomal biogenesis. *Science*, **2011**. **332**(6036): p. 1429-33.
28. Li, M., et al., TFEB: A Emerging Regulator in Lipid Homeostasis for Atherosclerosis. *Front Physiol*, **2021**. **12**: p. 639920.
29. Li, L., et al., A TFEB nuclear export signal integrates amino acid supply and glucose availability. *Nat Commun*, **2018**. **9**(1): p. 2685.
30. Napolitano, G., et al., mTOR-dependent phosphorylation controls TFEB nuclear export. *Nat Commun*, **2018**. **9**(1): p. 3312.
31. Puertollano, R., et al., The complex relationship between TFEB transcription factor phosphorylation and subcellular localization. *EMBO J*, **2018**. **37**(11).
32. Zhu, S.Y., et al., The Role and Regulatory Mechanism of Transcription Factor EB in Health and Diseases. *Front Cell Dev Biol*, **2021**. **9**: p. 667750.
33. Martina, J.A., et al., MTORC1 functions as a transcriptional regulator of autophagy by preventing nuclear transport of TFEB. *Autophagy*, **2012**. **8**(6): p. 903-14.
34. Pena-Llopis, S., et al., Regulation of TFEB and V-ATPases by mTORC1. *EMBO J*, **2011**. **30**(16): p. 3242-58.
35. Roczniak-Ferguson, A., et al., The transcription factor TFEB links mTORC1 signaling to transcriptional control of lysosome homeostasis. *Sci Signal*, **2012**. **5**(228): p. ra42.
36. Settembre, C., et al., A lysosome-to-nucleus signalling mechanism senses and regulates the lysosome via mTOR and TFEB. *EMBO J*, **2012**. **31**(5): p. 1095-108.

37. Martina, J.A., et al., TFEB and TFE3 are novel components of the integrated stress response. *EMBO J*, **2016**. 35(5): p. 479-95.
38. Martina, J.A., et al., The nutrient-responsive transcription factor TFE3 promotes autophagy, lysosomal biogenesis, and clearance of cellular debris. *Sci Signal*, **2014**. 7(309): p. ra9.
39. Medina, D.L., et al., Lysosomal calcium signalling regulates autophagy through calcineurin and TFEB. *Nat Cell Biol*, **2015**. 17(3): p. 288-99.
40. Wang, W., et al., Up-regulation of lysosomal TRPML1 channels is essential for lysosomal adaptation to nutrient starvation. *Proc Natl Acad Sci U S A*, **2015**. 112(11): p. E1373-81.
41. Yin, Q., et al., CDK4/6 regulate lysosome biogenesis through TFEB/TFE3. *J Cell Biol*, **2020**. 219(8).
42. Silvestrini, M.J., et al., Nuclear Export Inhibition Enhances HLH-30/TFEB Activity, Autophagy, and Lifespan. *Cell Rep*, **2018**. 23(7): p. 1915-1921.
43. Yorimitsu, T., et al., Endoplasmic reticulum stress triggers autophagy. *J Biol Chem*, **2006**. 281(40): p. 30299-304.
44. Ogata, M., et al., Autophagy is activated for cell survival after endoplasmic reticulum stress. *Mol Cell Biol*, **2006**. 26(24): p. 9220-31.
45. Deegan, S., et al., Stress-induced self-cannibalism: on the regulation of autophagy by endoplasmic reticulum stress. *Cell Mol Life Sci*, **2013**. 70(14): p. 2425-41.
46. Rashid, H.O., et al., ER stress: Autophagy induction, inhibition and selection. *Autophagy*, **2015**. 11(11): p. 1956-1977.
47. Nakashima, A., et al., Endoplasmic reticulum stress disrupts lysosomal homeostasis and induces blockade of autophagic flux in human trophoblasts. *Sci Rep*, **2019**. 9(1): p. 11466.
48. Kouroku, Y., et al., ER stress (PERK/eIF2alpha phosphorylation) mediates the polyglutamine-induced LC3 conversion, an essential step for autophagy formation. *Cell Death Differ*, **2007**. 14(2): p. 230-9.
49. Humeau, J., et al., Phosphorylation of eukaryotic initiation factor-2alpha (eIF2alpha) in autophagy. *Cell Death Dis*, **2020**. 11(6): p. 433.
50. B'Chir, W., et al., The eIF2alpha/ATF4 pathway is essential for stress-induced autophagy gene expression. *Nucleic Acids Res*, **2013**. 41(16): p. 7683-99.
51. Dang, T.T. and S.H. Back, Translation Inhibitors Activate Autophagy Master Regulators TFEB and TFE3. *Int J Mol Sci*, **2021**. 22(21).
52. Harding, H.P., et al., Ppp1r15 gene knockout reveals an essential role for translation initiation factor 2 alpha (eIF2alpha) dephosphorylation in mammalian development. *Proc Natl Acad Sci U S A*, **2009**. 106(6): p. 1832-7.
53. Kim, S., et al., Rescue of high-specificity Cas9 variants using sgRNAs with matched 5' nucleotides. *Genome Biol*, **2017**. 18(1): p. 218.



54. Bommasamy, H., et al., ATF6alpha induces XBP1-independent expansion of the endoplasmic reticulum. *J Cell Sci*, **2009**. 122(Pt 10): p. 1626-36.
55. Kim, S., et al., PARsylated transcription factor EB (TFEB) regulates the expression of a subset of Wnt target genes by forming a complex with beta-catenin-TCF/LEF1. *Cell Death Differ*, **2021**. 28(9): p. 2555-2570.
56. Kim, M.J., et al., Reduced EGFR Level in eIF2alpha PhosphorylationDeficient Hepatocytes Is Responsible for Susceptibility to Oxidative Stress. *Mol Cells*, **2020**. 43(3): p. 264-275.
57. Han, J., et al., ER-stress-induced transcriptional regulation increases protein synthesis leading to cell death. *Nat Cell Biol*, **2013**. 15(5): p. 481-90.
58. Back, S.H., et al., Translation attenuation through eIF2alpha phosphorylation prevents oxidative stress and maintains the differentiated state in beta cells. *Cell Metab*, **2009**. 10(1): p. 13-26.
59. Palam, L.R., T.D. Baird, and R.C. Wek, Phosphorylation of eIF2 facilitates ribosomal bypass of an inhibitory upstream ORF to enhance CHOP translation. *J Biol Chem*, **2011**. 286(13): p. 10939-49.
60. Glembotski, C.C., et al., ATF6 as a Nodal Regulator of Proteostasis in the Heart. *Front Physiol*, **2020**. 11: p. 267.
61. Luhr, M., et al., The kinase PERK and the transcription factor ATF4 play distinct and essential roles in autophagy resulting from tunicamycin-induced ER stress. *J Biol Chem*, **2019**. 294(20): p. 8197-8217.
62. Ganley, I.G., et al., Distinct autophagosomal-lysosomal fusion mechanism revealed by thapsigargin-induced autophagy arrest. *Mol Cell*, **2011**. 42(6): p. 731-43.
63. Chandrika, B.B., et al., Endoplasmic Reticulum Stress-Induced Autophagy Provides Cytoprotection from Chemical Hypoxia and Oxidant Injury and Ameliorates Renal Ischemia-Reperfusion Injury. *PLoS One*, **2015**. 10(10): p. e0140025.
64. Shen, H.M. and N. Mizushima, At the end of the autophagic road: an emerging understanding of lysosomal functions in autophagy. *Trends Biochem Sci*, **2014**. 39(2): p. 61-71.
65. Korolchuk, V.I., et al., Lysosomal positioning coordinates cellular nutrient responses. *Nat Cell Biol*, **2011**. 13(4): p. 453-60.
66. Pu, J., et al., Mechanisms and functions of lysosome positioning. *J Cell Sci*, **2016**. 129(23): p. 4329-4339.
67. Willett, R., et al., TFEB regulates lysosomal positioning by modulating TMEM55B expression and JIP4 recruitment to lysosomes. *Nat Commun*, **2017**. 8(1): p. 1580.
68. Arruda, A.P., et al., Chronic enrichment of hepatic endoplasmic reticulum-mitochondria contact leads to mitochondrial dysfunction in obesity. *Nat Med*, **2014**. 20(12): p. 1427-35.

69. Rutkowski, D.T., et al., Adaptation to ER stress is mediated by differential stabilities of pro-survival and pro-apoptotic mRNAs and proteins. *PLoS Biol*, **2006**. 4(11): p. e374.
70. Mauvezin, C., et al., Autophagosome-lysosome fusion is independent of V-ATPase-mediated acidification. *Nat Commun*, **2015**. 6: p. 7007.
71. Yoshii, S.R. and N. Mizushima, Monitoring and Measuring Autophagy. *Int J Mol Sci*, **2017**. 18(9).
72. Klionsky, D.J., et al., Guidelines for the use and interpretation of assays for monitoring autophagy (4th edition)(1). *Autophagy*, **2021**. 17(1): p. 1-382.
73. Perlmutter, D.H., Alpha-1-antitrypsin deficiency: importance of proteasomal and autophagic degradative pathways in disposal of liver disease-associated protein aggregates. *Annu Rev Med*, **2011**. 62: p. 333-45.
74. Silverman, G.A., S.C. Pak, and D.H. Perlmutter, Disorders of protein misfolding: alpha-1-antitrypsin deficiency as prototype. *J Pediatr*, **2013**. 163(2): p. 320-6.
75. Zheng, G., et al., TFEB, a potential therapeutic target for osteoarthritis via autophagy regulation. *Cell Death Dis*, **2018**. 9(9): p. 858.
76. Smith, M.D., et al., CCPG1 Is a Non-canonical Autophagy Cargo Receptor Essential for ER-Phagy and Pancreatic ER Proteostasis. *Dev Cell*, **2018**. 44(2): p. 217-232 e11.
77. Baltzis, D., et al., The eIF2alpha kinases PERK and PKR activate glycogen synthase kinase 3 to promote the proteasomal degradation of p53. *J Biol Chem*, **2007**. 282(43): p. 31675-87.
78. Pluquet, O., et al., Endoplasmic reticulum stress accelerates p53 degradation by the cooperative actions of Hdm2 and glycogen synthase kinase 3beta. *Mol Cell Biol*, **2005**. 25(21): p. 9392-405.
79. Huang, G., et al., ER stress disrupts Ca<sup>2+</sup>-signaling complexes and Ca<sup>2+</sup> regulation in secretory and muscle cells from PERK-knockout mice. *J Cell Sci*, **2006**. 119(Pt 1): p. 153-61.
80. van Vliet, A.R., et al., The ER Stress Sensor PERK Coordinates ER-Plasma Membrane Contact Site Formation through Interaction with Filamin-A and F-Actin Remodeling. *Mol Cell*, **2017**. 65(5): p. 885-899 e6.
81. Wang, R., et al., Insulin secretion and Ca<sup>2+</sup> dynamics in beta-cells are regulated by PERK (EIF2AK3) in concert with calcineurin. *J Biol Chem*, **2013**. 288(47): p. 33824-36.
82. Martina, J.A. and R. Puertollano, Rag GTPases mediate amino acid-dependent recruitment of TFEB and MITF to lysosomes. *J Cell Biol*, **2013**. 200(4): p. 475-91.
83. Nezich, C.L., et al., MiT/TFE transcription factors are activated during mitophagy downstream of Parkin and Atg5. *J Cell Biol*, **2015**. 210(3): p. 435-50.
84. Scheuner, D., et al., Translational control is required for the unfolded protein response and in vivo glucose homeostasis. *Mol Cell*, **2001**. 7(6): p. 1165-76.

85. Kaufman, R.J., Regulation of mRNA translation by protein folding in the endoplasmic reticulum. *Trends Biochem Sci*, **2004**. 29(3): p. 152-8.
86. Vatter, K.M. and R.C. Wek, Reinitiation involving upstream ORFs regulates ATF4 mRNA translation in mammalian cells. *Proc Natl Acad Sci U S A*, **2004**. 101(31): p. 11269-74.
87. Lu, P.D., H.P. Harding, and D. Ron, Translation reinitiation at alternative open reading frames regulates gene expression in an integrated stress response. *J Cell Biol*, **2004**. 167(1): p. 27-33.
88. Yamamoto, K., et al., Transcriptional induction of mammalian ER quality control proteins is mediated by single or combined action of ATF6alpha and XBP1. *Dev Cell*, **2007**. 13(3): p. 365-76.
89. Wu, J., et al., ATF6alpha optimizes long-term endoplasmic reticulum function to protect cells from chronic stress. *Dev Cell*, **2007**. 13(3): p. 351-64.
90. Yoshida, H., et al., Identification of the cis-acting endoplasmic reticulum stress response element responsible for transcriptional induction of mammalian glucose-regulated proteins. Involvement of basic leucine zipper transcription factors. *J Biol Chem*, **1998**. 273(50): p. 33741-9.
91. Spaan, C.N., et al., Expression of UPR effector proteins ATF6 and XBP1 reduce colorectal cancer cell proliferation and stemness by activating PERK signaling. *Cell Death Dis*, **2019**. 10(7): p. 490.
92. Ma, Y., et al., Two distinct stress signaling pathways converge upon the CHOP promoter during the mammalian unfolded protein response. *J Mol Biol*, **2002**. 318(5): p. 1351-65.
93. Yoshida, H., et al., ATF6 activated by proteolysis binds in the presence of NF-Y (CBF) directly to the cis-acting element responsible for the mammalian unfolded protein response. *Mol Cell Biol*, **2000**. 20(18): p. 6755-67.
94. Yang, H., et al., ATF6 Is a Critical Determinant of CHOP Dynamics during the Unfolded Protein Response. *iScience*, **2020**. 23(2): p. 100860.
95. Ishizawa, J., et al., Expression, function, and targeting of the nuclear exporter chromosome region maintenance 1 (CRM1) protein. *Pharmacol Ther*, **2015**. 153: p. 25-35.
96. Cullinan, S.B., et al., Nrf2 is a direct PERK substrate and effector of PERK-dependent cell survival. *Mol Cell Biol*, **2003**. 23(20): p. 7198-209.
97. Li, W., et al., Nrf2 Possesses a redox-insensitive nuclear export signal overlapping with the leucine zipper motif. *J Biol Chem*, **2005**. 280(31): p. 28430-8.
98. Zhang, Z., et al., The unfolded protein response regulates hepatic autophagy by sXBP1-mediated activation of TFEB. *Autophagy*, **2021**. 17(8): p. 1841-1855.

99. Andrejeva, G., et al., De novo phosphatidylcholine synthesis is required for autophagosome membrane formation and maintenance during autophagy. *Autophagy*, **2020**. 16(6): p. 1044-1060.
100. Schutter, M., et al., Local Fatty Acid Channeling into Phospholipid Synthesis Drives Phagophore Expansion during Autophagy. *Cell*, **2020**. 180(1): p. 135-149 e14.
101. Wu, J., et al., The unfolded protein response mediates adaptation to exercise in skeletal muscle through a PGC-1alpha/ATF6alpha complex. *Cell Metab*, **2011**. 13(2): p. 160-9.
102. Wang, Y., et al., The CREB coactivator CRTC2 links hepatic ER stress and fasting gluconeogenesis. *Nature*, **2009**. 460(7254): p. 534-7.
103. Gade, P., et al., An IFN-gamma-stimulated ATF6-C/EBP-beta-signaling pathway critical for the expression of Death Associated Protein Kinase 1 and induction of autophagy. *Proc Natl Acad Sci U S A*, **2012**. 109(26): p. 10316-21.
104. Blackwood, E.A., et al., Pharmacologic ATF6 activation confers global protection in widespread disease models by reprogramming cellular proteostasis. *Nat Commun*, **2019**. 10(1): p. 187.
105. Jin, J.K., et al., ATF6 Decreases Myocardial Ischemia/Reperfusion Damage and Links ER Stress and Oxidative Stress Signaling Pathways in the Heart. *Circ Res*, **2017**. 120(5): p. 862-875.
106. Inbal, B., et al., DAP kinase and DRP-1 mediate membrane blebbing and the formation of autophagic vesicles during programmed cell death. *J Cell Biol*, **2002**. 157(3): p. 455-68.

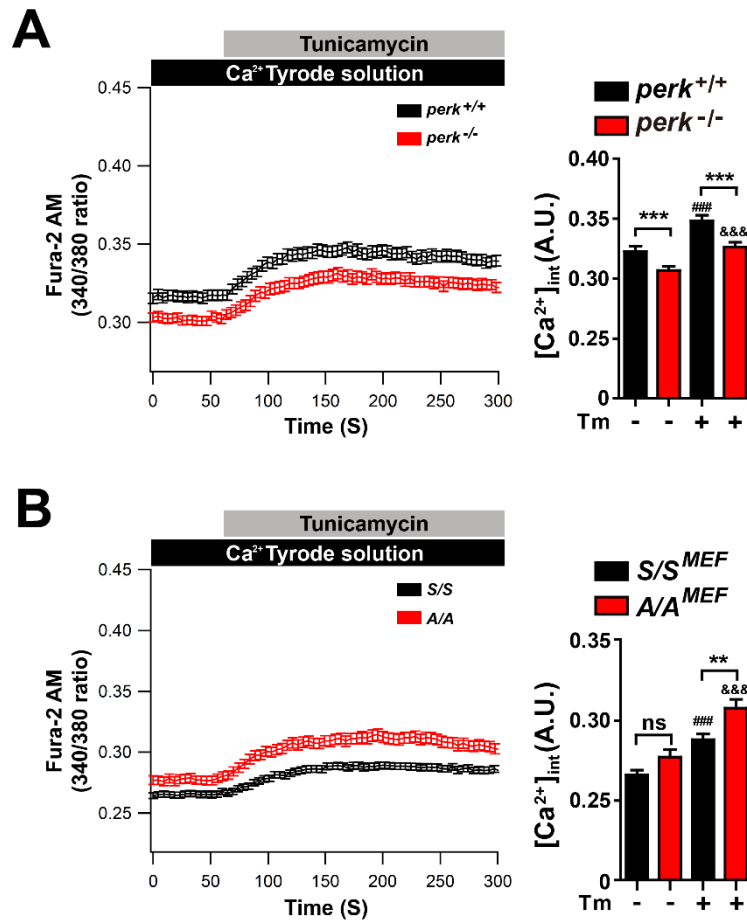
## **Appendix 1**

### **Translation Inhibitors Activate Autophagy Master Regulators TFEB and TFE3**

*Int. J. Mol. Sci.* 2021, 22(21), 12083; <https://doi.org/10.3390/ijms222112083>

## Appendix 2

### PERK but not eIF2 $\alpha$ phosphorylation is required for intracellular calcium dynamics during ER stress



**(A and B)** Representative measurements of Tm-induced cytosolic Ca<sup>2+</sup> changes. Wild-type (*perk*<sup>+/+</sup>) and *Perk*-KO (*perk*<sup>-/-</sup>) MEFs **(A)** and S/S<sup>MEF</sup> and A/A<sup>MEF</sup> cells **(B)** were treated with Tm (10  $\mu$ g/mL), and Fura-2 Ca<sup>2+</sup> imaging was performed as described in the Materials and Methods. The graphs depict the cytosolic Ca<sup>2+</sup> concentration in basal and Tm-stimulated MEFs (*perk*<sup>+/+</sup>, n = 169; *perk*<sup>-/-</sup>, n = 167; S/S<sup>MEF</sup>, n = 134; and A/A<sup>MEF</sup>, n = 131). Data are presented as mean  $\pm$  SEM. \*\*p < 0.01 and \*\*\*p < 0.001, *perk*<sup>+/+</sup> vs. *perk*<sup>-/-</sup> or S/S<sup>MEF</sup> vs. A/A<sup>MEF</sup>; ###p < 0.001, Mock vs. Tm in *perk*<sup>+/+</sup> or S/S<sup>MEF</sup>; &&&p < 0.001, Mock vs. Tm in *perk*<sup>-/-</sup> or A/A<sup>MEF</sup> (Student's t-test).

Appendix 2 was performed by Ms. Yoon Young Lee under the supervision of Prof. Chan Young Park, Department of Biological Sciences, School of Life Sciences, Ulsan National Institute of Science and Technology, Ulsan, Korea. (They are collaborators in this study).